UNIVERSITÀ DEGLI STUDI DI PALERMO
PhD Course in
Chemical, Environmental, Biomedical, Hydraulic and Materials Engineering

Biocomposites reinforced with biochar particles as a circular value-added filler

PhD Candidate

Giulia Infurna

Supervisor

Prof.ssa Nadka Tz. Dintcheva

XXXVI Cycle

Graduation Year 2023

Table of Contents

Aim of work

How can we meet the great green challenge we face? How can we reduce the environmental impact of urban and industrial waste? How can we give new life to waste materials? And how can we continue to perform in the new industrial era?

All these questions have led to the following research, with a strong focus on how industries are, or should be, moving from a linear to a circular economy. Within the circular economy, we therefore started by giving new life to waste materials from the agri-food industry. Through pyrolysis, we have started to convert matter into energy by producing low molecular weight fuel and gas.

The aim of this work is the formulation and characterization of biocomposites reinforced with biochar (BC) particles, the by-product of pyrolysis. In fact, biochar is a second-level waste product that holds great promise for materials science. The focus of this research was the employment of this particles to obtain biodegradable materials, with particular attention to energy optimisation, through the slow pyrolysis of two types of organic waste.

The first waste used was the residue of the carob fruits after their processing for the extraction of sugars and nutrients to produce candies. The lignocellulose residue was then subjected to pyrolysis and the resulting biochar was used as a reinforcing filler. A careful study of the pyrolysis temperature was carried out with two goals: energy optimization (quality and quantity of fuel) and optimization of the properties of the resulting biochar as a reinforcing particle.

The second pyrolysed waste material with the same objectives as the previous one was digestate, the product of anaerobic digestion of municipal solid organic waste for the production of biogas and biofuels. The first energy optimisation was therefore carried out on the waste. The resulting digestate was used as a feedstock for the pyrolysis carried out in our laboratories, resulting in the production of the three pyrolysis products: fuel, biogas and biochar. Once again, biochar was used as a reinforcing filler.

Another question was whether the properties of biochar could be comparable or better than carbonaceous particles widely used in materials science, such as carbon black, or whether it could be a co-component with carbon black or graphene in high-performance materials.

After answering these questions, supported by experimental work and literature review, several experimental studies were carried out, firstly on commercial biochar to define the operating conditions, optimise biochar concentration, for composite processing, then using carob waste and digestate biochar.

Carob-waste derived biochar particles at two different concentrations, *i.e.* 10 and 20 wt.%, were added to poly(butylene adipate terephthalate) (PBAT). As previously mentioned, in order to optimise the composition of the solid fractions and biofuels produced in the pyrolysis process, the BC were produced using three pyrolysis processing temperatures. The resulting particles from the pyrolysis process were considered to be suitable as a filler for the PBAT. First, the properties of the BC particles were characterized by elemental compositional and spectroscopic analysis, particle size measurements and evaluation of scavenger activity and efficiency. Furthermore, PBAT/BC composites were analysed regarding their rheological, thermal, morphological and mechanical properties. Accelerated weathering, monitored by both tensile test and spectroscopy analysis, was also performed and the

results obtained show that the biochar particles may have a beneficial effect on the photo-oxidative delay of the PBAT matrix.

Instead, digestate derived biochar has been added to the biopolymer blend with a focus on the effect of the biopolymer weight ratio on the final BC composites. The blends studied in this work were obtained by varying the weight ratio of poly butylene adipate co-terephthalate (PBAT) and poly lactic acid (PLA), due to their great importance in packaging and agricultural fields. It has been found that BC affects PBAT and PLA biopolymer matrices in different ways, and that the relative weight ratio between PBAT and PLA plays a significant role in blending compositions. In order to better investigate the filler/polymer interactions, biochar particles were dimensionally, morphologically and chemically characterised. The biocomposites blend has been fully characterised: rheological, morphological, mechanical and dynamic-mechanical characterisations have been carried out, highlighting that a strong chemical interaction takes place between PLA and BC particles.

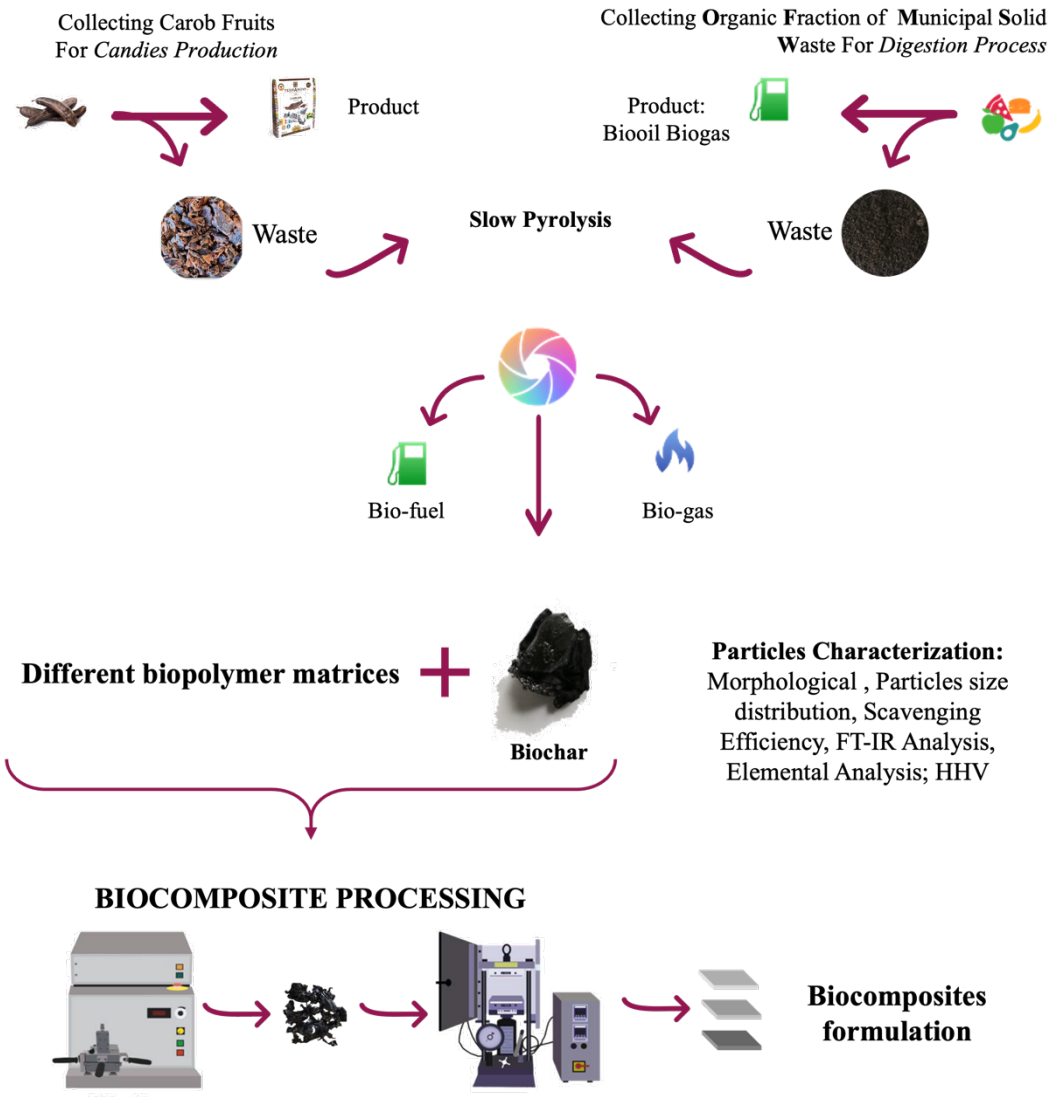

Biocomposites Characterization:

Morphological , FT-IR analysis, Rheological, Dynamic Mechanical Analysis, Tensile Test, Differential Scanning Calorimetry, Thermo-Gravimetric Analysis, Photo degradation Behaviour

1. Literature Overview

A key contribution to the EU's efforts to develop a sustainable, low-carbon, resource-efficient and competitive economy is the transition to a more circular economy, where the value of products, materials and resources is retained in the economy for as long as possible and the generation of waste is minimised. Such a transition is an opportunity to transform our economy and create new and sustainable competitive advantages for Europe [1].

In recent decades, scientific and industrial interest has been focused on the formulation of advanced polymer-based composites, with improved performance and properties through the addition of fillers, such as carbon-based fillers, and additives that could improve the intrinsic properties of the polymer matrix, combining the light weight, processability and flexibility of polymers with improved mechanical, chemical and physical properties of added fillers. Anyway, the generation of plastic waste and subsequent uncontrolled plastic pollution is one of the major environmental issues facing governments and authorities. The transition to a more sustainable society is closely linked to the production, use and disposal of plastics.

Due to the increasing production of plastics assets production, more and more studies have been focused on the conversion of polymer waste, municipal waste, biomass, and various residues into energy, fuels, and other materials, with the aim of achieving a circular economy and, above all, a zero-waste society.

In the competition for a circular economy, thermal decomposition processes, such as pyrolysis or hydrothermal-cracking, could be a challenging process to convert waste into three different new resources: gas (a mixed phase of light hydrocarbons), oil or bio-oil (a mixture of the heaviest hydrocarbons) and biochar, a solid phase.

In addition, it is necessary to support the biobased industry and create a framework for the use of bio-based plastics in order to address the shift towards a more sustainable society. Thus, the introduction of bioplastic (considered as biodegradable, bio-based or both polymer matrix) is under evaluation as a way to reduce the need for fossil resources, and to mitigate some environmental risks, such as plastic pollution.

An overview will be given of what biomasses are, their use as energy resources that also produce a value-added by-product, the benefits of using carbon based materials, their applications as reinforcing fillers for composites and biocomposites and their formulation. A particular focus will be placed on biochar particles, a carbonaceous filler produced as a by-product of thermal decomposition processes to recover energy, and their applications in materials science.

1.1. Biomass: a waste or a resource?

"Biomass' means the biodegradable fraction of products, waste and residues from biological origin from agriculture (including vegetal and animal substances), forestry and related industries including fisheries and aquaculture, as well as the biodegradable fraction of industrial and municipal waste" [2].

Biomass is divided into four macro categories: woody, herbaceous, animal and contaminated biomass. It can also be further subdivided into residual and non-residual biomass, depending on whether it comes from dedicated crops or processing waste.

Residual biomass can have a further classification on the basis of its field of origin:

- Agriculture: Residues from agricultural activities and crops;
- Forestry and agro-forestry: residues from agro-forestry activities such as straw, prunings, branches, bark, etc;
- Industrial: Residues from the wood or wood products processing industry and the paper industry, as well as residues from the agro-food industry (e.g. marc, vegetable waste, etc.).
- Zootechnical: biotechnical waste for biogas production;
- Municipal waste: residues from the maintenance of public green areas and the organic fraction of municipal solid waste (OFMSW).

Non-residual biomass is classified according to the type of crop that produces it:

- Alcoholic crops: characterised by a high sugar content (such as sugarcane, sugar beets, corn, wheat, etc.) and used for the production of ethanol;
- Oil crops: characterised by a high vegetable oil content, which can be used as such or processed into biodiesel;
- Lignocellulosic crops: characterised by high dry matter production that can be used for various energy applications (perennial woody species such as poplar and herbaceous species).

1.1.1. Lignocellulosic Biomass

Lignocellulosic biomass, one of the most abundant in nature, includes all compounds derived from crop residues and dedicated agricultural crops, herbaceous and/or woody in nature. Plant biomass is a complex mixture of organic compounds such as carbohydrates, proteins and fats, and minerals such as sodium, calcium, iron and phosphorus. The main components of lignocellulosic biomass are: extractives, cell wall components and ash [3]. Cell wall components include cellulose, hemicellulose and lignin, three essential polymers that give strength to the plant structure.

Cellulose, a polysaccharide consisting of glucose molecules linked by β-1-4 glycosidic linkages to form linear sugar chains, is the major component of plant biomass (30-60 % by weight). These chains are arranged parallel to each other and linked by hydrogen bonds to form fibrils. Fibrils are very long chains that are difficult to dissolve. The formation of fibrils gives the plant fibre strength and elasticity. Cellulose is characterised by the presence of six carbon atoms and is composed mainly of d-glucose. Cellulose is very difficult to dissolve and, although it is a carbohydrate, it cannot be digested by the human body. It is approximately 40-44% by weight on a dry basis and is one of the major constituents of wood.

Hemicellulose is a mixture of polysaccharides, mainly anhydrous sugars with 5 and 6 carbon atoms. Hemicellulose is a smaller polymer than cellulose. It forms hydrogen bonds with cellulose and, in combination with cellulose, acts as a structural material for the cell wall. It is highly soluble and has a more amorphous and random molecular structure than cellulose.Most hemicelluloses contain residues of simple sugars such as d-xylose or d-glucose, although the composition and structure of hemicellulose varies greatly depending on the type of biomass analysed. It makes up about 20-30% of the weight of dry wood.

Lignin is a complex, non-fibrous structure of high molecular weight. Chemically, it is an extremely branched three-dimensional polymer consisting of various acids and phenyl-propyl alcohols. The polymer is therefore the result of a large number of

combinations of polymerisation sites. It is mainly found in cell walls where it acts as a binder, cementing the cellulose fibres together and making them stable and resistant. It is highly insoluble, constituting 18-25% dry weight in hardwood and 25-30% in softwood.

The conversion of atmospheric carbon dioxide into carbohydrates is the process by which plant biomass is formed. This conversion uses sunlight as an energy source, which is absorbed by plants through a special photosensitive pigment called chlorophyll. Through chlorophyll, the incident solar radiation activates a chemical conversion mechanism involving the reaction between CO2 present in the air and water absorbed from the soil through the roots. This leads to the formation of organic compounds (mainly glucose) that will make up the plant's structure, and the release of oxygen as a waste product. This process is illustrated by the following equation [3]:

$$biomass + CO_2 + H_2O + h\nu \xrightarrow{chlorophyll} (CH_mO_n) + O_2 - 480\ kJ/mol$$

From the water that the plant has taken up from the atmosphere (in the form of water vapour) or from the soil, for every mole of CO_2 absorbed, one mole of O_2 is released into the atmosphere. The mechanism of photosynthesis is only one step in the process of biomass formation, as summarised by the above reaction. Glucose is subsequently converted into other, more complex molecules that are essential for structuring and stabilising plant biomass. In addition, the entire process requires not only light and water, but also appropriate environmental conditions and the availability of nutrients such as nitrogen, phosphorus and potassium fertilisers. At the end of their life cycle, plants give back to the environment the energy and substances they have stored in them through natural processes of decomposition or combustion.

Looking at the reaction described above, biomass can be considered a renewable energy source. In fact, the rate at which new biomass is produced is comparable to

the rate at which biomass is consumed, whereas fossil fuels take geological eras to produce and are therefore classified as non-renewable.

The production of energy from biomass offers significant socio-economic and environmental benefits, both locally and/or globally. For example, as discussed in the previous paragraph, since the CO_2 released during the energy production process is equal to the CO_2 absorbed during plant growth (photosynthesis process), the use of plant biomass for energy production is considered one of the most efficient systems for reducing greenhouse gas emissions. Fossil fuels, on the other hand, emit a quantity of CO_2 that accumulates in the atmosphere, exacerbating the already precarious environmental situation of modern society.

Biomass treatment processes for energy use can be divided into three macro-categories, as shown in Figure 1.

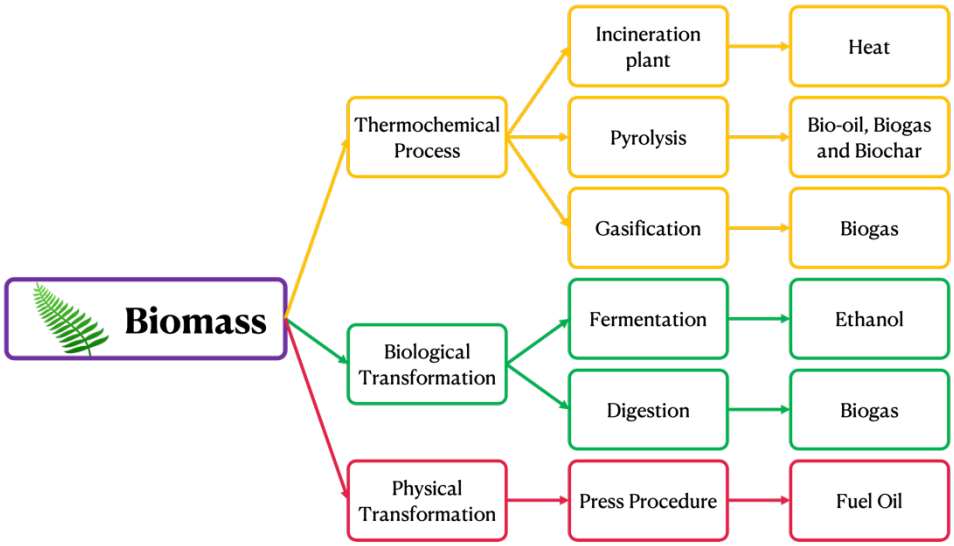

Figure 1 *Schematisation of the most important processes for the treatment of biomass for energy conversion*

These conversion processes produce products with higher added value and, above all, higher energy density. These products can be used for the production of electricity, heat and/or biofuels (solid, liquid or gaseous) or as biochemicals for industry. Choosing which process to use depends largely on the composition of the biomass, its physical properties, and its availability. It will also be necessary to carry

out pre-treatments to make the biomass to be processed suitable for the chosen conversion treatment.

The most important thermochemical processes include combustion, pyrolysis and gasification, and these will be discussed in more detail later on.

The most common biological processes used on an industrial scale include:

- Alcoholic fermentation: a biochemical conversion process that converts sugars to ethyl alcohol. It is the most widely used industrial process for producing liquid biofuels.
- Anaerobic digestion: conversion process carried out by bacteria that can produce biogas very rich in methane. Anaerobic digestion produces solid waste. Depending on the composition of the waste, it can be used as fertiliser, converted by pyrolysis or gasification, or simply disposed of.

Finally, physical treatments are mostly pressing and/or grinding processes. These can be used to obtain bio-oils. These may in turn undergo treatments to make them specific.

1.1.1. Municipal Waste

The daily activities of living beings continuously generate an enormous amount of waste, including organic and inorganic waste. The generation of solid waste is particularly high in developing countries. This is due to population growth, urbanisation, economic development and improved living standards.

Municipal waste consists of the organic fraction of municipal waste, defined as the organic fraction of municipal solid waste (OFMSW), and of residues from the maintenance of public green spaces. Partly due to waste disposal issues, but also due to its high carbohydrate content, biodegradability and high hydrogen potential, OFSMW is considered to be the substrate of choice for hydrogen production [4], [5].

Municipal solid waste generated by households is the third largest source of methane emissions, accounting for around 11 per cent of global methane emissions. Trying to

control and optimise the methane generated by fermenting this type of waste could certainly shift from and issue of disposing and managing the waste to a value-added process capable of creating a new resource. In this respect, a biological transformation such as anaerobic digestion has a key role to play.[6]

Anaerobic digestion is a series of biochemical processes that convert organic biomass into methane and carbon dioxide in the absence of oxygen, and more or less accounts for 35% of bioenergy production [7].

The main product of anaerobic digestion is biogas, a gaseous mixture consisting mainly of methane (50 to 75% by volume) and carbon dioxide. However, the main by-product of anaerobic digestion is the digestate. It can be subjected to a compaction and separation phase to separate a highly solid fraction from a predominantly liquid fraction, sent to a wastewater treatment plant and/or returned to the composting plant to be used as process water. After composting, the digestate can be used in gardening, in nurseries with pots and soil, in the sowing of meadows, etc. and can also be used and marketed as a "compost improver" on the basis of the provisions of the legislation on fertilisers.

Reference

[1] European Commission, 'COMMUNICATION FROM THE COMMISSION TO THE EUROPEAN PARLIAMENT, THE COUNCIL, THE EUROPEAN ECONOMIC AND SOCIAL COMMITTEE AND THE COMMITTEE OF THE REGIONS Closing the loop -An EU action plan for the Circular Economy', Brussels, 2018.

[2] C. Ervine, 'Directive 2004/39/Ec of the European Parliament and of the Council of 21 April 2004', in *Core Statutes on Company Law*, London: Macmillan Education UK, 2015, pp. 757–759. doi: 10.1007/978-1-137-54507-7_21.

[3] P. Basu, *Biomass gasification and pyrolysis: practical design and theory*. Burlington, MA: Academic Press, 2010.

[4] H. Shin, 'Hydrogen production from food waste in anaerobic mesophilic and thermophilic acidogenesis', *Int. J. Hydrog. Energy*, vol. 29, no. 13, pp. 1355–1363, Oct. 2004, doi: 10.1016/j.ijhydene.2003.09.011.

[5] J. Pan, R. Zhang, H. Elmashad, H. Sun, and Y. Ying, 'Effect of food to microorganism ratio on biohydrogen production from food waste via anaerobic fermentation', *Int. J. Hydrog. Energy*, vol. 33, no. 23, pp. 6968–6975, Dec. 2008, doi: 10.1016/j.ijhydene.2008.07.130.

[6] N. Kanaujia and J. Singh, '13 - Composition, characteristics and challenges of OFMSW for biogas production: Influence of mechanism and operating parameters to improve digestion process', in *Advanced Organic Waste Management*, C. Hussain and S. Hait, Eds., Elsevier, 2022, pp. 207–223. doi: 10.1016/B978-0-323-85792-5.00025-3.

[7] M. Rasapoor, B. Young, R. Brar, A. Sarmah, W.-Q. Zhuang, and S. Baroutian, 'Recognizing the challenges of anaerobic digestion: Critical steps toward improving biogas generation', *Fuel*, vol. 261, p. 116497, Feb. 2020, doi: 10.1016/j.fuel.2019.116497.

1.2. Waste management and valorisation

In recent years, governments and the public have become increasingly aware and concerned about the health and environmental impacts of poor waste management. The best, and certainly most effective, way to tackle this problem is to intervene upstream by reducing the generation of waste itself. Indeed, protecting the environment by minimising the generation of waste is one of the basic principles of the Basel Convention. With this in mind, there has been considerable interest and progress in redesigning plants and, more generally, entire industrial processes. However, this approach, while desirable, is not always feasible, particularly in the area of hazardous waste. Where the generation of hazardous waste cannot be avoided, the focus is on recycling. In addition, government programmes in many countries encourage the recycling of consumer products to recover potentially hazardous substances (such as heavy metals in batteries and electronic equipment) that would otherwise be disposed of in landfills. Some hazardous wastes can therefore be reused for purposes other than their original use. For example, some solvents can be mixed with fuels and used in industrial burners, while mining wastes can be used as aggregate in asphalt and reinforced concrete. However, the production of non-recyclable hazardous waste is unavoidable. For the latter, appropriate and safe treatment methods are required. Waste disposal represents a potentially huge loss of resources in terms of materials and energy. As analysed above, landfilling is still characterised by high volumes of treated waste, although in some countries significant amounts of waste are incinerated. Account must also be taken of the serious environmental impacts of waste management. Landfills, for example, occupy large areas and cause more or less significant air, water and soil pollution. Modern incineration technologies, on the other hand, have led to a drastic reduction in potentially polluting emissions and to significant energy recovery (waste-to-energy plants). The main techniques and technologies used to date for the disposal, treatment and/or valorisation of large quantities of waste are: landfilling, recycling and

incineration with or without energy recovery. Also worth mentioning are thermochemical, hydrothermal, and biological treatment processes. These treat smaller volumes than the above technologies but are expanding rapidly.

1.2.1. Recycling

Recycling refers to the set of strategies and methods used to recover useful materials from waste that would otherwise go to landfill or incineration for reuse. Recycling makes production/use cycles more sustainable, reducing raw material and energy consumption and atmospheric emissions. It is important to emphasise that recycling does not replace landfilling or incineration, but it significantly reduces the disposal and/or treatment of waste by the latter, to the benefit of economic and environmental sustainability. Mechanical and chemical recycling can be distinguished. Mechanical recycling consists of processing the compounds to be recycled into secondary raw materials (MPS) for the manufacture of new products.

Mechanical recycling starts with a sorting and separation phase, in which several techniques can be used: manual selection, separation by density, flotation, separation by aerodynamic properties, screening by blowing air, electrostatic separation.

After separation, the waste to be recycled is subjected to the grinding stage, using mills that coarsely crush the material, resulting in a significant reduction in the initial volume. The ground material is subsequently washed to eliminate any contaminants which may affect the next stage of the process. In the most common washing system, the ground material is passed through a tank in which a constant flow of water is maintained.

After a preliminary centrifugation to remove all the free water, the drying phase is carried out by drying in a stream of hot air or flue gas, with the aim of eliminating the adsorbed water (approximately 15-20%). This allows the water content to be reduced to 2-3% by weight so that the final conversion stage can be carried out. The

final conversion stage will be strictly dependent on the nature of the material to be recycled.

Chemical recycling, which is particularly popular for plastic waste, consists of breaking down waste compounds using heat, chemical agents or catalysts. In the case of plastics, a wide variety of raw materials can be recovered, ranging from monomers to mixtures of compounds, mainly hydrocarbons, which become new sources of chemicals or fuels. Products derived from chemical recycling have properties and qualities similar to those of virgin materials. Among the processes used, thermochemical process are of particular scientific and application interest.

1.2.2. Thermochemical Process

The main thermochemical decomposition processes studied are slow, fast and flash pyrolysis, torrefaction, gasification and hydrothermal liquefaction. All these processes essentially produce *i.* a solid phase, called *char* or *biochar* in the case of biomass feedstock, *ii. fuel*, a mixed liquid phase of the heaviest hydrocarbons, *iii. syngas*, a mixed gas phase of the lightest hydrocarbons [1]–[4]. Of course, depending on the chemical composition of the treated materials (*i.e.* biomass, mixed waste, synthetic polymers) and depending on the operating conditions (*i.e.* temperature process, heating rate, presence or absence of oxygen, residence time), the relative ratio between these three main products may change. Different thermal decomposition processes differ in terms of operating conditions such as operating temperatures, heating rates and pressures. Thermal decomposition processes are summarized in Table 1 in which the primary product of the process is also explained.

Table 1 Thermochemical Process and their main differences in terms of operative conditions, time of reactions and primary products [5]

Thermochemical Process	Temperature Range [°C]	Heating Rate	Pressure	Residence Time	Primary Product
Slow Pyrolysis	350-800	Slow (<10°C/min)	Atmospheric	Hours – Days	Char
Fast Pyrolysis	400-600	Very Fast (~1000°C/s)	Vacuum-Atmospheric	Seconds	Oil
Flash Pyrolysis	300-800	Fast	Moderate (2 – 25 atm)	Minutes	Biocarbon/ Char
Torrefaction	200-300	Slow (<10°C/min)	Atmospheric	Minutes - Hours	Friable Biomass
Gasification	700-1800	Moderate-Vary Fast	Atmospheric - Moderate	Seconds - Minutes	Syngas/ Producer gas
Hydrothermal Liquefaction	250-450	Moderate	Elevated 100-300 atm	Minutes - Hours	Bio-crude (oil)

Slow pyrolysis, carried out in the absence of oxygen, is characterised by slow heating rates and long residence times at atmospheric pressure with an operating temperature that can vary from 350 to 800°C; the energy required to pyrolyze the feedstock is usually provided internally by burning part of the feedstock; the main product is a high carbon solid char and the by-products are an aqueous low molecular weight liquid and a low energy combustible gas.

Like slow pyrolysis, fast pyrolysis is carried out in the absence of oxygen at temperatures between 400 and 600°C. However, it is different in that it uses a very high heating rate, a vacuum atmosphere, a short residence time and rapid quenching of the vapours, since the main objective of this process is to produce bio-oil. [6]–[8].

Flash pyrolysis is a batch process with an operating temperature range between 300 and 800°C, similar to slow pyrolysis but with a high heating rate, which uses moderate pressure (between 2 and 25 atm) to condense volatile elements and promote secondary formation, since the aim of this process is to produce a liquid biocarbon fraction or solid phase of biochar. [9].

Torrefaction differs from slow pyrolysis by the lower operating temperature range, between 200 and 300°C, which mainly removes water and some volatiles from the biomass, producing a "brown" char that is easy to grind, a stabilised and friable biomass.

Instead, gasification is characterised by a high process temperature (between 750 and 1800°C) with a limited and controlled oxygen concentration (usually calculated as the amount relative to stoichiometric combustion) [10] and/or steam [11]; as the name suggests, the primary products are a non-condensable gas mixture, called syngas, composed mainly by the presence of CO, H2, with a smaller amount of carbon dioxide, methane and other low molecular weight hydrocarbons [12].
Finally, hydrothermal liquefaction is a process carried out in the presence of water, with a temperature range of 250-450°C and under 100-300 bar; the main product of this process is called bio-crude, an energy dense intermediate renewable source equivalent to oil that can be fractionated into a variety of liquid fuels [13].
In general, biochar produced at high temperatures has a higher surface area and carbon content, mainly due to the increase of micro-pore volume caused by the removal of volatile organic compounds [14]. However, the biochar yields decreased with temperature increase [15].
As mentioned above, the quality and final chemical composition, as well as physical properties such as porosity, are influenced by the operating conditions and therefore the thermochemical process used to produce biochar, but also by the nature of the feedstock used to carry out the decomposition process. Depending on the nature and initial chemical composition of the feedstock, the final composition of the pyrolysis by-products will vary. The primary analysis normally carried out to characterise the feedstock, operating temperature and relative char quality is the proximate analysis. This thermogravimetric analysis provides information on the moisture content of the feedstock relative to the mass lost up to 110°C, the volatile matter relative to the mass lost in an inert atmosphere at 950°C, the fixed carbon relative to the mass lost in air at 750°C and the remainder relative to the ash content. To characterise the quality of char in terms of carbon content, elemental analysis is normally used, a technique in which a sample is burnt at a very high temperature in a small chamber with excess oxygen content, the gases relative to the combustion are trapped and, depending on the number of sensors available, it is possible to obtain information, in

terms of percentage by weight, on carbon, hydrogen and nitrogen, CHN elemental content (relative to CO_2, H_2O, NO), but also sulphur content, CHNS, and oxygen/sulphur content, CHNOS.

In general, organic or synthetic materials can be used as feedstock, with different thermo-decomposition processes depending on the physico-chemical properties of the feedstock and the desired product composition.

The value of a particular type of biomass depends on the chemical and physical properties of the molecules from which it is made. From the literature study, biomass is the main feedstock used for BC production for several advantageous reasons. First, for environmental reasons, biomass is more readily available in a renewable form, either through natural processes or as a product of human activities. In addition, if biomass is produced in a sustainable manner, its conversion produces approximately the same amount of carbon as is absorbed during plant growth, thus reducing the amount of CO_2 in the atmosphere [16].

Reference

[1] A. Tomczyk, Z. Sokołowska, and P. Boguta, 'Biochar physicochemical properties: pyrolysis temperature and feedstock kind effects', *Reviews in Environmental Science and Biotechnology*, vol. 19, no. 1, pp. 191–215, Mar. 2020, doi: 10.1007/s11157-020-09523-3.

[2] B. Sizirici, Y. H. Fseha, I. Yildiz, T. Delclos, and A. Khaleel, 'The effect of pyrolysis temperature and feedstock on date palm waste derived biochar to remove single and multi-metals in aqueous solutions', *Sustainable Environment Research*, vol. 31, no. 1, Dec. 2021, doi: 10.1186/s42834-021-00083-x.

[3] D. Mohan, C. U. Pittman, and P. H. Steele, 'Pyrolysis of wood/biomass for bio-oil: A critical review', *Energy and Fuels*, vol. 20, no. 3, pp. 848–889, May 2006, doi: 10.1021/ef0502397.

[4] V. Nagarajan, A. K. Mohanty, and M. Misra, 'Biocomposites with Size-Fractionated Biocarbon: Influence of the Microstructure on Macroscopic Properties', *ACS Omega*, vol. 1, no. 4, pp. 636–647, Oct. 2016, doi: 10.1021/acsomega.6b00175.

[5] G. Infurna, G. Caruso, and N. Tz. Dintcheva, 'Sustainable Materials Containing Biochar Particles: A Review', *Polymers*, vol. 15, no. 2, p. 343, Jan. 2023, doi: 10.3390/polym15020343.

[6] S. Al Arni, 'Comparison of slow and fast pyrolysis for converting biomass into fuel', *Renewable Energy*, vol. 124, pp. 197–201, Aug. 2018, doi: 10.1016/j.renene.2017.04.060.

[7] R. Palos, E. Rodríguez, A. Gutiérrez, J. Bilbao, and J. M. Arandes, 'Cracking of plastic pyrolysis oil over FCC equilibrium catalysts to produce fuels: Kinetic modeling', *Fuel*, vol. 316, p. 123341, May 2022, doi: 10.1016/j.fuel.2022.123341.

[8] J. K. Sarkar and Q. Wang, 'Different pyrolysis process conditions of South Asian waste coconut shell and characterization of gas, bio-char, and bio-oil', *Energies*, vol. 13, no. 8, Apr. 2020, doi: 10.3390/en13081970.

[9] M. J. Antal, S. G. Allen, X. Dai, B. Shimizu, M. S. Tam, and M. Grønli, 'Attainment of the theoretical yield of carbon from biomass', *Industrial and Engineering Chemistry Research*, vol. 39, no. 11, pp. 4024–4031, 2000, doi: 10.1021/ie000511u.

[10] C. Guizani *et al.*, 'Influence of temperature and particle size on the single and mixed atmosphere gasification of biomass char with H2O and CO2 Influence of temperature and particle size on the single and mixed atmosphere gasification of biomass char with H 2 O and CO 2', *Fuel Processing Technology*, vol. 134, pp. 175–188, 2015, doi: 10.1016/j.fuproc.2015.01.031ï.

[11] D. Barisano *et al.*, 'Investigation of an Intensified Thermo-Chemical Experimental Set-Up for Hydrogen Production from Biomass: Gasification Process Integrated to a Portable Purification System—Part II', *Energies*, vol. 15, no. 13, Jul. 2022, doi: 10.3390/en15134580.

[12] R. W. Breault, 'Gasification processes old and new: A basic review of the major technologies', *Energies*, vol. 3, no. 2, pp. 216–240, 2010, doi: 10.3390/en3020216.

[13] L. Grande, I. Pedroarena, S. A. Korili, and A. Gil, 'Hydrothermal liquefaction of biomass as one of the most promising alternatives for the synthesis of advanced liquid biofuels: A review', *Materials*, vol. 14, no. 18, Sep. 2021, doi: 10.3390/ma14185286.

[14] B. Chen, D. Zhou, and L. Zhu, 'Transitional Adsorption and Partition of Nonpolar and Polar Aromatic Contaminants by Biochars of Pine Needles with Different Pyrolytic Temperatures', *Environ. Sci. Technol.*, vol. 42, no. 14, pp. 5137–5143, Jul. 2008, doi: 10.1021/es8002684.

[15] G. Xu, X. Yang, and L. Spinosa, 'Development of sludge-based adsorbents: Preparation, characterization, utilization and its feasibility assessment', *Journal of Environmental Management*, vol. 151, pp. 221–232, Mar. 2015, doi: 10.1016/j.jenvman.2014.08.001.

[16] P. McKendry, 'Energy production from biomass (part 1): overview of biomass', *Bioresource Technology*, vol. 83, no. 1, pp. 37–46, May 2002, doi: 10.1016/S0960-8524(01)00118-3.

1.3. Carbon particles: why use them in material science?

In composite science and technology, the use of carbon-based particles and nanoparticles has been extensively studied due to their outstanding mechanical, electrical, and thermal properties. Indeed, when incorporated into a polymer matrix, they are expected to improve or significantly alter the properties of the host matrix, with the addition of small amounts of filler. Among the wide variety of fillers, the carbon-based materials play an important role in composite formulation. The carbon atom, C, is the most versatile element due to its ability to combine with other atoms to form *sp, $sp^2$and* sp^3 hybridized structure and its ability to form a wide range of stable molecules [1]–[3]. Elemental carbon has three main forms: diamond (consisting of sp^3-bonded carbon in crystalline form), graphite (consisting of sp^2-bonded carbon in planar layers) and fullerene. Various forms of carbon exhibit sp^2-bonded hybridization forms, and of interest to materials science are graphene, carbon nanotubes and carbon black. The performance of carbon-based composites and nanocomposites depends on the intrinsic properties of the nanofillers (geometric dimension, surface area, aspect ratio, etc.), the interaction between filler and polymer matrices, the degree of dispersion and the distribution of the filler in the polymer matrix [4]–[8].

Carbon black (CB) differ from other forms of bulk carbon, such as diamond graphite and cokes since they are composed of aggregates having complex configuration, quasi-graphitic in structure, and colloidal dimension [9].

Carbon Nanotubes (CNT) are a hexagonal network of carbon atoms rolled up into a seamless and hollow cylinder. CNTs can be divided into single-walled (SWNTs), double-walled (DWNTs) and multi-walled carbon nanotubes (MWCNTs), depending on the number of graphene sheets they consist of [10], [11]. However, because of van der Waals interactions, CNT are susceptible to agglomeration and the aggregates formed act as defects in the host matrix, leading to a reduction in mechanical properties [11], [12]. In order to overcome the disadvantages related to

the poor dispersion of CNTs in polymers, several strategies have been pursued, including high shear mixing [25], the addition of surfactants or dispersants [13] and the chemical functionalisation of the CNT surface [14]–[16]. Due to their unique combination of mechanical, electrical and magnetic properties, carbon nanotubes are one of the most promising candidates for the formulation of innovative nanocomposites [17]–[19]. Moreover, their shape factor makes CNTs particularly interesting for formulating engineered materials with enhanced anisotropic properties such as electrical and thermal conductivity, etc. [20]. The high mechanical properties of CNTs are well known in the literature, suggesting that they can be used as reinforcing fibres in high-toughness nanocomposites, where stiffness, strength and low weight are relevant properties, such as applications in aerospace structural panels, sporting goods, ultra-lightweight thin-walled space structures for use in space, and high stiffness-to-weight space mirror substrates [21]. In addition, the excellent electrical and thermal properties of nanotubes are particularly important in nanocomposites. In fact, thanks to their high aspect ratio, CNTs are able to impart a percolation-like behaviour due to the random orientation of the CNTs, which could create a conductive network even at extremely low CNT content [22]–[24].

Graphene, in nanoplatelets forms (GNP), is considered a two-dimensional carbon nanofiller with a one-atom thick planar layer of sp^2 hybridized carbon atoms [25]. GNP-based nanocomposites are ideal candidates for the development of protective layers, chemical filters, adhesive layers, sensors and electrical devices due to the multifunctional properties of GNP and its sp^2-bonded carbon in planar layers [26], [27]. Graphene has received much attention for its ability in improving the mechanical [28], [29], thermal [30], [31] and electrical properties [30], [32] of composites, as well as their thermo-mechanical and photo-oxidative degradation behavior [33]. Furthermore, the presence of GNPs increases the effect of extensional flow, thereby improving the mechanical properties with the draw ratio of the composites compared to the matrix alone [34]. For these reasons, applications in

energy devices such as fuel cells, supercapacitors and battery fabrication [35]–[37] or for flexible electrochemical energy storage are well known [38], [39].

Thus, CNTs, GNPs and CB in different application field play a fundamental role in the formulation of composites and nanocomposites in automotive industry, aerospace, military industry, and other applications fields, imparting high performance to the final product thanks to their light weight, hight strength and toughness [40], [41]. Several studies have also been carried out with these different carbon nanofillers, which have different geometric dimensions, showing that hybrid concentrations can effectively inhibit the re-agglomeration/aggregation of fillers, with the creation of a three-dimensional network. These properties allow them to produce advanced multifunctional polymer materials with great mechanical, thermal and electrical stability [26], [42]–[44].

References

[1] B. Dittrich, K.-A. Wartig, D. Hofmann, R. Mülhaupt, and B. Schartel, 'Carbon black, multiwall carbon nanotubes, expanded graphite and functionalized graphene flame retarded polypropylene nanocomposites: GRAPHENE FLAME RETARDED POLYPROPYLNE NANOCOMPOSITES', *Polym. Adv. Technol.*, vol. 24, no. 10, pp. 916–926, Oct. 2013, doi: 10.1002/pat.3165.

[2] L. Bokobza, J.-L. Bruneel, and M. Couzi, 'Raman Spectra of Carbon-Based Materials (from Graphite to Carbon Black) and of Some Silicone Composites', *C*, vol. 1, no. 1, pp. 77–94, Dec. 2015, doi: 10.3390/c1010077.

[3] T. C. Bond and R. W. Bergstrom, 'Light Absorption by Carbonaceous Particles: An Investigative Review', *Aerosol Science and Technology*, vol. 40, no. 1, pp. 27–67, Jan. 2006, doi: 10.1080/02786820500421521.

[4] J. Chen, B. Liu, X. Gao, and D. Xu, 'A review of the interfacial characteristics of polymer nanocomposites containing carbon nanotubes', *RSC Adv.*, vol. 8, no. 49, pp. 28048–28085, 2018, doi: 10.1039/C8RA04205E.

[5] A. Rostami, M. Vahdati, and H. Nazockdast, 'Unraveling the localization behavior of MWCNTs in binary polymer blends using thermodynamics and viscoelastic approaches', *Polym. Compos.*, vol. 39, no. 7, pp. 2356–2367, Jul. 2018, doi: 10.1002/pc.24216.

[6] F. Faridirad, M. Barmar, and S. Ahmadi, 'The effect of MWCNT on dynamic mechanical properties and crystallinity of in situ polymerized polyamide 12 nanocomposite', *Polym Adv Technol*, vol. 29, no. 7, pp. 2134–2146, Jul. 2018, doi: 10.1002/pat.4322.

[7] A. Rostami and M. I. Moosavi, 'High-performance thermoplastic polyurethane nanocomposites induced by hybrid application of functionalized graphene and carbon nanotubes', *J Appl Polym Sci*, vol. 137, no. 14, p. 48520, Apr. 2020, doi: 10.1002/app.48520.

[8] G. Giovinco, S. Sibilia, and A. Maffucci, 'Characterization of the thermal conductivity and diffusivity of graphene nanoplatelets strips: a low-cost technique', *Nanotechnology*, vol. 34, no. 34, p. 345703, Aug. 2023, doi: 10.1088/1361-6528/acd5da.

[9] Y. Fan, G. D. Fowler, and M. Zhao, 'The past, present and future of carbon black as a rubber reinforcing filler – A review', *Journal of Cleaner Production*, vol. 247, p. 119115, Feb. 2020, doi: 10.1016/j.jclepro.2019.119115.

[10] O. Breuer and U. Sundararaj, 'Big returns from small fibers: A review of polymer/carbon nanotube composites', *Polym Compos*, vol. 25, no. 6, pp. 630–645, Dec. 2004, doi: 10.1002/pc.20058.

[11] J. N. Coleman, U. Khan, W. J. Blau, and Y. K. Gun'ko, 'Small but strong: A review of the mechanical properties of carbon nanotube–polymer composites', *Carbon*, vol. 44, no. 9, pp. 1624–1652, Aug. 2006, doi: 10.1016/j.carbon.2006.02.038.

[12] N. T. Dintcheva, R. Arrigo, G. Nasillo, E. Caponetti, and F. P. La Mantia, 'Effect of the nanotube aspect ratio and surface functionalization on the morphology and properties of multiwalled carbon nanotube polyamide-based fibers', *J. Appl. Polym. Sci.*, vol. 129, no. 5, pp. 2479–2489, Sep. 2013, doi: 10.1002/app.38898.

[13] E. Morici, R. Arrigo, R. Teresi, and N. T. Dintcheva, 'Improved carbon nanotubes dispersion through polar dispersant agents in polyamide', presented at the VIII INTERNATIONAL CONFERENCE ON "TIMES OF POLYMERS AND COMPOSITES": From Aerospace to Nanotechnology, Naples, Italy, 2016, p. 020030. doi: 10.1063/1.4949605.

[14] M. Li, W. Tu, X. Chen, H. Wang, and J. Chen, 'NR/SBR composites reinforced with organically functionalized MWCNTs: simultaneous improvement of tensile strength and elongation and enhanced thermal stability', *Journal of Polymer Engineering*, vol. 36, no. 8, pp. 813–818, Oct. 2016, doi: 10.1515/polyeng-2015-0136.

[15] R. Arrigo *et al.*, 'Thermo-oxidative resistant nanocomposites containing novel hybrid-nanoparticles based on natural polyphenol and carbon nanotubes', *Polymer Degradation and Stability*, vol. 115, pp. 129–137, 2015, doi: 10.1016/j.polymdegradstab.2015.02.014.

[16] N. Tz. Dintcheva *et al.*, 'Multi-functional hindered amine light stabilizers-functionalized carbon nanotubes for advanced ultra-high molecular weight

Polyethylene-based nanocomposites', *Composites Part B: Engineering*, vol. 82, pp. 196–204, Dec. 2015, doi: 10.1016/j.compositesb.2015.07.017.

[17] R. Arrigo, E. Morici, and N. T. Dintcheva, 'High-performance thermoplastic elastomers/carbon nanotubes nanocomposites: Mechanical behavior, rheology, and durability', *Polymer Composites*, vol. 38, no. S1, Sep. 2017, doi: 10.1002/pc.23835.

[18] L. G. Pedroni, J. R. Araujo, M. I. Felisberti, and A. F. Nogueira, 'Nanocomposites based on MWCNT and styrene–butadiene–styrene block copolymers: Effect of the preparation method on dispersion and polymer–filler interactions', *Composites Science and Technology*, vol. 72, no. 13, pp. 1487–1492, Aug. 2012, doi: 10.1016/j.compscitech.2012.06.009.

[19] Q. C. Tan, R. A. Shanks, D. Hui, and I. Kong, 'Functionalised graphene-multiwalled carbon nanotube hybrid poly(styrene-b-butadiene-b-styrene) nanocomposites', *Composites Part B: Engineering*, vol. 90, pp. 315–325, Apr. 2016, doi: 10.1016/j.compositesb.2015.12.020.

[20] N. T. Dintcheva *et al.*, 'High performance composites containing perfluoropolyethers-functionalized carbon-based nanoparticles: Rheological behavior and wettability', *Composites Part B: Engineering*, vol. 95, pp. 29–39, Jun. 2016, doi: 10.1016/j.compositesb.2016.03.095.

[21] K. Prashantha, J. Soulestin, M. F. Lacrampe, and P. Krawczak, 'Present Status and Key Challenges of Carbon Nanotubes Reinforced Polyolefins: A Review on Nanocomposites Manufacturing and Performance Issues', *Polymers and Polymer Composites*, vol. 17, no. 4, pp. 205–245, May 2009, doi: 10.1177/096739110901700402.

[22] R. Andrews, D. Jacques, M. Minot, and T. Rantell, 'Fabrication of Carbon Multiwall Nanotube/Polymer Composites by Shear Mixing', *Macromol. Mater. Eng.*, vol. 287, no. 6, p. 395, Jun. 2002, doi: 10.1002/1439-2054(20020601)287:6<395::AID-MAME395>3.0.CO;2-S.

[23] E. Mulazzi *et al.*, 'Optical properties of carbon nanotube-PPVcomposites: influence of the PPV conversion temperature and nanotube concentration', *Synthetic Metals*, vol. 154, no. 1–3, pp. 221–224, Sep. 2005, doi: 10.1016/j.synthmet.2005.07.056.

[24] S. I. Moseenkov, A. V. Zavorin, A. V. Ishchenko, A. N. Serkova, A. G. Selyutin, and V. L. Kuznetsov, 'Using Current-Voltage Characteristics to Control the Structure of Contacts in Polyethylene Based Composites Modified by Multiwalled Carbon Nanotubes', *J Struct Chem*, vol. 61, no. 4, pp. 628–639, Apr. 2020, doi: 10.1134/S0022476620040174.

[25] T. Kuilla, S. Bhadra, D. Yao, N. H. Kim, S. Bose, and J. H. Lee, 'Recent advances in graphene based polymer composites', *Progress in Polymer Science*, vol. 35, no. 11, pp. 1350–1375, Nov. 2010, doi: 10.1016/j.progpolymsci.2010.07.005.

[26] Q. Wang, T. Wang, J. Wang, W. Guo, Z. Qian, and T. Wei, 'Preparation of antistatic high-density polyethylene composites based on synergistic effect of graphene nanoplatelets and multi-walled carbon nanotubes', *Polym Adv Technol*, vol. 29, no. 1, pp. 407–416, Jan. 2018, doi: 10.1002/pat.4129.

[27] S. Wan, J. Peng, L. Jiang, and Q. Cheng, 'Bioinspired Graphene-Based Nanocomposites and Their Application in Flexible Energy Devices', *Adv. Mater.*, vol. 28, no. 36, pp. 7862–7898, Sep. 2016, doi: 10.1002/adma.201601934.

[28] L. Botta, F. P. La Mantia, M. Ceraulo, and M. C. Mistretta, 'Effect of processing temperature and mixing time on the properties of PP/GnP nanocomposites', *Polymer Degradation and Stability*, vol. 181, p. 109321, Nov. 2020, doi: 10.1016/j.polymdegradstab.2020.109321.

[29] X. Zhao, Q. Zhang, D. Chen, and P. Lu, 'Enhanced Mechanical Properties of Graphene-Based Poly(vinyl alcohol) Composites', *Macromolecules*, vol. 43, no. 5, pp. 2357–2363, Mar. 2010, doi: 10.1021/ma902862u.

[30] Y. Li, H. Zhang, H. Porwal, Z. Huang, E. Bilotti, and T. Peijs, 'Mechanical, electrical and thermal properties of in-situ exfoliated graphene/epoxy nanocomposites', *Composites Part A: Applied Science and Manufacturing*, vol. 95, pp. 229–236, Apr. 2017, doi: 10.1016/j.compositesa.2017.01.007.

[31] Y. Liu, J. Lu, and Y. Cui, 'Improved thermal conductivity of epoxy resin by graphene–nickel three-dimensional filler', *Carbon Resources Conversion*, vol. 3, pp. 29–35, 2020, doi: 10.1016/j.crcon.2019.12.003.

[32] M. López-González, A. Flores, F. Marra, G. Ellis, M. Gómez-Fatou, and H. J. Salavagione, 'Graphene and Polyethylene: A Strong Combination Towards Multifunctional Nanocomposites', *Polymers*, vol. 12, no. 9, p. 2094, Sep. 2020, doi: 10.3390/polym12092094.

[33] M. C. Mistretta, L. Botta, A. D. Vinci, M. Ceraulo, and F. P. La Mantia, 'Photo-oxidation of polypropylene/graphene nanoplatelets composites', *Polymer Degradation and Stability*, vol. 160, pp. 35–43, Feb. 2019, doi: 10.1016/j.polymdegradstab.2018.12.003.

[34] F. P. La Mantia, M. Ceraulo, M. C. Mistretta, and L. Botta, 'Effect of the elongational flow on morphology and properties of polypropylene/graphene nanoplatelets nanocomposites', *Polymer Testing*, vol. 71, pp. 10–17, Oct. 2018, doi: 10.1016/j.polymertesting.2018.08.016.

[35] X. Wang and G. Shi, 'Flexible graphene devices related to energy conversion and storage', *Energy Environ. Sci.*, vol. 8, no. 3, pp. 790–823, 2015, doi: 10.1039/C4EE03685A.

[36] N. G. Sahoo, Y. Pan, L. Li, and S. H. Chan, 'Graphene-Based Materials for Energy Conversion', *Adv. Mater.*, vol. 24, no. 30, pp. 4203–4210, Aug. 2012, doi: 10.1002/adma.201104971.

[37] X. Wan, G. Long, L. Huang, and Y. Chen, 'Graphene - A Promising Material for Organic Photovoltaic Cells', *Adv. Mater.*, vol. 23, no. 45, pp. 5342–5358, Dec. 2011, doi: 10.1002/adma.201102735.

[38] C. Xu, B. Xu, Y. Gu, Z. Xiong, J. Sun, and X. S. Zhao, 'Graphene-based electrodes for electrochemical energy storage', *Energy Environ. Sci.*, vol. 6, no. 5, p. 1388, 2013, doi: 10.1039/c3ee23870a.

[39] M. Mao, J. Hu, and H. Liu, 'Graphene-based materials for flexible electrochemical energy storage: Flexible graphene energy storage', *Int. J. Energy Res.*, vol. 39, no. 6, pp. 727–740, May 2015, doi: 10.1002/er.3256.

[40] G. D. Goh, W. Toh, Y. L. Yap, T. Y. Ng, and W. Y. Yeong, 'Additively manufactured continuous carbon fiber-reinforced thermoplastic for topology optimized unmanned aerial vehicle structures', *Composites Part B:*

Engineering, vol. 216, p. 108840, Jul. 2021, doi: 10.1016/j.compositesb.2021.108840.

[41] A. Pearson *et al.*, 'Role of interfacial adhesion and fiber length on the mechanical performance fiber reinforced thermoplastic elastomers', *Composites Science and Technology*, vol. 213, p. 108928, Sep. 2021, doi: 10.1016/j.compscitech.2021.108928.

[42] M. Wegrzyn, A. Ortega, A. Benedito, and E. Gimenez, 'Thermal and electrical conductivity of melt mixed polycarbonate hybrid composites co-filled with multi-walled carbon nanotubes and graphene nanoplatelets', *J. Appl. Polym. Sci.*, vol. 132, no. 37, p. n/a-n/a, Oct. 2015, doi: 10.1002/app.42536.

[43] N. Bagotia, V. Choudhary, and D. K. Sharma, 'A review on the mechanical, electrical and EMI shielding properties of carbon nanotubes and graphene reinforced polycarbonate nanocomposites', *Polym Adv Technol*, vol. 29, no. 6, pp. 1547–1567, Jun. 2018, doi: 10.1002/pat.4277.

[44] G. Infurna, P. F. Teixeira, N. T. Dintcheva, L. Hilliou, F. P. La Mantia, and J. A. Covas, 'Taking advantage of the functional synergism between carbon nanotubes and graphene nanoplatelets to obtain polypropylene-based nanocomposites with enhanced oxidative resistance', *European Polymer Journal*, vol. 133, Jun. 2020, doi: 10.1016/j.eurpolymj.2020.109796.

1.4. Biochar particles

1.4.1. Characteristics and properties

Biochar (BC) is a carbon-rich material, widely employed in environmental applications such as soil remediation, carbon sequestration, water treatment, and wastewater treatment because of its unique properties, such as high surface area, recalcitrant, and catalysis [1]–[3], and it is undoubtedly a way of recovering waste at the end of its life and giving it new added value. Nowadays Biochar has attracted interest as a filler for polymer [4]–[8] and biopolymer [9]–[12] composites due to the fact that it is characterised by a high amount of aromatic carbon atoms and condensed aromatic structure, in different forms, including graphite. It also contains hydrogen, oxygen, nitrogen, sulphur, calcium and silica, the ratio of which to carbon is highly dependent on the type of biomass used and the thermal decomposition conditions.

Biochar can be produced from a variety of waste feedstocks, either as a primary product or as a by-product for energy recovery. Municipal solid waste and agricultural waste are just two examples of the many organic wastes that can be used as feedstocks for biochar production. Common wastes such as sewage sludge and agricultural waste are produced in large quantities around the world, for sludge production alone, it reached 6.25 million tonnes in China in 2013 [13]. Sludge is a solid waste that must be treated and disposed of as it is produced during the wastewater treatment process. However, because it is rich in carbon and nutrients such as ammonia, it is a viable feedstock for biochar synthesis [14].

Converting common household wastes to biochar could be an option for environmental sustainability. Different feedstock has different proportions of element composition, and thus exhibits different properties, so the biochar derived

from different feedstocks has various performances. How to deal with these wastes is directly link to the impact they have on the environment.

Table 2 Proximate analysis of different biomass raw materials and relative elemental composition after pyrolysis process [15]

Feedstock	Proximate Analysis			Elemental Analysis			
	Volatile Matter [wt.%]	**Fixed Carbon [wt.%]**	**Ash [wt.%]**	**C [wt.%]**	**H [wt.%]**	**N [wt.%]**	**O [wt.%]**
Alfalfa [16] (*Medicago sativa)*	78.90	15.80	5.30	49.90	6.30	2.80	40.80
Almond Shell[17]	74.90	21.80	3.30	50.30	6.20	1.00	42.50
Bagasse [18]	71.00	13.70	2.10	51.71	5.32	0.33	42.64
Bamboo[19]	81.60	17.50	0.90	52.00	5.10	0.40	42.50
Carob Waste[20], [21]	38.80	52.80	3.80	46.94	1.63	5.44	-
Coconut Fiber[22]	80.85	11.10	8.05	47.75	5.61	0.90	45.51
Corncob [23]	69.50	15.90	2.90	48.12	6.48	-	43.51
Cornstalk [23]	65.30	15.60	11.70	46.21	6.01	-	45.87
Cocopeat [18]	49.10	25.30	4.60	61.57	4.37	1.02	33.04
Dead Eucalyptus leaves [24]	77.60	16.90	0.80	52.90	8.10	0.30	47.90
Hamlin citrus [16]	77.90	17.80	9.40	50.70	6.60	1.60	42.90
Hornbeem Shell[25]	78.83	9.37	9.52	41.78	5.36	0.60	52.26
Loblolly Pine [16] (*Pinus taeda)*	77.60	14.50	2.30	55.50	5.60	0.40	45.90
Maize straw [26]	-	-	5.31	42.20	7.21	1.28	49.20
Mesocarp fibre[24] (*Oil palm*)	72.80	18.90	8.30	51.50	6.60	1.50	40.10
Oak sawdust [27]	69.24	16.51	0.81	52.28	5.74	0.06	41.92
Olive wood [28]	79.60	17.20	3.20	49.00	5.40	0.70	44.90
Paddy straw [18]	56.40	15.40	20.90	48.75	5.98	1.99	43.28
Pinewood [22]	85.45	13.15	1.40	48.15	6.70	1.35	43.60
Palm Kernel Shell[18]	66.80	17.90	3.40	55.82	5.62	0.84	37.73
Raw Pine sawdust [26]	83.10	16.80	3.76	50.60	6.18	0.05	43.10
Rice husk	62.80	19.20	18.00	49.30	6.10	0.80	43.70
Sawdust [23]	70.40	18.50	1.20	48.37	4.98	-	46.27
Tea waste [29]	70.29	18.57	3.88	48.60	5.43	3.80	42.17
Wood Stem [18]	80.10	10.70	0.40	50.52	5.81	0.23	43.44
Wood Bark [18]	68.90	16.30	4.90	53.42	6.12	1.40	39.06

In summary, the type of feedstock has a significant effect on the physicochemical properties of biochar [30], the carbon content in biochar is an important parameter,

and depending on the type of feedstock, different thermal processes discussed previously could be used to optimise it to the desired product yield.
Due to different composition (carbon with presence of alkali metals *e.g.* Li, Na, and K or alkaline metals *e.g.* Ca, Mg and Ba metals) depending on the nature of feedstock, biochar could have versatile properties leading to many applications: bioenergy (co-gasification co-firing and combustion), chemical field (as a catalyst or catalyst support), agronomy (as water retention, plant nutrients or soil conditioner), pharmacy field (as adsorption of drugs and toxins), environment remediation (as carbon sequestration and sorption of pollutants) and biomaterials for production of biocomposites, fuel cells and photovoltaic plants [31].

1.4.2. How to tailor Biochar properties with Pyrolysis Operative Condition

The temperature employed, together with the heating rate, pressure and residence time, determines the type of plant required for biomass conversion and the preferred products of the thermal decomposition section. Slow pyrolysis is characterized by slow heating rates and long residence times at atmospheric pressure, with operating temperatures varying from 350 to 800°C; the energy required for pyrolysis of the feed is usually provided internally by combustion of a portion of the feed. The main product is a high-carbon solid char, and the co-products are an aqueous, low-molecular-weight liquid and a low-energy combustible gas [32]–[34]. Fast pyrolysis is carried out at temperatures between 400 and 600 °C. In contrast to slow pyrolysis, it uses a very high heating rate in a vacuum atmosphere, a short residence time and rapid quenching of the vapour, as the main aim of this process is to produce bio-oil [32], [35], [36]. Flash pyrolysis is a batch process with an operating temperature range between 300 and 800 °C and is similar to slow pyrolysis, but with a high heating rate, using moderate pressure (between 2 and 25 atm) to condense volatile

elements and promote secondary formation, since the aim of this process is to produce a liquid biocarbon fraction or a solid phase of biochar [37]. Torrefaction is a slow pyrolysis process with a lower temperature range, between 200 and 300 °C, which removes mainly water and some volatile compounds from the biomass to produce a "brown" char that is easy to grind. This is a stabilised and friable biomass. Gasification is characterised by a high process temperature (between 750 and 1800°C) with limited and controlled oxygen concentration (usually calculated relative to stoichiometric combustion) [38] and/or steam [39]. As the name suggests, the primary products are a non-condensable gas mixture, called syngas, which is essentially composed by the presence of CO, H2, with a smaller amount of carbon dioxide, methane and other low molecular weight hydrocarbons [40].

From this perspective, the yield of products such as biochar is primarily determined by the influence of the operating conditions and the temperature used in the thermal degradation process. For the same type of feedstock, the yield of biochar decreases as the pyrolysis temperature increases. The results reported by Chen *et al.* [19] of the slow pyrolysis of bamboo carried out at different temperatures (from 300 to 700 °C) showed how the biochar yield decreases from 49.3% when the pyrolysis was carried out at 300 °C to 23.6% when it was carried out at 700 °C. Instead, the co-products increase: the yield of bio-oil increases from 26.5% to 34.1%, and the yield of non-condensable gases increases from 23.2% to 42.3%. For corncob biochar obtained at different pyrolysis temperatures, ranging from 300 to 600 °C, the biochar yield decreases from 77.3% to 21.7% [23]. The yield of BCs was almost reduced from 37% to 22% for soybean- and peanut- shell derived biochar obtained by pyrolysis at 300 and 700°C [41]. Similarly, when pyrolysis temperatures were increased, biochar yields decreased for several type of feedstock: hickory and hamlin citrus [16], [22], [42] for sewage sludge [43] the residual wastes after palm oi extraction [44], residual shell of carob fruit after sugar extraction [21] woody fraction of mallee eucalyptus loxophleba [45], wheat straw and oat straw [46], pineapple peel [47] douglas fir wood, douglas fir bark, and hybrid poplar wood[30]. For lignocellulosic feedstocks,

the low pyrolysis temperature determines minimal condensation of aliphatic compounds and lower losses of CH_4, H_2 and CO. Above a certain temperature, which depends on the nature of the lignocellulosic feedstock, the yield decreases significantly due to dehydration of hydroxyl groups and thermal degradation of lignocellulosic structures [48], [49]. For the same reasons, also in the fast pyrolysis regime, which implies a higher heating rate, a study of the effect of operating conditions, such as temperature, on pine wood-derived biochar was carried out. In terms of biochar yield as a function of temperature, the trend remains unchanged; in fact, a decrease from about 0.42 kg/kg dry biomass (obtained by fast pyrolysis at 325 °C) to about 0.11 kg/kg dry biomass (obtained by fast pyrolysis at 575 °C) was shown, with a decrease curve that shows an exponential decrease [50].

Proximate analysis is a useful analysis carried out on feedstock to determine the suitability of the feedstock for conversion to biogas, biofuel or biochar, as it provides information on the fixed carbon, volatile matters and ash in the feedstock [51]. The fixed carbon represents the solid carbon in the biomass that is expected to remain in the char after devolatilisation in the pyrolysis process [52].

At the same time, proximate analysis could be a great resource for characterising the biochar after the pyrolysis process, as the fixed carbon of the char represents the material that remains after the volatiles have been driven off [53], and this data is certainly highly dependent on the process temperature. Proximate analysis can be used also to understand the amount of residual volatiles in biochar samples, which are the product of insufficient thermal degradation during the pyrolysis process. Thus, as the process temperature increase as volatile matter decrease and fixed carbon increase. Moreover, due to the accumulation of mineral components resulting from the decomposition of organic constituents, the ash content of biochar increased with increasing production temperature. Several studies confirm these trends in fixed carbon, volatile matter and ash contents a function of pyrolysis temperature. Chen *et al.* [19] pyrolysed Bamboo from 300 to 700 °C, and performed proximate analysis on resulting biochar showing that volatile matters decrease as the increases

of temperature: from 30% at 300°C to 9% at 700°C, and the relative fixed carbon increase from 65% at 300°C to 86% at 700°C. The same trend has been reported by proximate analysis of resulting biochar derived from pyrolysis of soybean stover and peanut shell [41] corn cob [23], cocoa pods waste coming from cocoa industry, and resulting digestate of cocoa pods for biogas production [54], coconut fiber and pine wood [22] wood hybrid poplar (*Populous deltoids*) and Douglas fir *(Pseudotsuga Menziessii*) wood and bark [30].

An important parameter of biochar is its elemental composition: total carbon, nitrogen and hydrogen in biochar samples, and in some study sulphur, are often analysed with a CHN elemental analyser and oxygen content is often obtained as the weight difference between raw biochar and sum of C, H, N and non-volatile elements. C, H, N and O are elements that are really sensitive to pyrolysis temperature unlike non-volatile and inorganic elements whose total content depends more on the nature of the pyrolysed feedstock. In particular, as the pyrolysis temperature increased, the biochar became richer in carbon, while the oxygen and hydrogen contents decreased. The ratios of hydrogen to carbon (H/C) and oxygen to carbon (O/C), which are considered pyrolysis indicators, can be calculated as a ratio of the amount of carbon, hydrogen and oxygen, respectively. In fact, there is a correlation between these two ratios and the chemical structure of the resulting biochar. In fact, as hydrogen or oxygen decreases relative to the feedstock and relative to the total carbon content, the formation of aromatic structures occurs, as well as the condensation of carbon atoms through the loss of O-containing functional groups. As mentioned earlier, if biochar became richer in carbon while the oxygen and hydrogen contents decreased with increasing temperature, it follows that the H/C and O/C ratios decrease with increasing pyrolysis temperature. Thus, at a higher temperature, the biochar gradually became richer in carbon with an aromatic structure. This results are largely confirmed by the experimental study present in the literature and for several type of biomass, woody and non woody waste: moso bamboo [19], corn-cob, sawdust and cornstalk [23], soybean stover and peanut shells

[41], loblolly pine, citrus, alfalfa, and switchgrass [16], pine wood and coconut fiber [22], hickory wood, bagasse and bamboo [42], peanut hull, pecan shell, poulty litter and switchgrass [48], carob waste [20], wood apple shells [55], cassava rhizome, durian peel and pineapple peel [56], wood [57], cocoa pods waste coming from cocoa industry, and resulting digestate of cocoa pods for biogas production [54], palm waste [1], pine needle [58] and others [59]–[72]. The H/C and O/C ratios decrease as the pyrolysis temperature increases, regardless of the variation in heating rate and thus, in a sense, the type of pyrolysis used (slow or fast). In fact, Amine Hmid *et al.* have shown that pyrolysis of olive mill waste at pyrolysis temperatures of 430, 480 and 530 °C at different heating rates (i.e. 25, 35 and 45 °C/min) results in an increase in carbon content and a decrease in oxygen and hydrogen content with increasing pyrolysis temperature [28]. Likewise, Onay fast pyrolysed safflower seeds for biochar production at pyrolysis temperatures of 400, 600 and 700 °C at much higher heating rates (*i.e.* 100, 300 and 800 °C/min), confirming the same carbon, hydrogen and oxygen content trends as previously shown [73].

Considering how the variation in elemental composition contributes to the variation in biochar chemical structure as pyrolysis temperature varies, complex molecular chains (such as cellulose, lignin and hemicellulose) are transformed into very different chemical structures, with the appearance or disappearance of functional groups on the biochar surface, strictly dependent on pyrolysis temperature. In fact, functional groups typical of oxygenated hydrocarbons, reflecting the carbohydrate structure of cellulose and hemicelluloses, dominate the FT-IR spectra of biochar. Pyrolysis can cause absorption bands characteristic of raw materials to disappear and new bands typical of biochar samples to appear. A typical FT-IR spectra is normally composed by: a broad band from 3000-3600 cm^{-1} attributed to the presence of OH functional groups (alcoholic and phenolic) [74], [75], a smaller band from 2700 to 3000 cm^{-1}, attributed to alkyl C–H stretching [76], a band at 1600 cm^{-1} attributed to aromatic C–C and C–O stretching of conjugated ketones and quinones [55], a band occurring at 1735 cm^{-1} attributed to C=O stretching of ketones, aldehydes and esters

[78], [79], a band centered at 1238 cm^{-1} attributed to the presence of C–O–C groups and aryl ethers, phenolic associated with lignin [80], a band at 1130 cm^{-1} attributed to of C–O–C stretching of ester groups in cellulose and hemicelluloses [76]. When heated to a high temperature, the chemical bonds are broken and rearranged and new functional groups are formed, which it is possible to distinguish as acidic (*i.e.* carboxyl, carbonyl, lacton, phenol, pyrone, ether, anhydride) and basic groups (*i.e.* pyridine, pyridine, pyrrole) [81]. Suliman *et al.* showed how the increase of pyrolysis temperature of three different biomass, determines a linear decrease in the content of oxygenated functional groups (*i.e.* phenolic, lactone and carboxylic group) and a reverse trend for the total basic surface functional groups [30]. All of these functional group are present on outer surface of biochar and on its pore [82]–[85]. Biochar produced at low temperature displays more of this functional groups due to the retainment of aliphatic and cellulose structure [48], [76], higher temperature leads to dehydration and deoxidation of the biomass with a consequent high hydrophobic nature with well-organized C layers [78], [86]. In particular, the band related to the -OH stretching due to hydrogen-bonded hydroxyl groups (3200-3500 cm^{-1}) is the first to disappear with increasing pyrolysis temperature for biomass-derived biochar. Then the asymmetric (2935 cm^{-1}) and symmetric (2885 cm^{-1}) CH stretching of aliphatic functional groups decreases and then disappears, as does the symmetric C-O stretching (1030 and 1110 cm^{-1}). Instead, for the carboxylic acid C=O (1700-1740 cm^{-1}), the aromatic C=C stretching of conjugated ketones and quinones (1600 cm^{-1}) first increases and then decreases with the increase of the pyrolysis temperature. As the temperature increases, the CH bending for aromatic out-of-plane deformation (750, 815 and 885 cm^{-1}) becomes more prominent, reaching a spectrum at the highest temperature that could be related to that of pure graphite [57], [64], [80], [87]–[89]. The pH of biochar depends firstly on the pH of the biomass feedstock. However, biochar is generally alkaline or has a higher pH than the starting biomass. The alkaline nature of biochar can be attributed to two factors: *(i)* the acidic functional groups, such as carboxyl, hydroxyl or formyl groups, in the biomass are stripped off

during pyrolysis and (ii) the pyrolysis process led to an increase in the concentration of metals (present as ash). Liu *et al.* [23] pyrolysed corncob at 300 400 500 and 600°C, founding that corncob pH results slightly acid and equal to 6.4, but already pyrolyzing at 300°C pH results equal to 8.1, and at high temperature equal to 10.4. Organic functional groups and inorganic alkali influenced the alkalinity of biochar. The contribution of inorganic alkali such as Na and K became significant at temperatures above 500 °C, whereas the contribution of organic functional groups decreased with increasing pyrolysis temperature as thermal decomposition progressed [18]. As noted above, as the pyrolysis temperature increases, the functional group concentration of the biochar surface decreases and the ash content increases. It follows, that pH increases with pyrolysis temperature, tending to be more alkaline, and this result is well documented in the literature [30], [41], [42], [48], [65], [67], [90].

The surface area of the biochar is one of the key characteristics that can greatly influence its behaviour, helping to absorb chemical compound, affecting its reactivity and the combustion characteristics of the biochar. It is a parameter that depends on the nature of the feedstock, since a complex lignocellulosic structure already has a high surface area with a relative high pore volume, and on the temperature used in the pyrolysis process. The devolatilisation step promoted pyrolysis process, seems to be responsible on the formation of pores [16]. By increasing the driving force of the devolatilisation process, the increase in pyrolysis temperature changes the morphology of the char particles. The higher temperature causes a rapid release of volatiles during pyrolysis, this leads to an internal overpressure which causes smaller pores to merge. This merging process results in the formation of large internal voids with a porous biochar structure, hence, the macroporosity increases with increasing temperature [23], [41], [42], [64], [88]. A higher temperature pyrolysis creates also a porous structure due to several cracks and holes generated by the releasing of volatile matter [91]. Sizirici *et al.* shown a BET surface area that increase from 1.1 $m^2 g^{-1}$ and 3.5 $m^2 g^{-1}$ of frond and leaf respectively

of palme waste pyrolysed at 400°C to 246 $m^2\ g^{-1}$ and 289 $m^2\ g^{-1}$ pyrolysing them at 600°C [1]. The orange peels derived biochar shown a surface area of 22.8 $m^2\ g^{-1}$ when pyrolysed at 150 °C, and of 201 $m^2\ g^{-1}$ when pyrolysed at 700°C [61]. A complete characterization of pore structure and surface area done by Tsai *et al.* [47], correlated the pore structure on their adsorption-desorption isotherms, showing a coexistence of microporous and mesoporous in biochar structure, and their value increases as the increases of pyrolysis temperature and of residence time. In contrast, fast pyrolysis with higher heating rates results in faster devolatilization step that affects the resulting morphology of the biochar. Onay *et al.* [73] that pyrolysed at heating rate of 100, 300 and 800 °C/min, at three different temperatures, *i.e.* 400, 600 and 800 °C, shown low values of surface area at every heating rate and pyrolysis temperature, and for all heating rates the surface area firstly slightly increases, then it decreases as the increase of pyrolysis temperatures. The decrease in surface area value observed at high temperature is due to structural ordering and the decrease in the number of micropores and increase in macropores due to the evolution of volatile bubbles at higher devolatilization rates.

Another important parameter affected by the pyrolysis temperature is the high heating value (HHV), which is defined as the energy released per unit mass or volume of fuel when the fuel is completely burnt. In the case of solid fuels, such as biochar, this is referred to unit mass. There are two methods of assessing HHV, the first is experimental and is carried out using bomb calorimeters, the second is theoretical and uses elemental composition for the calculation. Since elemental composition is known to be affected by pyrolysis temperature, this property is again dependent on pyrolysis temperature. Generally, the theoretical methos employed for HHV calculation are based on Dulong' s formula [92] and its modification after experimental data fitting [63], [93] are summarize in the following relation:

$$HHV = aC_{wt.\%} + bH_{wt.\%} + cO_{wt.\%} + dS_{wt.\%} + eN_{wt.\%} + fA_{wt.\%}$$

C, H, O, N, S, and A represents carbon, hydrogen, oxygen, nitrogen, sulphur and ash, respectively, and the coefficients depend on the nature of the fuel. From an experimental point of view, Azargohar *et al.* [67] found that for biochars produced from wheat straw and flax straw, the heating value increased by an increase in the pyrolysis temperature, while for biochars derived from sawdust and poultry litter no trends has been found. This maybe due to a decrease in the oxygen content by pyrolysis temperature for the first two raw materials, differently to the others. Again the highest value of HHV has been correlated to the lower oxygen content and lower H/C ratio when canola meal has been pyrolysed at different temperature [62].

The HHVs of biochars prepared at 300, 400, 500, 600, and 700 °C were 25.9, 29.8, 27.4, 26.1, and 27.2 MJ/kg, respectively. These data show that the biochar produced at a pyrolysis temperature of 400 °C had the largest HHV and that the maximum difference between HHVs was 15%. The larger HHVs of biochars relative the parent biomass (20.1 MJ/kg) were expected on the basis of the lower oxygen content and H/ C ratio for the biochars relative to canola meal (see Table 1). The energy recovery of biochar is defined as the percent energy content (yield × HHV) of biochar relative to that for a unit mass of canola meal. The energy recovery of biochar decreased from 64.9 to 43.0% with increasing temperature from 300 to 700 °C. The decrease in the energy recovery of biochar with pyrolysis temperature is due to the decrease in biochar yield with increasing pyrolysis temperature and the narrow range of biochar HHVs (25.9−29.8 MJ/kg). Other studies demonstrates how as the increase of pyrolysis temperature, the decrease of H and O content in synergy with the increase of carbon content increases the HHV values [19], [21], [22], [28], [63]. However, it has been reported that the ash content increases as the pyrolysis temperature increases. The contribution of ash to the HHV is contradictory to the increase in carbon content. In fact, as the ash contribution increases, the HHV decreases. In some study the ash content results predominant, decreasing strongly the HHV value [43]. In another study, as the pyrolysis temperature is increased, first

the contribution of carbon is predominant, thus HHV increases its value, then the amount of ash determines the decrease of HHV [65].

Reference

[1] B. Sizirici, Y. H. Fseha, I. Yildiz, T. Delclos, and A. Khaleel, 'The effect of pyrolysis temperature and feedstock on date palm waste derived biochar to remove single and multi-metals in aqueous solutions', *Sustainable Environment Research*, vol. 31, no. 1, Dec. 2021, doi: 10.1186/s42834-021-00083-x.

[2] A. Tomczyk, Z. Sokołowska, and P. Boguta, 'Biochar physicochemical properties: pyrolysis temperature and feedstock kind effects', *Reviews in Environmental Science and Biotechnology*, vol. 19, no. 1, pp. 191–215, Mar. 2020, doi: 10.1007/s11157-020-09523-3.

[3] E. W. Bruun, P. Ambus, H. Egsgaard, and H. Hauggaard-Nielsen, 'Effects of slow and fast pyrolysis biochar on soil C and N turnover dynamics', *Soil Biology and Biochemistry*, vol. 46, pp. 73–79, Mar. 2012, doi: 10.1016/j.soilbio.2011.11.019.

[4] R. Arrigo, P. Jagdale, M. Bartoli, A. Tagliaferro, and G. Malucelli, 'Structure-property relationships in polyethylene-based composites filled with biochar derived from waste coffee grounds', *Polymers*, vol. 11, no. 8, Aug. 2019, doi: 10.3390/polym11081336.

[5] C. Gheorghe-Bulmau, A. Volceanov, I. Stanciulescu, G. Ionescu, C. Marculescu, and M. Radoiu, 'Production and properties assessment of biochars from rapeseed and poplar waste biomass for environmental applications in Romania', *Environmental Geochemistry and Health*, 2021, doi: 10.1007/s10653-021-01061-3.

[6] O. Das, N. K. Kim, A. L. Kalamkarov, A. K. Sarmah, and D. Bhattacharyya, 'Biochar to the rescue: Balancing the fire performance and mechanical properties of polypropylene composites', *Polymer Degradation and Stability*, vol. 144, pp. 485–496, Oct. 2017, doi: 10.1016/j.polymdegradstab.2017.09.006.

[7] M. Giorcelli, A. Khan, N. M. Pugno, C. Rosso, and A. Tagliaferro, 'Biochar as a cheap and environmental friendly filler able to improve polymer mechanical

properties', *Biomass and Bioenergy*, vol. 120, pp. 219–223, Jan. 2019, doi: 10.1016/j.biombioe.2018.11.036.

[8] O. Das, D. Bhattacharyya, D. Hui, and K. T. Lau, 'Mechanical and flammability characterisations of biochar/polypropylene biocomposites', *Composites Part B: Engineering*, vol. 106, pp. 120–128, Dec. 2016, doi: 10.1016/j.compositesb.2016.09.020.

[9] J. George, L. B. Azad, A. M. Poulose, Y. An, and A. K. Sarmah, 'Nano-mechanical behaviour of biochar-starch polymer composite: Investigation through advanced dynamic atomic force microscopy', *Composites Part A: Applied Science and Manufacturing*, vol. 124, Sep. 2019, doi: 10.1016/j.compositesa.2019.105486.

[10] T. Haeldermans *et al.*, 'Bio-Based Poly(3-hydroxybutyrate)/Thermoplastic Starch Composites as a Host Matrix for Biochar Fillers', *Journal of Polymers and the Environment*, vol. 29, no. 8, pp. 2478–2491, Aug. 2021, doi: 10.1007/s10924-021-02049-x.

[11] T. Haeldermans *et al.*, 'Poly(Lactic acid) bio-composites containing biochar particles: Effects of fillers and plasticizer on crystallization and thermal properties', *Express Polymer Letters*, vol. 15, no. 4, pp. 343–360, 2021, doi: 10.3144/expresspolymlett.2021.30.

[12] R. Arrigo, M. Bartoli, and G. Malucelli, 'Poly(lactic Acid)-biochar biocomposites: Effect of processing and filler content on rheological, thermal, and mechanical properties', *Polymers*, vol. 12, no. 4, Apr. 2020, doi: 10.3390/POLYM12040892.

[13] G. Yang, G. Zhang, and H. Wang, 'Current state of sludge production, management, treatment and disposal in China', *Water Research*, vol. 78, pp. 60–73, Jul. 2015, doi: 10.1016/j.watres.2015.04.002.

[14] A. Sepehri and M.-H. Sarrafzadeh, 'Effect of nitrifiers community on fouling mitigation and nitrification efficiency in a membrane bioreactor', *Chemical Engineering and Processing - Process Intensification*, vol. 128, pp. 10–18, Jun. 2018, doi: 10.1016/j.cep.2018.04.006.

[15] G. Infurna, G. Caruso, and N. Tz. Dintcheva, 'Sustainable Materials Containing Biochar Particles: A Review', *Polymers*, vol. 15, no. 2, p. 343, Jan. 2023, doi: 10.3390/polym15020343.

[16] S. Wang *et al.*, 'Physicochemical and sorptive properties of biochars derived from woody and herbaceous biomass', *Chemosphere*, vol. 134, pp. 257–262, Sep. 2015, doi: 10.1016/j.chemosphere.2015.04.062.

[17] A. Elleuch, A. Boussetta, J. Yu, K. Halouani, and Y. Li, 'Experimental investigation of direct carbon fuel cell fueled by almond shell biochar: Part I. Physico-chemical characterization of the biochar fuel and cell performance examination', *International Journal of Hydrogen Energy*, vol. 38, no. 36, pp. 16590–16604, Dec. 2013, doi: 10.1016/j.ijhydene.2013.08.090.

[18] Y. Lee *et al.*, 'Comparison of biochar properties from biomass residues produced by slow pyrolysis at 500°C', *Bioresource Technology*, vol. 148, pp. 196–201, Nov. 2013, doi: 10.1016/j.biortech.2013.08.135.

[19] D. Chen, D. Liu, H. Zhang, Y. Chen, and Q. Li, 'Bamboo pyrolysis using TG–FTIR and a lab-scale reactor: Analysis of pyrolysis behavior, product properties, and carbon and energy yields', *Fuel*, vol. 148, pp. 79–86, May 2015, doi: 10.1016/j.fuel.2015.01.092.

[20] G. Infurna *et al.*, 'Biochar Particles Obtained from Agricultural Carob Waste as a Suitable Filler for Sustainable Biocomposite Formulations', *Polymers*, vol. 14, no. 15, p. 3075, Jul. 2022, doi: 10.3390/polym14153075.

[21] M. Maniscalco, G. Infurna, G. Caputo, L. Botta, and N. T. Dintcheva, 'Slow pyrolysis as a method for biochar production from carob waste: Process investigation and products' characterization', *Energies*, vol. 14, no. 24, Dec. 2021, doi: 10.3390/en14248457.

[22] Z. Liu and G. Han, 'Production of solid fuel biochar from waste biomass by low temperature pyrolysis', *Fuel*, vol. 158, pp. 159–165, Oct. 2015, doi: 10.1016/j.fuel.2015.05.032.

[23] X. Liu, Y. Zhang, Z. Li, R. Feng, and Y. Zhang, 'Characterization of corncob-derived biochar and pyrolysis kinetics in comparison with corn stalk and

sawdust', *Bioresource Technology*, vol. 170, pp. 76–82, Oct. 2014, doi: 10.1016/j.biortech.2014.07.077.

[24] N. Jafri, W. Y. Wong, V. Doshi, L. W. Yoon, and K. H. Cheah, 'A review on production and characterization of biochars for application in direct carbon fuel cells', *Process Safety and Environmental Protection*, vol. 118, pp. 152–166, Aug. 2018, doi: 10.1016/j.psep.2018.06.036.

[25] U. Moralı and S. Şensöz, 'Pyrolysis of hornbeam shell (Carpinus betulus L.) in a fixed bed reactor: Characterization of bio-oil and bio-char', *Fuel*, vol. 150, pp. 672–678, Jun. 2015, doi: 10.1016/j.fuel.2015.02.095.

[26] L. Luo, C. Xu, Z. Chen, and S. Zhang, 'Properties of biomass-derived biochars: Combined effects of operating conditions and biomass types', *Bioresource Technology*, vol. 192, pp. 83–89, Sep. 2015, doi: 10.1016/j.biortech.2015.05.054.

[27] J. Zhang, Z. Zhong, J. Zhao, M. Yang, W. Li, and H. Zhang, 'Study on the preparation of activated carbon for direct carbon fuel cell with oak sawdust', *Can. J. Chem. Eng.*, vol. 90, no. 3, pp. 762–768, Jun. 2012, doi: 10.1002/cjce.20549.

[28] A. Hmid, D. Mondelli, S. Fiore, F. P. Fanizzi, Z. Al Chami, and S. Dumontet, 'Production and characterization of biochar from three-phase olive mill waste through slow pyrolysis', *Biomass and Bioenergy*, vol. 71, pp. 330–339, Dec. 2014, doi: 10.1016/j.biombioe.2014.09.024.

[29] B. B. Uzun, E. Apaydin-Varol, F. Ateş, N. Özbay, and A. E. Pütün, 'Synthetic fuel production from tea waste: Characterisation of bio-oil and bio-char', *Fuel*, vol. 89, no. 1, pp. 176–184, Jan. 2010, doi: 10.1016/j.fuel.2009.08.040.

[30] W. Suliman, J. B. Harsh, N. I. Abu-Lail, A.-M. Fortuna, I. Dallmeyer, and M. Garcia-Perez, 'Influence of feedstock source and pyrolysis temperature on biochar bulk and surface properties', *Biomass and Bioenergy*, vol. 84, pp. 37–48, Jan. 2016, doi: 10.1016/j.biombioe.2015.11.010.

[31] S. Nanda, A. K. Dalai, F. Berruti, and J. A. Kozinski, 'Biochar as an Exceptional Bioresource for Energy, Agronomy, Carbon Sequestration,

Activated Carbon and Specialty Materials', *Waste Biomass Valor*, vol. 7, no. 2, pp. 201–235, Apr. 2016, doi: 10.1007/s12649-015-9459-z.

[32] S. Al Arni, 'Comparison of slow and fast pyrolysis for converting biomass into fuel', *Renewable Energy*, vol. 124, pp. 197–201, Aug. 2018, doi: 10.1016/j.renene.2017.04.060.

[33] M. Volpe, D. Panno, R. Volpe, and A. Messineo, 'Upgrade of citrus waste as a biofuel via slow pyrolysis', *Journal of Analytical and Applied Pyrolysis*, vol. 115, pp. 66–76, Sep. 2015, doi: 10.1016/j.jaap.2015.06.015.

[34] D. R. Vardon *et al.*, 'Complete utilization of spent coffee grounds to produce biodiesel, bio-oil, and biochar', *ACS Sustainable Chemistry and Engineering*, vol. 1, no. 10, pp. 1286–1294, Oct. 2013, doi: 10.1021/sc400145w.

[35] R. Palos, E. Rodríguez, A. Gutiérrez, J. Bilbao, and J. M. Arandes, 'Cracking of plastic pyrolysis oil over FCC equilibrium catalysts to produce fuels: Kinetic modeling', *Fuel*, vol. 316, p. 123341, May 2022, doi: 10.1016/j.fuel.2022.123341.

[36] J. K. Sarkar and Q. Wang, 'Different pyrolysis process conditions of South Asian waste coconut shell and characterization of gas, bio-char, and bio-oil', *Energies*, vol. 13, no. 8, Apr. 2020, doi: 10.3390/en13081970.

[37] M. J. Antal, S. G. Allen, X. Dai, B. Shimizu, M. S. Tam, and M. Grønli, 'Attainment of the theoretical yield of carbon from biomass', *Industrial and Engineering Chemistry Research*, vol. 39, no. 11, pp. 4024–4031, 2000, doi: 10.1021/ie000511u.

[38] C. Guizani *et al.*, 'Influence of temperature and particle size on the single and mixed atmosphere gasification of biomass char with H2O and CO2 Influence of temperature and particle size on the single and mixed atmosphere gasification of biomass char with H 2 O and CO 2', *Fuel Processing Technology*, vol. 134, pp. 175–188, 2015, doi: 10.1016/j.fuproc.2015.01.031ï.

[39] D. Barisano *et al.*, 'Investigation of an Intensified Thermo-Chemical Experimental Set-Up for Hydrogen Production from Biomass: Gasification Process Integrated to a Portable Purification System—Part II', *Energies*, vol. 15, no. 13, Jul. 2022, doi: 10.3390/en15134580.

[40] R. W. Breault, 'Gasification processes old and new: A basic review of the major technologies', *Energies*, vol. 3, no. 2, pp. 216–240, 2010, doi: 10.3390/en3020216.

[41] M. Ahmad *et al.*, 'Effects of pyrolysis temperature on soybean stover- and peanut shell-derived biochar properties and TCE adsorption in water', *Bioresource Technology*, vol. 118, pp. 536–544, Aug. 2012, doi: 10.1016/j.biortech.2012.05.042.

[42] Y. Sun *et al.*, 'Effects of feedstock type, production method, and pyrolysis temperature on biochar and hydrochar properties', *Chemical Engineering Journal*, vol. 240, pp. 574–578, Mar. 2014, doi: 10.1016/j.cej.2013.10.081.

[43] T. N. Trinh, P. A. Jensen, K. Dam-Johansen, N. O. Knudsen, and H. R. Sørensen, 'Influence of the Pyrolysis Temperature on Sewage Sludge Product Distribution, Bio-Oil, and Char Properties', *Energy Fuels*, vol. 27, no. 3, pp. 1419–1427, Mar. 2013, doi: 10.1021/ef301944r.

[44] J. Li, R. Yan, B. Xiao, X. Wang, and H. Yang, 'Influence of Temperature on the Formation of Oil from Pyrolyzing Palm Oil Wastes in a Fixed Bed Reactor', *Energy Fuels*, vol. 21, no. 4, pp. 2398–2407, Jul. 2007, doi: 10.1021/ef060548c.

[45] M. Garcia-Perez *et al.*, 'Fast Pyrolysis of Oil Mallee Woody Biomass: Effect of Temperature on the Yield and Quality of Pyrolysis Products', *Ind. Eng. Chem. Res.*, vol. 47, no. 6, pp. 1846–1854, Mar. 2008, doi: 10.1021/ie071497p.

[46] F. Ateş and M. A. Işıkdağ, 'Evaluation of the Role of the Pyrolysis Temperature in Straw Biomass Samples and Characterization of the Oils by GC/MS', *Energy Fuels*, vol. 22, no. 3, pp. 1936–1943, May 2008, doi: 10.1021/ef7006276.

[47] W. T. Tsai, R. Ayestas, C. H. Tsai, and Y. Q. Lin, 'Preparation and Characterization of Porous Materials from Pineapple Peel at Elevated Pyrolysis Temperatures', *Materials*, vol. 15, no. 13, Jul. 2022, doi: 10.3390/ma15134686.

[48] J. M. Novak *et al.*, 'Characterization of Designer Biochar Produced at Different Temperatures and Their Effects on a Loamy Sand', vol. 3, 2009.

[49] M. J. Antal and M. Grønli, 'The Art, Science, and Technology of Charcoal Production', *Ind. Eng. Chem. Res.*, vol. 42, no. 8, pp. 1619–1640, Apr. 2003, doi: 10.1021/ie0207919.

[50] R. J. M. Westerhof, D. W. F. (Wim) Brilman, W. P. M. Van Swaaij, and S. R. A. Kersten, 'Effect of Temperature in Fluidized Bed Fast Pyrolysis of Biomass: Oil Quality Assessment in Test Units', *Ind. Eng. Chem. Res.*, vol. 49, no. 3, pp. 1160–1168, Feb. 2010, doi: 10.1021/ie900885c.

[51] S. V. Vassilev, D. Baxter, L. K. Andersen, C. G. Vassileva, and T. J. Morgan, 'An overview of the organic and inorganic phase composition of biomass', *Fuel*, vol. 94, pp. 1–33, Apr. 2012, doi: 10.1016/j.fuel.2011.09.030.

[52] Pabir Basu, 'Chapter 3 - Biomass Characteristics', in *Biomass Gasification, Pyrolysis and Torrefaction - Practical Design and Theory*, Third Edition., 2018, p. Pages 49-91.

[53] J. G. Speight, 'Assessing fuels for gasification', in *Gasification for Synthetic Fuel Production*, Elsevier, 2015, pp. 175–198. doi: 10.1016/B978-0-85709-802-3.00008-4.

[54] S. Ghysels *et al.*, 'Integrating anaerobic digestion and slow pyrolysis improves the product portfolio of a cocoa waste biorefinery', *Sustainable Energy Fuels*, vol. 4, no. 7, pp. 3712–3725, 2020, doi: 10.1039/D0SE00689K.

[55] S. Pradhan, V. Prakash, S. Majhi, L. Mohapatra, N. Mohanta, and S. K. Acharya, 'Dry Sliding Wear Behaviour of Epoxy/Biochar Composites', *Transactions of the Indian Institute of Metals*, 2022, doi: 10.1007/s12666-022-02617-2.

[56] K. Aup-Ngoen and M. Noipitak, 'Effect of carbon-rich biochar on mechanical properties of PLA-biochar composites', *Sustainable Chemistry and Pharmacy*, vol. 15, Mar. 2020, doi: 10.1016/j.scp.2019.100204.

[57] R. Ayadi, A. Koubaa, F. Braghiroli, S. Migneault, H. Wang, and C. Bradai, 'Effect of the Pyro-Gasification Temperature of Wood on the Physical and Mechanical Properties of Biochar-Polymer Biocomposites', *Materials*, vol. 13, no. 6, p. 1327, Mar. 2020, doi: 10.3390/ma13061327.

[58] B. Chen, D. Zhou, and L. Zhu, 'Transitional Adsorption and Partition of Nonpolar and Polar Aromatic Contaminants by Biochars of Pine Needles with Different Pyrolytic Temperatures', *Environ. Sci. Technol.*, vol. 42, no. 14, pp. 5137–5143, Jul. 2008, doi: 10.1021/es8002684.

[59] Y. Lin, P. Munroe, S. Joseph, R. Henderson, and A. Ziolkowski, 'Water extractable organic carbon in untreated and chemical treated biochars', *Chemosphere*, vol. 87, no. 2, pp. 151–157, Apr. 2012, doi: 10.1016/j.chemosphere.2011.12.007.

[60] G. Duman, C. Okutucu, S. Ucar, R. Stahl, and J. Yanik, 'The slow and fast pyrolysis of cherry seed', *Bioresource Technology*, vol. 102, no. 2, pp. 1869–1878, Jan. 2011, doi: 10.1016/j.biortech.2010.07.051.

[61] B. Chen and Z. Chen, 'Sorption of naphthalene and 1-naphthol by biochars of orange peels with different pyrolytic temperatures', *Chemosphere*, vol. 76, no. 1, pp. 127–133, Jun. 2009, doi: 10.1016/j.chemosphere.2009.02.004.

[62] R. Azargohar, S. Nanda, B. V. S. K. Rao, and A. K. Dalai, 'Slow Pyrolysis of Deoiled Canola Meal: Product Yields and Characterization', *Energy Fuels*, vol. 27, no. 9, pp. 5268–5279, Sep. 2013, doi: 10.1021/ef400941a.

[63] A. Demirbas, 'Properties of charcoal derived from hazelnut shell and the production of briquettes using pyrolytic oil', 1999.

[64] M. Uchimiya, L. H. Wartelle, K. T. Klasson, C. A. Fortier, and I. M. Lima, 'Influence of Pyrolysis Temperature on Biochar Property and Function as a Heavy Metal Sorbent in Soil', *J. Agric. Food Chem.*, vol. 59, no. 6, pp. 2501–2510, Mar. 2011, doi: 10.1021/jf104206c.

[65] K. B. Cantrell, P. G. Hunt, M. Uchimiya, J. M. Novak, and K. S. Ro, 'Impact of pyrolysis temperature and manure source on physicochemical characteristics of biochar', *Bioresource Technology*, vol. 107, pp. 419–428, Mar. 2012, doi: 10.1016/j.biortech.2011.11.084.

[66] P. Fu, S. Hu, J. Xiang, L. Sun, S. Su, and J. Wang, 'Evaluation of the porous structure development of chars from pyrolysis of rice straw: Effects of pyrolysis temperature and heating rate', *Journal of Analytical and Applied Pyrolysis*, vol. 98, pp. 177–183, Nov. 2012, doi: 10.1016/j.jaap.2012.08.005.

[67] R. Azargohar, K. L. Jacobson, E. E. Powell, and A. K. Dalai, 'Evaluation of properties of fast pyrolysis products obtained, from Canadian waste biomass', *Journal of Analytical and Applied Pyrolysis*, vol. 104, pp. 330–340, Nov. 2013, doi: 10.1016/j.jaap.2013.06.016.

[68] I. F. Titiladunayo, A. G. McDonald, and O. P. Fapetu, 'Effect of Temperature on Biochar Product Yield from Selected Lignocellulosic Biomass in a Pyrolysis Process', *Waste Biomass Valor*, vol. 3, no. 3, pp. 311–318, Sep. 2012, doi: 10.1007/s12649-012-9118-6.

[69] M. Keiluweit, P. S. Nico, M. G. Johnson, and M. Kleber, 'Dynamic Molecular Structure of Plant Biomass-Derived Black Carbon (Biochar)', *Environ. Sci. Technol.*, vol. 44, no. 4, pp. 1247–1253, Feb. 2010, doi: 10.1021/es9031419.

[70] J. W. Lee *et al.*, 'Characterization of Biochars Produced from Cornstovers for Soil Amendment', *Environ. Sci. Technol.*, vol. 44, no. 20, pp. 7970–7974, Oct. 2010, doi: 10.1021/es101337x.

[71] F. Karaosmanoğlu, A. Işığıgür-Ergüdenler, and A. Sever, 'Biochar from the Straw-Stalk of Rapeseed Plant', *Energy Fuels*, vol. 14, no. 2, pp. 336–339, Mar. 2000, doi: 10.1021/ef9901138.

[72] C. A. Mullen, A. A. Boateng, N. M. Goldberg, I. M. Lima, D. A. Laird, and K. B. Hicks, 'Bio-oil and bio-char production from corn cobs and stover by fast pyrolysis', *Biomass and Bioenergy*, vol. 34, no. 1, pp. 67–74, Jan. 2010, doi: 10.1016/j.biombioe.2009.09.012.

[73] O. Onay, 'Influence of pyrolysis temperature and heating rate on the production of bio-oil and char from safflower seed by pyrolysis, using a well-swept fixed-bed reactor', *Fuel Processing Technology*, vol. 88, no. 5, pp. 523–531, May 2007, doi: 10.1016/j.fuproc.2007.01.001.

[74] Pretsch E., Buhlmann P., and Badertscher M., *Structure Determination of Organic Compounds: Tables of Spectral Data*. Berlin, Heidelberg: Springer Berlin Heidelberg, 2009. doi: 10.1007/978-3-540-93810-1.

[75] W. A. W. A. K. Ghani *et al.*, 'Biochar production from waste rubber-wood-sawdust and its potential use in C sequestration: Chemical and physical characterization', *Industrial Crops and Products*, vol. 44, pp. 18–24, Jan. 2013, doi: 10.1016/j.indcrop.2012.10.017.

[76] N. Claoston, A. Samsuri, M. Ahmad Husni, and M. Mohd Amran, 'Effects of pyrolysis temperature on the physicochemical properties of empty fruit bunch

and rice husk biochars', *Waste Manag Res*, vol. 32, no. 4, pp. 331–339, Apr. 2014, doi: 10.1177/0734242X14525822.

[77] E. C. Abdullah, K. R. Thines, M. Ruthiraan, and N. M. Mubarak, 'Synthesis of magnetic biochar from Garcinia Mangostana peel using muffle furnace for adsorption of Zn2 ions from aqueous solution', in *Fourth International Conference On Advances in Applied Science and Environmental Engineering - ASEE 2015*, Institute of Research Engineers and Doctors, Sep. 2015, pp. 9–12. doi: 10.15224/978-1-63248-068-2-03.

[78] M. Uchimiya, S. Chang, and K. T. Klasson, 'Screening biochars for heavy metal retention in soil: Role of oxygen functional groups', *Journal of Hazardous Materials*, vol. 190, no. 1–3, pp. 432–441, Jun. 2011, doi: 10.1016/j.jhazmat.2011.03.063.

[79] S.-X. Zhao, N. Ta, and X.-D. Wang, 'Effect of Temperature on the Structural and Physicochemical Properties of Biochar with Apple Tree Branches as Feedstock Material', *Energies*, vol. 10, no. 9, p. 1293, Aug. 2017, doi: 10.3390/en10091293.

[80] Y. Liu, Z. He, and M. Uchimiya, 'Comparison of Biochar Formation from Various Agricultural By-Products Using FTIR Spectroscopy', *MAS*, vol. 9, no. 4, p. p246, Mar. 2015, doi: 10.5539/mas.v9n4p246.

[81] S. Mia, B. Singh, and F. A. Dijkstra, 'Aged biochar affects gross nitrogen mineralization and recovery: a ^{15} N study in two contrasting soils', *GCB Bioenergy*, vol. 9, no. 7, pp. 1196–1206, Jul. 2017, doi: 10.1111/gcbb.12430.

[82] P. J. F. Harris and S. C. Tsang, 'High-resolution electron microscopy studies of non-graphitizing carbons', *Philosophical Magazine A*, vol. 76, no. 3, pp. 667–677, Sep. 1997, doi: 10.1080/01418619708214028.

[83] P. J. F. Harris, 'Structure of non-graphitising carbons'.

[84] L. Van Zwieten *et al.*, 'Effects of biochar from slow pyrolysis of papermill waste on agronomic performance and soil fertility', *Plant Soil*, vol. 327, no. 1–2, pp. 235–246, Feb. 2010, doi: 10.1007/s11104-009-0050-x.

[85] W. Zheng, B. K. Sharma, and N. Rajagopalan, 'Using Biochar as a Soil Amendment for Sustainable Agriculture'.

[86] M. Ahmad *et al.*, 'Speciation and phytoavailability of lead and antimony in a small arms range soil amended with mussel shell, cow bone and biochar: EXAFS spectroscopy and chemical extractions', *Chemosphere*, vol. 95, pp. 433–441, Jan. 2014, doi: 10.1016/j.chemosphere.2013.09.077.

[87] Q. Zhang, M. U. Khan, X. Lin, H. Cai, and H. Lei, 'Temperature varied biochar as a reinforcing filler for high-density polyethylene composites', *Composites Part B: Engineering*, vol. 175, p. 107151, Oct. 2019, doi: 10.1016/j.compositesb.2019.107151.

[88] A. Shaaban, S. M. Se, N. M. M. Mitan, and M. F. Dimin, 'Characterization of biochar derived from rubber wood sawdust through slow pyrolysis on surface porosities and functional groups', in *Procedia Engineering*, Elsevier Ltd, 2013, pp. 365–371. doi: 10.1016/j.proeng.2013.12.193.

[89] O. Das, A. K. Sarmah, and D. Bhattacharyya, 'Biocomposites from waste derived biochars: Mechanical, thermal, chemical, and morphological properties', *Waste Management*, vol. 49, pp. 560–570, Mar. 2016, doi: 10.1016/j.wasman.2015.12.007.

[90] H. Maljaee, R. Madadi, H. Paiva, L. Tarelho, and V. M. Ferreira, 'Incorporation of biochar in cementitious materials: A roadmap of biochar selection', *Construction and Building Materials*, vol. 283, p. 122757, May 2021, doi: 10.1016/j.conbuildmat.2021.122757.

[91] X. Gai *et al.*, 'Effects of Feedstock and Pyrolysis Temperature on Biochar Adsorption of Ammonium and Nitrate', *PLoS ONE*, vol. 9, no. 12, p. e113888, Dec. 2014, doi: 10.1371/journal.pone.0113888.

[92] S. Hosokai, K. Matsuoka, K. Kuramoto, and Y. Suzuki, 'Modification of Dulong's formula to estimate heating value of gas, liquid and solid fuels', *Fuel Processing Technology*, vol. 152, pp. 399–405, Nov. 2016, doi: 10.1016/j.fuproc.2016.06.040.

[93] S. A. Channiwala and P. P. Parikh, 'A unifed correlation for estimating HHV of solid, liquid and gaseous fuelsq', 2002.

1.5. Biochar-based composites

1.5.1. Biochar as a Filler of Polymer-based composites

In recent times, biochar (BC) has attracted increasing interest for its use as a filler in polymer-based composite materials, either in thermoplastics or in thermosetting plastics [1], [2]. As discussed previously, the final properties of BC particulates are a function of several factors including the nature of the raw material from which the BC particulates are produced, the type of process employed and the relative operating conditions. The final properties of the composites in terms of interfacial adhesion, dispersion, thermal and mechanical stability, and ageing resistance are therefore determined by the final fixed carbon and ash content, the grinding and screening process used to control the final particle size, surface area and pore volume sill, and also by the polymer matrix used.

In order to assess how pyrolysis temperature and type of feedstock could determine a difference in the final properties of composites, Das *et al.* [3] added biochar particles as a co-filler for the production of wood plastic polypropylene-based composites, pyrolyzing different feedstocks (landfill pine sawdust, sewage sludge, and poultry litter) at a different temperatures, with the aim of identifying a routing process for waste employing. Keeping the weight of landfill pine at 30 wt.%, the 24 wt.% of biochar particles obtained from the different feedstocks with different pyrolysis conditions (*i.e.* temperature, heating rate and residence time, see [3] for more details) were added. The fixed biochar concentration of 24 wt.% was determined thanks to a previous work by the same research group [4], in which BC produced from pine wood was added to the PP matrix at different loadings ranging from 6 to 30 wt.%. In this study, a BC content of 24 wt.% showed a general improvement in tensile and flexural strength and in the young modulus of the final composite. Taking these results into account, it was found that the increase in tensile

strength and the modulus is strongly related to the increase in surface area. Furthermore, the presence of residual minerals (*i.e.* $CaCO_3$ found in BC from poultry litter and relative ash content) increases the composite impact strength and exhibits lower heat release rate during combustion compared to the other composite. These results can be explained by the fact that inorganic particles generally impede the diffusion of oxygen through the material, thus creating a physical barrier between the combustible and the oxidising agent. This allows BC composites to be used in a flame-retardant field.

In addition, a generally good dispersion of BC particles and infiltration of polypropylene into biochar pores was also observed for all composites, thanks to the maleic anhydride grafted polypropylene/maleated anhydride polypropylene (MAPP) used as coupling agent.

Without the presence of wood for PP-based composites, a flame retardant ability of pine wood biochar was demonstrated in a study by Das *et al.* [5], in which by varying the BC loading from 0 to 35 wt%, the composites exhibited an increasingly stable compact char structure during controlled combustion tests that masked O_2 diffusion in the polypropylene matrix. In addition, the addition of char significantly reduced the peak heat release and smoke production. The increase in flame retardancy conferred by the presence of biochar particles in wood-polypropylene composites has also been investigated in the presence of conventional inorganic flame retardants such as magnesium hydroxide and ammonium polyphosphates [6], [7]. On the other hand, the presence of biochar, the two flame retardant particles were trapped in BC pores instead of polypropylene with a final reduction of PP flow during processing and consequent reduction of interfacial adhesion and relative mechanical stability. Furthermore, the addition of biochar particles to wood-polypropylene composites imparts water resistance to the composite. This result remains valid without exceeding a threshold concentration above which the composites become more susceptible to water. In addition, it has been found that a high pyrolysis temperature generates a more hydrophilic particle, due to an absorption by capillary action of the

pores [8]. Furthermore, the reason for the addition of biochar particles to a wood-polypropylene composite is that WPCs usually suffer from thermal instability and thickness swelling due to the high hydrophilic behaviour of wood dust. Ayrilmis *et al.* [9] gradually reduced the concentration of wood dust from 60 to 0 wt% and increased the concentration of commercial Quercus charcoal flour from 0 to 60 wt%, respectively, and showed that thickness swelling is reduced by 50% after 30 days when wood dust is completely replaced by BC, thus increasing the global dimensional stability. The same stabilization behaviour is observed for the water absorption after 30 days of WPC, which decreases from about 21% for PP/wood composites to about 15% for PP/char composites. A study by DeVallance *et al.* confirms the same result of dimensional stabilization and overall improvement in resistance to thermal degradation by adding BC particles to WPC [10], [11].

Giorcelli *et al.* [12] also investigated the relationship between the pyrolysis temperature and the electrical conductivity of the biochar particles, with the aim of using biochar particles as a filler in epoxy resin based conductive composites. The residues of *Miscantus* residues were pyrolyzed at 650, 700 and 750°C and activated with CO_2 to increase the surface area, then 20 wt.% of the particles were incorporated into and epoxy resins and electrically characterized. As already shown by other studies, it was found that an increase in pyrolysis temperature corresponds to and increase in carbon content with a corresponding reduction of other elements (*i.e.* O, Mg, Si, K, Ca) [13], and the ratio between disordered and graphitized structure of the carbon structure increases with the increase in pyrolysis temperature. All these properties allow an increase in the conductivity of the biochar particles as a function of the pyrolysis temperature, with a consequent increase in the electrical performance of the composites obtained with the adding of particles produced at higher pyrolysis temperature. In the same low viscosity Epoxy resin LPL, two different biochar obtained by pyrolyzing *Maple tree* waste at low and high temperatures (600 and 1000°C) were added at different weight percentages in order to improve mechanical properties of the resin [1]. It was observed that an addition of small amounts of

carbon fillers, lower than 2 wt.%, increased the load bearing capacity of the epoxy matrix, modifying the mechanical properties of the polymer matrix; on the other hand, a concentration equal or higher to 2 wt.% transformed the pristine epoxy resin from brittle to a ductile composite, different from what it has already seen for polypropylene-based composites.

The optimum filler concentration depends on the type of polymer, the pyrolysis temperature and the type of feedstock used for biochar production, as well as the presence of other additives in composites production. By adding a curing agent (*i.e.* cycloaliphatic polyamine) and an embedding medium during the processing of epoxy-based composite, it is possible to increase the filler content above a critical level that normally reduces the tensile strength. In this configuration, a critical level of chars obtained from natural substance is found to be equal to 25 wt.%, and in composites with plastic waste char, the critical level appears to be quite low, equal to 15 wt% [14]. Nevertheless, waste plastic char, PWC (obtained from the pyrolysis of polyethylene terephthalate, PET) increases the global conductivity of a polymer composite due to the terephthalic acid present in the char structure [15].

Another way to activate biochar particles was investigated by Zhang *et al.* [16] by impregnating the biomass feedstock in H_3PO_4 solution prior to the carbonization process by varying the concentration of H_3PO_4 in the solutions. In general, the activation of BC improved the thermal stability of the resulting composites, but a different concentration of activating agent affected the characteristics of biochar in terms of chemical and morphological structure. In fact, a low concentration of H_3PO_4 improved the porous structure, which improved the resulting mechanical properties, thanks to better adhesion between particles and HDPE polymer matrix, including flexural properties, stiffness elasticity, creep resistance and anti-stress relaxation. On the other hand, a high concentration of H_3PO_4 in the activation solution, generated fouling in the porous structure, reducing all mechanical properties.

The electrical properties of UHMWPE/LLDPE [17], [18] blends have been obtained by adding a char obtained by carbonization of bamboo at 1110°C. Irregular shaped

particles have been obtained with a global transformation of the amorphous structure into a graphite-like structure with a higher degree of crystallinity, with high specific surface due to the creation of a nanoporous structure. These particles were added to UHMWPE blended with LLDPE as a flow accelerator to reduce the melt viscosity of UHMDPE and improve the processability of the composite and the final particle dispersion. The highly filled composites (with carbon loading up to 80 wt%) showed excellent electromagnetic interference shielding performance and one of the highest values reported for conductive polymer composites was found, in fact at maximum biochar concentration a conductivity of 107.6 S/m was found. An increase in nanoporous structure, crystallinity, hardness and thermal stability was found to be higher for biochar obtained by carbonisation at 800 °C followed by pyrolysis at 1110 °C as the biochar activation step [19]. At the same time, if the goal is bicompatibility, achieving a high temperature is not useful because of the global reduction in hydrophilicity and higher specific surface energy, which promote protein adhesion and cell proliferation.

With the aim of reducing waste for environmental purposes, Kane *et al.* [20] recently compared recycled high-density polyethylene, rHDPE, with and without biochar, looking at both improvements in mechanical properties and environmental impact. From a mechanical point of view, the tensile behaviour of rHDPE was significantly modified by the addition of biochar particles derived from forest residues, increasing the strength and stiffness due to the global increase in the crystallinity of rHDPE, to the reinforcing effect of the polymer matrix, and thanks to a good interfacial adhesion that led to a polymer interlocking with the porous structure of biochar. In addition, using life cycle assessment, it has been found that the addition of biochar as a filler reduces the global amount of plastic used to produce a manufactured product, which of course provides a benefit in terms of global warming potential when referring to the CO_2 emitted in the production of plastic. It has been calculated that rHDPE CO2 equivalent by adding less than 40 wt% of biochar particles, giving a composite with similar strength and stiffness to that obtained by adding 40 - 50 wt% of biochar

particles to virgin HDPE [21]. Another way to reduce the amount of polyolefin waste and the amount of virgin polyolefin used in the industrial field was addressed in a study by Idress *et al.* [22], in which a composite based on recycled polyethylene terephthalate rPET was produced by adding biochar. The biochar used in this work was obtained from high-temperature pyrolysis (1100 °C) under autogenous pressure of approximately 150 bar of PET waste. In this study, the researchers were able to extrude recycled PET and PET/BC composites, highlighting that the incorporation of biochar improves the mechanical properties and imparts thermal properties to PET, suggesting that BC could supply the need for commercial graphene materials in polymer composites. As noted with other polyolefins, the responsibility of the improvement in mechanical properties must be related to high surface porosity of BC particles and high affinity between BC particles and polymer matrix. Instead, the improvement in thermal properties must be attributed to the known barrier effect of BC.

1.5.2. Biochar as a Filler of Bio-Polymer-based composites

In the context of a sustainable and circular economy, the recovery of bio-waste and its incorporation into bioplastic for the formulation of sustainable biocomposites is a challenging issue. Bioplastics should be defined as polymers that meet one or both of two criteria: the polymer is bio-based and biodegradable [23].

Among the biopolymer-based composites containing biochar particles, a significant number of studies are reported in the literature. One of the most biochar-added polyester matrices is polylactic acid (PLA), which suffers from poor thermal stability, high brittleness that reduce its use in many fields, *i.e.* textile, biomedical and food packaging [24]. In short, the use of BC in PLA can lead to a growth in the PLA market thanks to a global improvement in the mechanical stability of this polymer [25]–[27]. Kane *et al.* [28] investigated BC-added PLA composites and compared them with high density polyethylene (HDPE) composites. Unlike HDPE,

for PLA/BC composites this work highlights an impact of BC in the thermal degradation behaviour, shown in a decrease of the onset degradation temperature and a global reduction of the melt viscosity of PLA, probably due to the presence of inorganic element of the BC surface, responsible of catalysing the thermal decomposition of PLA. The same behaviour was found in the study by Arrigo *et al.* [29] in which BC particles derived from spent ground coffee were added to the PLA matrix and the composites were processed by melt mixing and solvent casting methods. A significant change in the rheological behaviour of PLA was found when the composites were obtained by melt processing. In fact, the author reports a progressive increase of the melt viscosity in composites obtained by solvent casting and a progressive decrease of the melt viscosity in composites obtained by melt mixing, as the BC content increases, suggesting in the latter case a strong reduction of the polymer molar mass due to thermal degradation [30], and a preservation of PLA when processing has been carried out at room temperature by solvent casting. In any case, a strong polymer-filler or filler-filler interaction has been found, as evidenced by the appearance of a yield stress behaviour. A significant reduction in the molecular weight of poly(3-hydroxybutyrate) (PHB) processed at high temperature with the addition of biochar particles has been demonstrated by Haeldermans *et al.* [31]. In this study, different PHB/char with BC loading (from 20 wt% to 50 wt%) were produced and this formulation was compared with PHB/thermoplastic starch (TPS)/BC composites. Despite the best biodegradability compared to other biopolymers, it is well known in the literature that PHB suffers a significant reduction in molecular weight after processing, which limits its application due to a really small operational processing window [32], *e.g.* unprocessed PHB-M_w of 611 Kg/mol and melt-processed PHB-M_w of approx. 463 Kg/mol [31]. Unfortunately, increasing the amount of biochar particles from 20 to 50 wt% reduces PHB-Mw even more, reaching a reduction of 218 Kg/mol for 50 wt% BC, which reduces the global thermal stability of BC biocomposites. Consistent with the reduction in molecular weight, a reduction in thermal properties has been

found, such as a decrease in melting point with the decrease in molecular weight [33]. Thanks to the presence of thermoplastic starch in the biocomposites, the decrease in Mw is more gradual and controlled, and molecular weight analysis showed that at low BC load, TPS can act as an intermediary between PHB and PHB, controlling the decrease in molecular weight.

Differently, the addition of BC particles as a filler in Ecovio commercial polymer blend containing of poly (1,4-butylene adiphat-co-1,4-butylene terephthalate), PBAT, 47 mol% of aromatic segment, and PLA, 25 mol%, significantly increase the application field of BC particles in biopolymers matrix [34]. In fact, it has been found a significantly reduction of resistivity of obtained-biocomposites as the increase of BC load, added up to 30 wt.%, suggesting and employment of the composites in equipment element in laboratories for precise measurement or as an antistatic agent in the packaging industry. Moreover, thermal stability has not been affected by the presence of BC compared to Ecovio polymer matrix. Moreover, thanks to a global improvement of modulus showed in DMA analysis in all temperature range (-50 to 120°C), mechanical properties result higher for composites with respect to neat matrix, suggesting a better mechanical stability.

Polyvinyl alcohol (PVA)/corn starch/BC biocomposites have been successfully formulated by means of the solvent casing method in the presence of citric acid and glutaraldehyde, which were added for the fixing effect before the casting period [35]. The interaction between the biopolymer blend and the BC particles significantly affects the degradation path of PVA/starch composites. In fact, a significant decrease, a narrowing of the peak relative to the hydroxy band, was observed with increasing BC loading. This phenomenon was attributed by the author to the good compatibility of the PVA, the starch and the BC [36]. In any case, as was the case for composites based on PLA and PHB, the overall thermal stability of the biocomposites is lower when BC is added in the blend.

A noticeable improving of mechanical properties has been obtained introducing a suitable concentration of biochar particles in a eco-friendly biocomposites

manufactured by a green epoxy matrix reinforced with short agave fibers for replacing synthetic materials in structural applications [37]. In this case, with the optimum amount of BC particles (in this case founded equal to 2 wt.%) by means of synergic effect of short fiber and biochar particles, a better adhesion has been achieved between epoxy matrix and fiber, demonstrated by fiber pull-out test. This aspect involves in an increase of global Young's modulus and tensile strength, and, moreover in an increase of fatigue performance with an increase of fatigue strength by about 67% and fatigue lifetime by least 3 order of magnitude. This remarkable enhancement of mechanical performance increases the possibility of employing a green epoxy matrix fiber reinforced for structural and semi-structural applications, especially in automotive and naval applications.

Green composites have been formulated adding biochar particles in partially biobased polymer or biobased polymers that are non-biodegradable. Nagarajan *et al.* [38] performed a study varying particle size distribution of biochar particles produced from low-temperature slow pyrolysis process of *Miscanthus* fibers. After pyrolysis, size-fractionation of BC was performed with sieves having different opening, *e.g.,* 300, 212, 150, 125, 75 and 20 μm. The different size-fractioned BC were added to poly(trimethylene terephthalate) (PTT) 70 /poly(lactic acid) (PLA) 30- ethylene-methyl acrylate-glycidyl methacrylate terpolymer (EMAGMA) polymer blend (85-15), using in some formulation an epoxy-functionalized chain extender (CE). A good range of particle size distribution, combined with the presence of chain extender, helps to obtain a morphology with better dispersion of the blend components, *i.e.* particle size distribution of 75-20 μm. Biochar particles under 20 μm of size diameter stabilized the blend morphologies, showing a coalescence PLA-EMAGMA particles that turn in smaller and finer morphologies in presence of CE. This evaluation obtained from SEM images observation are consistent with rheological test and mechanical analysis, showing that with an appropriate BC particle size and shape, morphologies and properties can be tailored achieving desired properties, with solid cost reduction. The partially biobased PTT was

combined with 20 wt.% high temperature biocarbon from peanut hulls pyrolysis, founding superior mechanical performance that could be optimize for non-structural automotive components or electrical housing applications [39]. Also in this case, particle size distribution and particle size of the original biomass can play a crucial role on the resulting biochar and impact the concentration of volatiles and bio-oil of pyrolysis process [40], [41] and, as expected, in biocomposites properties, reason why a milling process before pyrolysis has been conducted [39]. The adding of peanut hulls biochar, its sheet-like surface morphology with high graphitic carbon content and its relatively low electrical conductivity, improved thermal stability of PTT based green composites, increasing both in flexural and tensile moduli, suggesting nonstructural and anti-static applications.

References

[1] M. Giorcelli, A. Khan, N. M. Pugno, C. Rosso, and A. Tagliaferro, 'Biochar as a cheap and environmental friendly filler able to improve polymer mechanical properties', *Biomass and Bioenergy*, vol. 120, pp. 219–223, Jan. 2019, doi: 10.1016/j.biombioe.2018.11.036.

[2] E. O. Ogunsona, A. Codou, M. Misra, and A. K. Mohanty, 'Thermally Stable Pyrolytic Biocarbon as an Effective and Sustainable Reinforcing Filler for Polyamide Bio-composites Fabrication', *Journal of Polymers and the Environment*, vol. 26, no. 9, pp. 3574–3589, Sep. 2018, doi: 10.1007/s10924-018-1232-5.

[3] O. Das, A. K. Sarmah, and D. Bhattacharyya, 'Biocomposites from waste derived biochars: Mechanical, thermal, chemical, and morphological properties', *Waste Management*, vol. 49, pp. 560–570, Mar. 2016, doi: 10.1016/j.wasman.2015.12.007.

[4] O. Das, A. K. Sarmah, and D. Bhattacharyya, 'A novel approach in organic waste utilization through biochar addition in wood/polypropylene composites', *Waste Management*, vol. 38, no. 1, pp. 132–140, 2015, doi: 10.1016/j.wasman.2015.01.015.

[5] O. Das, D. Bhattacharyya, D. Hui, and K. T. Lau, 'Mechanical and flammability characterisations of biochar/polypropylene biocomposites', *Composites Part B: Engineering*, vol. 106, pp. 120–128, Dec. 2016, doi: 10.1016/j.compositesb.2016.09.020.

[6] O. Das, N. K. Kim, A. K. Sarmah, and D. Bhattacharyya, 'Development of waste based biochar/wool hybrid biocomposites: Flammability characteristics and mechanical properties', *Journal of Cleaner Production*, vol. 144, pp. 79–89, Feb. 2017, doi: 10.1016/j.jclepro.2016.12.155.

[7] O. Das, N. K. Kim, A. L. Kalamkarov, A. K. Sarmah, and D. Bhattacharyya, 'Biochar to the rescue: Balancing the fire performance and mechanical properties of polypropylene composites', *Polymer Degradation and Stability*, vol. 144, pp. 485–496, Oct. 2017, doi: 10.1016/j.polymdegradstab.2017.09.006.

[8] O. Das, 'Wettability Properties of Biochar Added Wood/Polypropylene Composites', *Academic Journal of Polymer Science*, vol. 1, no. 4, Aug. 2018, doi: 10.19080/ajop.2018.01.555570.

[9] N. Ayrilmis, J. H. Kwon, T. H. Han, and A. Durmus, 'Effect of wood-derived charcoal content on properties of wood plastic composites', *Materials Research*, vol. 18, no. 3, pp. 654–659, May 2015, doi: 10.1590/1516-1439.001515.

[10] D. B. Devallance, G. S. Oporto, and P. Quigley, 'Investigation of hardwood biochar as a replacement for wood flour in wood-polypropylene composites', *Journal of Elastomers and Plastics*, vol. 48, no. 6, pp. 510–522, Oct. 2016, doi: 10.1177/0095244315589655.

[11] M. Zouari, D. B. Devallance, and L. Marrot, 'Effect of Biochar Addition on Mechanical Properties, Thermal Stability, and Water Resistance of Hemp-Polylactic Acid (PLA) Composites', *Materials*, vol. 15, no. 6, Mar. 2022, doi: 10.3390/ma15062271.

[12] M. Giorcelli, P. Savi, A. Khan, and A. Tagliaferro, 'Analysis of biochar with different pyrolysis temperatures used as filler in epoxy resin composites', *Biomass and Bioenergy*, vol. 122, pp. 466–471, Mar. 2019, doi: 10.1016/j.biombioe.2019.01.007.

[13] S. Nanda, A. K. Dalai, F. Berruti, and J. A. Kozinski, 'Biochar as an Exceptional Bioresource for Energy, Agronomy, Carbon Sequestration, Activated Carbon and Specialty Materials', *Waste Biomass Valor*, vol. 7, no. 2, pp. 201–235, Apr. 2016, doi: 10.1007/s12649-015-9459-z.

[14] G. Ahmetli, S. Kocaman, I. Ozaytekin, and P. Bozkurt, 'Epoxy composites based on inexpensive char filler obtained from plastic waste and natural resources', *Polymer Composites*, vol. 34, no. 4, pp. 500–509, Apr. 2013, doi: 10.1002/pc.22452.

[15] İ. Özaytekin and Y. Kar, 'Synthesis and properties of composites of oligoazomethine with char', *J. Appl. Polym. Sci.*, vol. 123, no. 2, pp. 815–823, Jan. 2012, doi: 10.1002/app.34509.

[16] Q. Zhang *et al.*, 'Properties evaluation of biochar/high-density polyethylene composites: Emphasizing the porous structure of biochar by activation', *Science of the Total Environment*, vol. 737, Oct. 2020, doi: 10.1016/j.scitotenv.2020.139770.

[17] S. Li, A. Huang, Y. J. Chen, D. Li, and L. S. Turng, 'Highly filled biochar/ultra-high molecular weight polyethylene/linear low density polyethylene composites for high-performance electromagnetic interference shielding', *Composites Part B: Engineering*, vol. 153, pp. 277–284, Nov. 2018, doi: 10.1016/j.compositesb.2018.07.049.

[18] S. Li, X. Li, Q. Deng, and D. Li, 'Three kinds of charcoal powder reinforced ultra-high molecular weight polyethylene composites with excellent mechanical and electrical properties', *Materials & Design*, vol. 85, pp. 54–59, Nov. 2015, doi: 10.1016/j.matdes.2015.06.163.

[19] S. Li, Y. Xu, X. Jing, G. Yilmaz, D. Li, and L. S. Turng, 'Effect of carbonization temperature on mechanical properties and biocompatibility of biochar/ultra-high molecular weight polyethylene composites', *Composites Part B: Engineering*, vol. 196, Sep. 2020, doi: 10.1016/j.compositesb.2020.108120.

[20] S. Kane, E. Van Roijen, C. Ryan, and S. Miller, 'Reducing the environmental impacts of plastics while increasing strength: Biochar fillers in biodegradable, recycled, and fossil-fuel derived plastics', *Composites Part C: Open Access*, vol. 8, Aug. 2022, doi: 10.1016/j.jcomc.2022.100253.

[21] Q. Zhang *et al.*, 'Biochar filled high-density polyethylene composites with excellent properties: Towards maximizing the utilization of agricultural wastes', *Industrial Crops and Products*, vol. 146, p. 112185, Apr. 2020, doi: 10.1016/j.indcrop.2020.112185.

[22] M. Idrees, S. Jeelani, and V. Rangari, 'Three-Dimensional-Printed Sustainable Biochar-Recycled PET Composites', *ACS Sustainable Chemistry and Engineering*, vol. 6, no. 11, pp. 13940–13948, Nov. 2018, doi: 10.1021/acssuschemeng.8b02283.

[23] Y. Tokiwa, B. Calabia, C. Ugwu, and S. Aiba, 'Biodegradability of Plastics', *IJMS*, vol. 10, no. 9, pp. 3722–3742, Aug. 2009, doi: 10.3390/ijms10093722.

[24] M. Murariu and P. Dubois, 'PLA composites: From production to properties', *Advanced Drug Delivery Reviews*, vol. 107, pp. 17–46, Dec. 2016, doi: 10.1016/j.addr.2016.04.003.

[25] S. Wang *et al.*, 'Physicochemical and sorptive properties of biochars derived from woody and herbaceous biomass', *Chemosphere*, vol. 134, pp. 257–262, Sep. 2015, doi: 10.1016/j.chemosphere.2015.04.062.

[26] M. Ho, K. Lau, H. Wang, and D. Hui, 'Improvement on the properties of polylactic acid (PLA) using bamboo charcoal particles', *Composites Part B: Engineering*, vol. 81, pp. 14–25, Nov. 2015, doi: 10.1016/j.compositesb.2015.05.048.

[27] S. Qian, K. Sheng, W. Yao, and H. Yu, 'Poly(lactic acid) biocomposites reinforced with ultrafine bamboo-char: Morphology, mechanical, thermal, and water absorption properties', *J. Appl. Polym. Sci.*, vol. 133, no. 20, p. n/a-n/a, May 2016, doi: 10.1002/app.43425.

[28] S. Kane and C. Ryan, 'Biochar from food waste as a sustainable replacement for carbon black in upcycled or compostable composites', *Composites Part C: Open Access*, vol. 8, Aug. 2022, doi: 10.1016/j.jcomc.2022.100274.

[29] R. Arrigo, M. Bartoli, and G. Malucelli, 'Poly(lactic Acid)-biochar biocomposites: Effect of processing and filler content on rheological, thermal, and mechanical properties', *Polymers*, vol. 12, no. 4, Apr. 2020, doi: 10.3390/POLYM12040892.

[30] I. Valentina, A. Haroutioun, L. Fabrice, V. Vincent, and P. Roberto, 'Poly(Lactic Acid)-Based Nanobiocomposites with Modulated Degradation Rates', *Materials*, vol. 11, no. 10, p. 1943, Oct. 2018, doi: 10.3390/ma11101943.

[31] T. Haeldermans *et al.*, 'Bio-Based Poly(3-hydroxybutyrate)/Thermoplastic Starch Composites as a Host Matrix for Biochar Fillers', *Journal of Polymers and the Environment*, vol. 29, no. 8, pp. 2478–2491, Aug. 2021, doi: 10.1007/s10924-021-02049-x.

[32] W. M. Pachekoski, C. Dalmolin, and J. A. M. Agnelli, 'The influence of the industrial processing on the degradation of poly(hidroxybutyrate) - PHB', *Mat.*

Res., vol. 16, no. 2, pp. 237–332, Dec. 2012, doi: 10.1590/S1516-14392012005000180.

[33] S. Luo, D. T. Grubb, and A. N. Netravali, 'The effect of molecular weight on the lamellar structure, thermal and mechanical properties of poly(hydroxybutyrate-co-hydroxyvalerates)', *Polymer*, vol. 43, no. 15, pp. 4159–4166, Jul. 2002, doi: 10.1016/S0032-3861(02)00242-2.

[34] M. Musioł *et al.*, '(Bio)degradable biochar composites – Studies on degradation and electrostatic properties', *Materials Science and Engineering B: Solid-State Materials for Advanced Technology*, vol. 275, Jan. 2022, doi: 10.1016/j.mseb.2021.115515.

[35] P. Terzioğlu and F. N. Parın, 'Biochar Reinforced Polyvinyl Alcohol /Corn Starch Biocomposites', *Süleyman Demirel Üniversitesi Fen Bilimleri Enstitüsü Dergisi*, pp. 35–42, Apr. 2020, doi: 10.19113/sdufenbed.568229.

[36] Z. W. Abdullah and Y. Dong, 'Preparation and characterisation of poly(vinyl) alcohol (PVA)/starch (ST)/halloysite nanotube (HNT) nanocomposite films as renewable materials', *J Mater Sci*, vol. 53, no. 5, pp. 3455–3469, Mar. 2018, doi: 10.1007/s10853-017-1812-0.

[37] B. Zuccarello, M. Bartoli, F. Bongiorno, C. Militello, A. Tagliaferro, and A. Pantano, 'New concept in bioderived composites: Biochar as toughening agent for improving performances and durability of agave-based epoxy biocomposites', *Polymers*, vol. 13, no. 2, pp. 1–14, Jan. 2021, doi: 10.3390/polym13020198.

[38] V. Nagarajan, A. K. Mohanty, and M. Misra, 'Biocomposites with Size-Fractionated Biocarbon: Influence of the Microstructure on Macroscopic Properties', *ACS Omega*, vol. 1, no. 4, pp. 636–647, Oct. 2016, doi: 10.1021/acsomega.6b00175.

[39] M. Picard, S. Thakur, M. Misra, D. F. Mielewski, and A. K. Mohanty, 'Biocarbon from peanut hulls and their green composites with biobased poly(trimethylene terephthalate) (PTT)', *Scientific Reports*, vol. 10, no. 1, Dec. 2020, doi: 10.1038/s41598-020-59582-3.

[40] D. V. Suriapparao and R. Vinu, ‘Effects of Biomass Particle Size on Slow Pyrolysis Kinetics and Fast Pyrolysis Product Distribution’, *Waste Biomass Valor*, vol. 9, no. 3, pp. 465–477, Mar. 2018, doi: 10.1007/s12649-016-9815-7.

[41] X. Hu and M. Gholizadeh, ‘Biomass pyrolysis: A review of the process development and challenges from initial researches up to the commercialisation stage’, *Journal of Energy Chemistry*, vol. 39, pp. 109–143, Dec. 2019, doi: 10.1016/j.jechem.2019.01.024.

2. Experimental part

2.1. Biochar production from slow pyrolysis

The recovery of biowaste for sustainable biocomposites formulation is a challenging issue in the context of sustainable and circular economy. The aim of this chapter is the characterisation of *(i)* the two biowastes used as feedstock for the pyrolysis process and *(ii)* the resultant biochar. The first feedstock used was carob waste after glucose extraction from a local carob candy factory. The second bio-waste used was digestate from the anaerobic digestion of organic fraction of municipal solid waste (OFMSW).

Thus, the two biomasses were first characterised. A pyrolysis process was performed on biowaste to produce biofuel and later the solid residual fraction of pyrolysis was characterised as an interesting filler for biocomposites production.

Since it was investigated that the pyrolysis temperature could affect the properties of the resulting biochar, carob waste was pyrolysed at three processing temperatures (*i.e.* 280, 340 and 400 °C) to optimise the compositions of the produced solid fractions and biofuels. Instead, the digestate was subjected to pyrolysis at 400 °C. Subsequently, the properties of the resulting BC particles were chemically characterised by elemental composition and/or EDX analysis and spectroscopic analysis. Morphology, particle size distribution and evaluation of radical scavenging activity and efficiency were also investigated.

2.1.1. Materials and Methods

2.1.1.1. Materials

In this dissertation study two kind of organic waste has been used as a feedstock for slow pyrolysis process:

- *Carob Waste*, residual waste after syrup extraction for candies production, kindly provided by Terranova Candy Factory, Palermo, Sicily, Italy;
- *Digestate,* residual waste after anaerobic digestion for biogas production of OFMSW, Organic Fraction of Municipal Solid Waste, kindly supplied by Archimede s.r.l., Caltanisetta.

2.1.1.2. Analysis of Feedstock

A Netzsch STA 449 F1 Jupiter thermogravimetric analyser was used for the proximate analysis and thermogravimetric study of the waste. Approximately 90 ± 5 mg of the sample under consideration was crushed to reduce the waste to powder. The powder was transferred to the crucible of the analyser. Each analysis was repeated at least in duplicate. Tests were performed at a flow rate of 40 ml/min under an inert nitrogen atmosphere. The sample was heated to a temperature of 600ºC at four different heating rates: 5ºC/min, 10ºC/min, 20ºC/min and 40ºC/min. Both thermodynamic aspects (global exo- or endothermicity of the process) and kinetic aspects of processes involving mass loss, such as pyrolysis, can thus be studied.
In the case of proximate analysis, 100 ± 5 mg of the sample was heated from room temperature to 900 °C in a nitrogen atmosphere. In this case, in the last part of the analysis, the sample is exposed to air for oxidation and determination of the ash content.

2.1.1.3. Operative Condition

In order to carry out the experimental analyses, it is necessary to determine the appropriate operating temperatures. These are chosen on the basis of the results of the thermogravimetric analysis. From the TG curve, it is possible to determine the degradation temperature range of the sample under study; looking at both the TG curve and the corresponding derived curve (DTG), it is possible to identify the temperature of maximum degradation rate as the minimum of the DTG curve and the corresponding inflection point of the TG curve.
The thermogravimetric study is carried out by heating a sample quantity (of the order of mg), specific for each model compound analysed, from room temperature to 600 ºC in an inert atmosphere at a heating rate of 10 ºC/min.
On the basis of the curves obtained, the operating temperature for each compound to be pyrolysed is selected around the temperature of maximum degradation rate. This is done in order to optimise the pyrolysis process and to evaluate the effect of temperature on it. Pyrolysis of the feedstock is carried out once the operating temperatures have been determined.

2.1.1.4. Experimental apparatus and Procedure

A half-batch reactor under atmospheric pressure and an inert atmosphere of argon was used to thermally treat the waste used in this thesis. The piping and instrumentation diagram (P&ID) of the apparatus is shown in Figure 2.

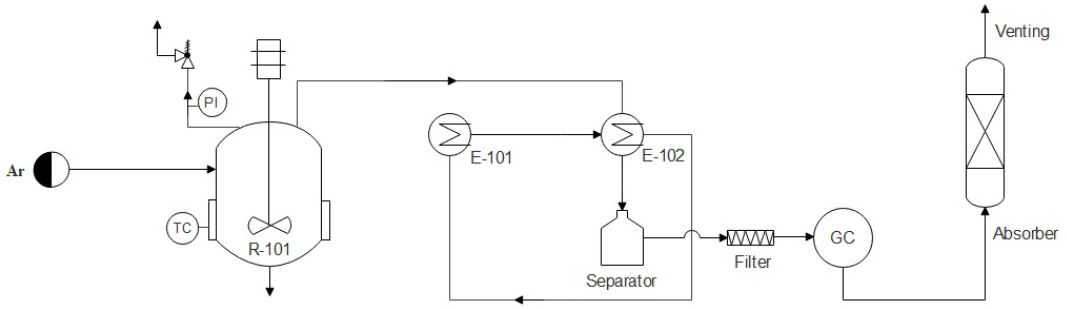

Figure 2 *P&ID of the experimental apparatus used for slow pyrolysis*

The R-101 reactor is an autoclave stirred reactor with a volume of 500 mL. It was purged with argon to remove air from the system and to avoid oxidation phenomena. The reactor was heated by electric heating bands at an average rate of 10°C/min from room temperature to the temperature selected for pyrolysis according to the maximum degradation rate of the feedstock determined by thermogravimetric tests. The gas stream produced was sent to the E-102 condenser and cooled with a water-glycol mixture. The heavier and condensable species were collected in the separator. The temperature was kept constant at 20°C by the E-101 refrigeration unit. In this way, the gas fraction was sent to the gas chromatograph (GC) for analysis of its composition. The adsorption column with activated carbon is necessary for the significant reduction of the content of hazardous compounds from the gas stream prior to venting. All experiments were performed at least twice. Finally, the biochar that was produced was collected.

Biochar produced by pyrolysing carob waste at three different temperatures (i.e. 280, 340 and 400°C) is referred to as BC280, BC340 and BC400. Biochar produced from carob waste is generally referred to as *cw*BC. Biochar produced by pyrolysis of digestate is called *d*BC.

2.1.1.5. Biochar Particle Characterization

Solid fractions higher heating value, HHVs, were determined with Parr 6200 calorimeter. In this case, 1 g of the sample was introduced in Parr 1108 style oxygen bomb and each analysis was repeated in duplicates.

The size of biochar particles was measured using a Malvern Mastersizer 2000 granulometer. The Mastersizer 2000 granulometer was equipped with Malvern Hydro 2000 MU that uses a stirrer for the dispersion of 1 gr of samples into 800 mL of deionized water. All the analyses were carried out at two different stirrer velocities of 2000 and 3000 rpm, after 5 min of sonication. The diameter size distribution was plotted after performing measurements on six different samples. From this measurement, it was extrapolated the particle distribution curves. Three factors, d10, d50 and d90, have been calculated, they represent the maximum diameter value of 10%, 50% and 90% of the particles, respectively.

The microstructure of biochar particles obtained after pyrolysis treatment was investigated using a scanning electron microscope (SEM, Quanta 200 ESEM, FEI, Hillsboro, OR, USA). Prior to SEM analysis, biochar particles were sputtered (Scancoat Six Edwards, Crawley, UK), with a thin layer of gold under argon atmosphere for 90 s, in order to avoid electrostatic charging under electron beam.

A Spectrum One (Perkin Elmer, Shelton, CT, USA) was used to record IR spectra using eight scans at a resolution of 4 cm^{-1}, on attenuated total reflectance (ATR) mode in the range 4000–450 cm^{-1}.

On biochar obtained from carob waste (*cw*BC), the elemental analysis, *i.e.* the determination of carbon hydrogen and nitrogen has been performed by means of a TruSpec CHN LECO 628 (ASTM D5373) analyser. In this case, about 100 ÷ 150 mg of dried grinded and homogenized sample was introduced in the apparatus.

On biochar obtained from digestate (*d*BC), EDX analysis has been carried out for the characterisation of the elemental composition of the *d*BC surface at two different

magnifications: 50x and 1000x, to evaluate the elemental concentration of the *d*BC in qualitative and quantitative terms.

The 1,1.diphenyl-2-pycryl (DPPH, supplied by Sigma Aldrich) free radical scavenging assay was carried out [1]–[3]. First, a methanol solution of DPPH (10^{-4} M) was prepared, then 1 mg of solid was placed in 2 ml of this solution for 24h at 25 °C. The solutions were kept at 25 °C during the time required by the measurement. Then the supernatant liquid was removed, and the UV-vis spectrum recorded at different step times achieving 24h in a Beckmann DU-800 spectrometer. Spectra were recorded on a spectrophotometer equipped with a Peltier temperature controller. Moreover, a study of *cw*BC and *d*BC concentration was performed, adding 1, 2, 5 and 10 mg of solid in the methanol solution of DPPH (10^{-4} M), recording spectra at the end of 24h. Scavenging activities were determined from the drop in absorbance at 517 nm of each sample compared with that of the DPPH solution in the absence of contact with the material. Scavenging efficiency values were calculated by the following equation:

$$Radical\ Scavenging\ Efficiency\ (\%) = \frac{A - B}{A - 0.1} \times 100$$

where A is the absorbance at 517 nm of the DPPH solution and B the one of the DPPH solution after contact with the solid.

2.1.2. Results and discussion

2.1.2.1. Carob Waste Properties

In order to evaluate the suitability of the carob waste as a feedstock for pyrolysis conversion to biochar, the proximate analysis (air-dried basis) was performed using thermogravimetric analysis. The trend obtained is shown in Figure 3. It is well known that the content of fixed carbon is related to the yield of solids, while the content of volatiles is related to the yield of gases and liquids [4].

The carob waste is characterised by a relatively low moisture content, which is 5.1 % by weight (on an air-dried basis). The volatile matter and the fixed carbon are 38.3 % by weight and 52.8 % by weight, respectively. Furthermore, the final ash value is 3.8 %wt. Therefore, the high value of fixed carbon suggests that the carob waste can be considered as a suitable feedstock for producing biochar particles.

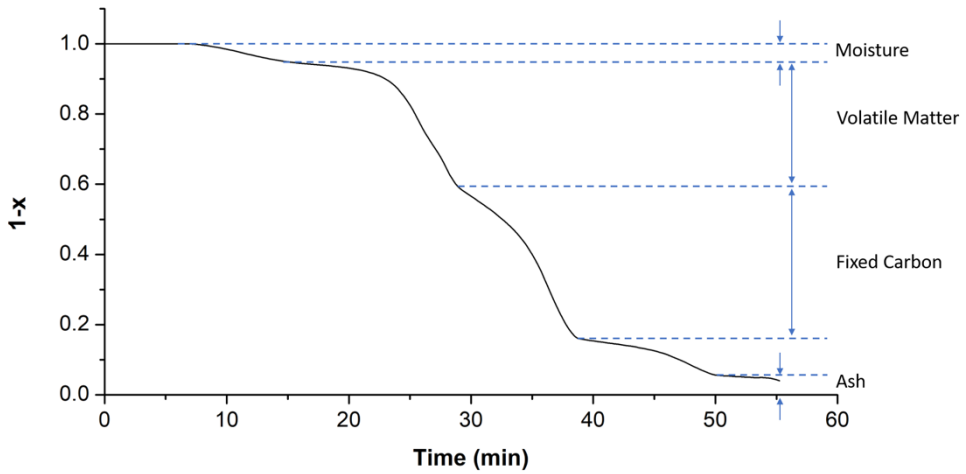

Figure 3 *Proximate Analysis of carob waste*

The Figure 4 shows the TG and DTG curves of carob waste obtained in an inert atmosphere at different heating rates (5, 10, 20 and 40 ºC/min), heating 90±5 mg of the sample from room temperature to 600 ºC.

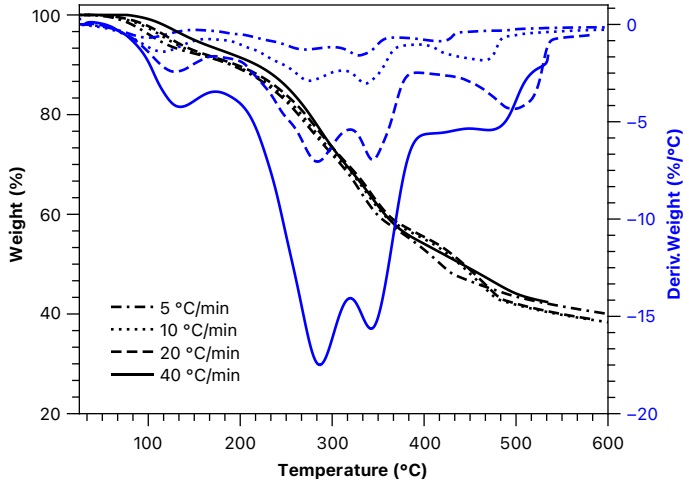

Figure 4 *TG and DTG curves of carob waste*

Table 3 Degradation temperature and weight loss as a function of heating rate of Carob Waste

	1st Peak [°C]	2nd Peak [°C]	3rd Peak [°C]	4th Peak [°C]	Weight Loss [%]
5 °C/min	99.98	270.49	328.98	416.48	60,29
10 °C/min	116.05	274.55	336.55	464.54	61.93
20 °C/min	128.50	284.01	344.00	498.50	67.21
40 °C/min	135.01	286.51	342.51	470.51	-

As the heating rate is increased, there is a slight shift in the TG and DTG curves towards values of higher temperature, even though the TG curves can be considered to overlap on the whole. It is possible to deduce a slight influence of heating rate on pyrolysis of feedstock. In addition, the DTG trends show four different well-differentiated peaks corresponding to four different stages of carob waste degradation phenomena. The thermal degradation of carob waste, comparable to a biomass degradation pathway, is a complex process consisting of:

- *Moisture Removal* (related to moisture and very high volatiles components)
- *Hemicellulose degradation* (270 ÷286 °C)

- *Cellulose and lignin degradation* (329 ÷ 343 °C)
- *Lignin decomposition* (416 ÷ 470°C).

Thus, carob waste was pyrolysed at three different operating temperatures, *i.e.* 280, 340 and 400 °C, considering a slow pyrolysis heating rate of 10 °C/min and based on TG/DTG curves. In fact, at this heating rate, the carob waste shows that the degradation of hemicellulose takes place at 274.5 ◦C, while the degradation of lignin and cellulose structure and the decomposition of lignin take place at 336.3 ◦C and 464.5 ◦C, respectively. The temperatures at 280 °C and 340 °C were chosen to maximize the rate of decomposition, while the temperature at 400 °C was chosen as a compromise between the need for high weight loss and the need for energy conservation compared to 464.5 °C.

The pyrolysis was carried out at a heating rate of 10 °C/min from room temperature to the final temperature. With regard to the mass yield of the products, the mass of the gas phase produced was calculated from the mass balance of the system as follows:

$$m_{gas} = m_{feed} - m_{liquid} - m_{biochar}$$

Figure 5 compares the yields obtained for each experiment, considering the three different pyrolysis temperatures, *i.e.* 280, 340 and 400°C. At the end of each pyrolysis experiment, when the temperature of the system was low enough, the liquid phase and the biochar were collected and weighed. Liquid phase yields increase with increasing temperature from 17% wt at 280°C to 27% wt at 400°C. The solid phase is the predominant fraction, and the mass yields decrease with increasing temperature from 67 wt% at 280 °C to 48 wt% at 400 °C. This is typical for slow biomass pyrolysis [5], [6]. The results obtained can be understood by considering that the slow pyrolysis regime maximises the production of the solid fraction. This is also reported in the literature [7]. Furthermore, a high value of fixed carbon, which typically leads to a higher solid yield, was observed in the proximate analysis of the carob waste.

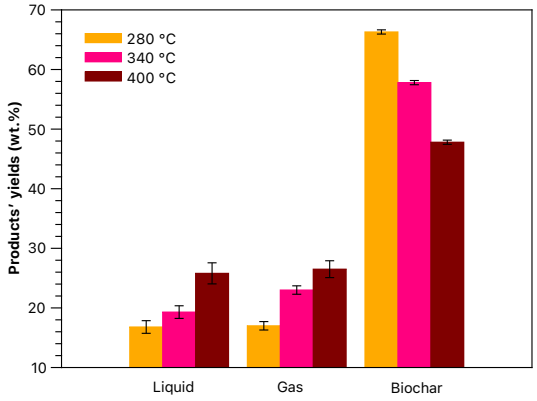

Figure 5 *Product's yields at each pyrolysis temperature*

2.1.2.2. Carob Waste-derived Biochar (cwBC) Properties

Carob waste biochar (*cw*BC) has been fully characterised. Firstly, the HHV of the solid fractions, which is the amount of heat released by the unit mass once it has been burned and the products have returned to a temperature of 25 °C (including the latent heat of vaporisation of water), was determined using a Parr 6200 calorimeter. The HHVs of the solid fractions are 23.5 MJ/kg at 280 °C, 25.1 MJ/kg at 340 °C and 28.6 MJ/kg at 400 °C and increase with increasing temperature.

The size of the *cw*BC particles obtained at the three different pyrolysis temperatures were measured using a sonic granulometer, which allowed the size distribution curves of the particles to be obtained, see Figure 6(a). Since the grinding conditions were the same for all three particles, the difference in the dimensions of the three different *cw*BC is a direct result of the pyrolysis conditions and the resulting fragility. The factors d10, d50 and d90 were also calculated. They represent the maximum diameter values of 10%, 50% and 90% of the particles, respectively, see Figure 6(b). Looking at the decrease of d90, as the pyrolysis temperature increases, and at the size distribution curves, it's possible to assume that overall BC400 show the smaller dimension compared to the other particles. As far as d50 is concerned, the maximum

value was obtained for the particles pyrolysed at 340°C. Interestingly, the d10 remains almost the same for the three different particles.

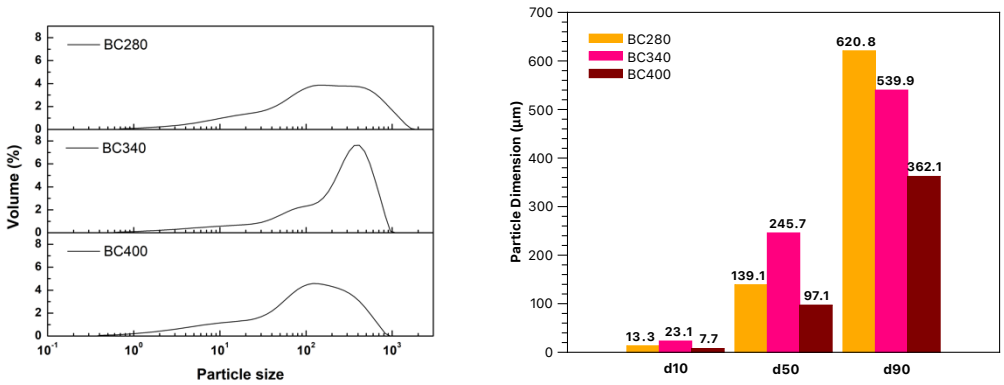

(a) *(b)*

Figure 6 *(a) Curve of diameter distribution and (b) d10, d50 and d90 factors for cwBC produced at different temperatures from the pyrolysis of carob waste.*

In Figure 7(a), the ATR-FTIR spectra of the carob waste prior to the pyrolysis process and of the biochar obtained at the three different process temperatures are shown. The ATR-FTIR spectra show the reduction of typical lignocellulosic peaks with increasing pyrolysis temperature. In fact, the ATR-FTIR spectrum of carob waste shows a broad band between 3300-3600 cm^{-1} due to ν_{OH}. This band decreases significantly for BC280 and even more so for BC340 and BC400. Furthermore, in agreement with the DTG curve, the signals of the saturated symmetric and asymmetric peaks of ν_{C-H} at 2930 and 2850 cm^{-1} begin to disappear at BC340, the temperature at which the maximum degradation rate of hemicellulose occurs, and no signal is detected at BC400. In addition, $\nu_{C=O}$ (1732 cm^{-1}) and $\nu_{C=C}$ between 1680 and 1480 cm^{-1}, usually attributed to the presence of aromatic structures, remain also for BC400. This is because lignin degradation occurs at a higher temperature according to the DTG curve. Thus, the predominant functional group related to the hemicellulose structure and part of the lignin structure are lost as the temperature increases. This result is also apparent in the following SEM micrograph. In fact, Figure 7(b), the micrograph of BC280, shows a typical lignocellulosic structure,

whereas Figure 7(d), the micrograph of BC400, appears as a carbonaceous particle. In addition, the morphology of BC340 in Figure 7(c), shows an intermediate structure.

Furthermore, CHN elemental analysis was performed on the ground carob waste and *cw*BC particles pyrolysed at different temperatures. The results obtained are presented in Table 4. The results show that, according to the literature [8], the carbon content in *cw*BC increases with increasing pyrolysis temperature. This is due to the carbonisation and thermochemical decomposition of the biomass. Thus, the structures of cellulose, hemicellulose and lignin are involved to a different resistant graphitic bond, which can be related to the different dimension of the particles after the same milling process.

The radical scavenging activities of the *cw*BC particles were investigated in order to assess their chemical activity. In particular, the scavenger activities of *cw*BC were determined from the decrease in absorbance at 517 nm of each sample caused by the interaction of DPPH and *cw*BC upon dispersion in methanol solution. Initially, the kinetics of the scavenger activity was studied by monitoring the scavenger efficiency as a function of time, see Figure 8*(a)*, keeping the amount of *cw*BC constant.

The graph in Figure 8*(a)* shows a similar scavenging efficiency from BC280 to BC340, although in the latter case a slightly slower scavenging kinetic was observed. On the other hand, for BC400, there is a significant decrease in both the efficiency and the rate of scavenging, with the efficiency never exceeding 40% even after 24 h.

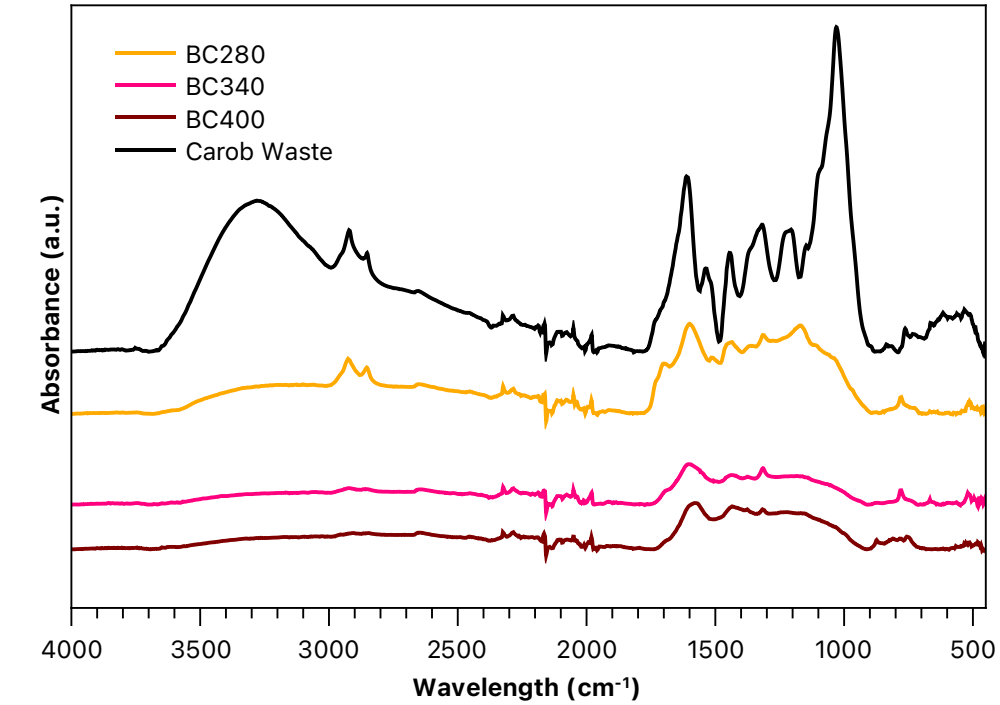

(a)

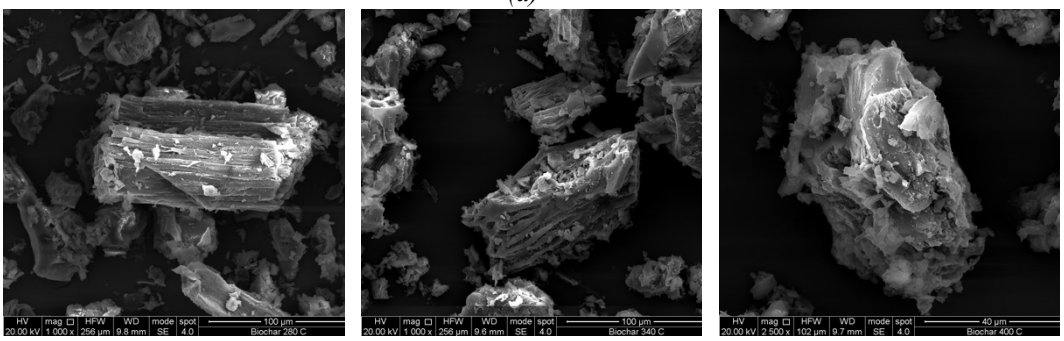

(b) *(c)* *(d)*

Figure 7 *(a) ATR-FTIR spectra of carob waste before pyrolysis process and of biochar obtained at different pyrolysis temperature and SEM morphologies of (b) BC280, (c) BC340 and (d) BC400.*

Table 4 Elemental Composition of Carob Waste and Biochar particles

	%C	%H	%N
Carob Waste	46.94 ± 0.7	1.63 ± 0.04	5.44 ± 0.04
BC 280	65.20 ± 0.2	1.75 ± 0.07	4.29 ± 0.02
BC 340	68.90 ± 0.3	1.87 ± 0.09	3.79 ± 0.03
BC 400	73.10 ± 0.2	2.09 ± 0.02	3.34 ± 0.06

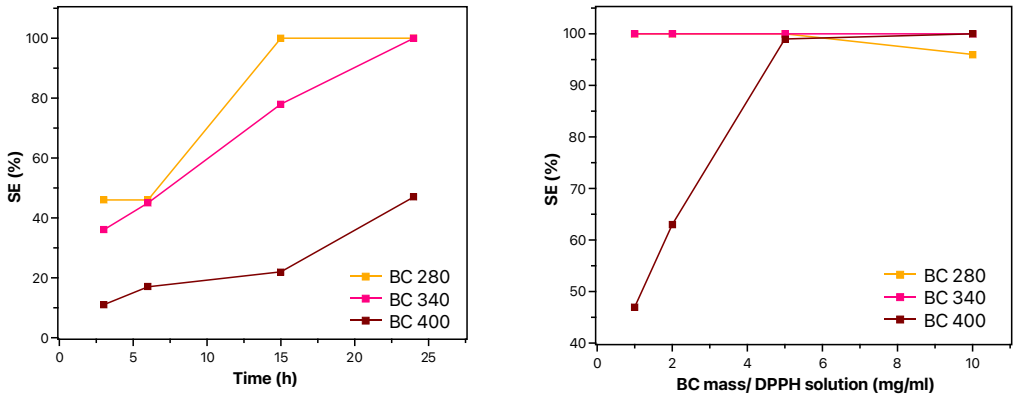

(a) *(b)*

Figure 8 *Scavenging Efficiency of (a) 1 mg/ml of solid as function of time and (b) varying the content of solid in DPPH solution after 24h*

The above result is in perfect agreement with the information obtained from the FT-IR and SEM studies, taking into account the carbonaceous nature of the BC400 sample. An analysis was then carried out by increasing the amount of *cw*BC and measuring after 24 hours, see Figure 8(b). Owing to the presence of some residual functional groups in BC280 and BC340, the particles show faster kinetics in scavenging free radicals in solution and the scavenging efficiency remains almost constant with increasing *cw*BC amount, see Figure 3b. Instead, it is necessary to increase the amount of BC400 to 5 mg in 2 ml of DPPH solution to achieve approximately 100% scavenging efficiency for BC400.

2.1.2.3. Digestate Properties

Anaerobic digestion is a biological treatment that uses micro-organisms that degrade biodegradable material in the absence of oxygen, in our case the organic fraction of municipal solid waste (OFMSW), for waste management or energy production. The products of anaerobic digestion are: Biogas, which is essentially a mixture of CH_4 and CO_2 (and trace amounts of molecular nitrogen and hydrogen), digestate and water [9]–[11]. Thus, digestate represents a by-product of anaerobic digestion and it can be used in horticulture, nursery in pots and in soil, in seeding meadows, etc. and also be used and marketed as "compost improver" based on the provisions of the fertiliser legislation.

In this thesis digestate has been used as a feedstock for biochar production after characterisation. Firstly, a proximate analysis was carried out on dried digestate to determine the partitioning into moisture, volatiles, fixed carbon and ash. Figure 9 and Table 5 show the results of this analysis.

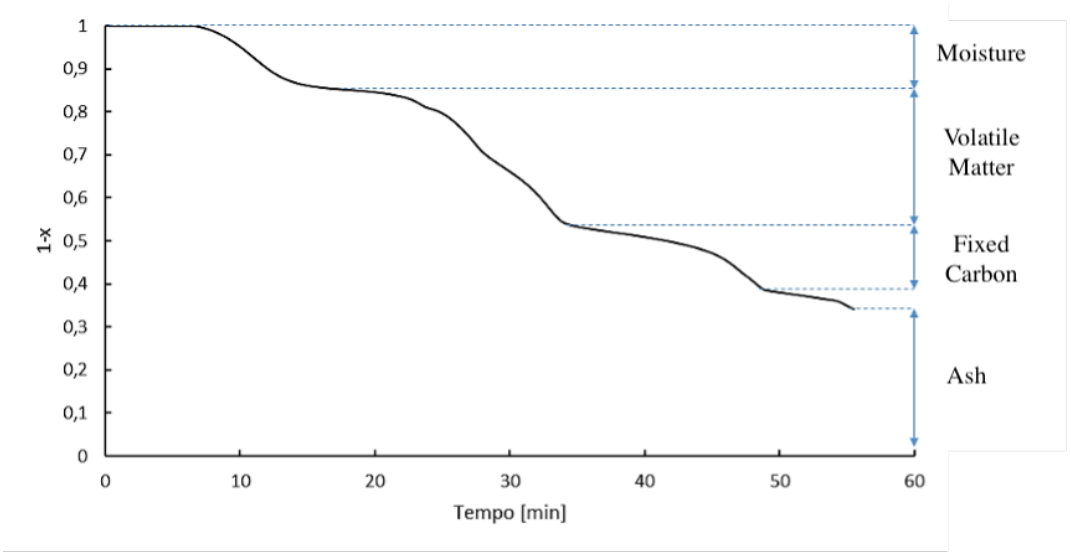

Figure 9 *Proximate Analysis of Digestate*

Table 5 Proximate Analysis air-dried basis

	[%wt]
Moisture	14,8
Volatile Matter	32,0
Fixed Carbon	19,1
Ash	34,1

As can be seen from the Table 5, the digestate has a relatively high moisture content of 14.8 wt.%. This means that it must be dried prior to pyrolysis in order to reduce its content. At 19.1 wt.% and 34.1 wt.% respectively, the amount of fixed carbon and ash exceeds 50 wt.% of the initial weight of the sample. From this it can be concluded that the predominant fraction produced by the pyrolysis process will be the solid fraction. In fact, the percentage of fixed carbon is related to the biochar yield of the pyrolysis process. Finally, the content of volatile compounds is 32 wt.% by weight. These results are consistent with those reported in the literature for similar feedstocks [12].

Figure 10 shows the TG and DTG curves of digestate obtained in an inert atmosphere at different heating rates (5, 10, 20 and 40 ºC/min), heating 60±5 mg of the sample from room temperature to 600 ºC. It is evident that as the heating speed rises, the TG and DTG curves shift towards higher temperatures. In this case, this phenomenon is more pronounced compared to the curves for carob waste (see Figure 4). From this, it is possible to deduce that the heating rate has a more significant effect on the degradation process of the digestate. Due to the heterogeneity of the digestate, the DTG curves have four peaks for each heating rate analysed. This implies that the degradation process takes place in at least three reactive steps and that at each detectable peak temperature will correspond to the degradation of a specific compound that constitutes the digestate.

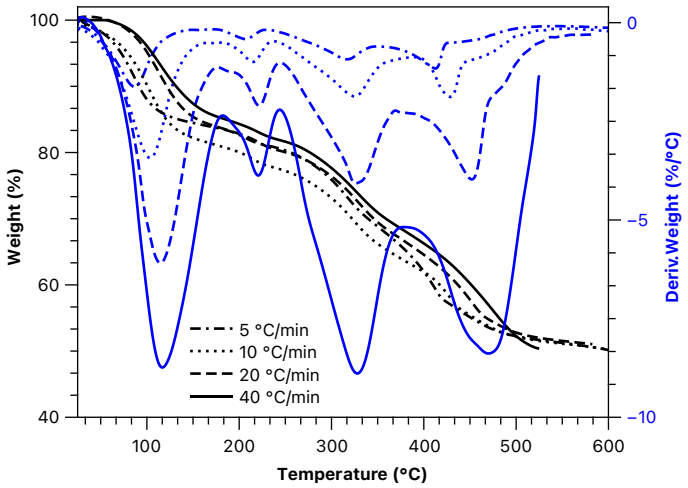

Figure 10 *TG and DTG curves of Digestate*

Table 6 Degradation temperature and weight loss as a function of heating rate of Digestate

	1st Peak [°C]	2nd Peak [°C]	3rd Peak [°C]	4th Peak [°C]	Weight Loss [%]
5 °C/min	86.45	206.94	316.92	412.44	50.1
10 °C/min	103.88	214.87	325.38	428.88	49.6
20 °C/min	114.58	221.56	326.08	452.08	49.3
40 °C/min	116.97	220.47	327.96	460.94	-

The Table 6 summarizes the peak temperatures and their weight loss obtained by thermogravimetric analyses at different heating speeds. Also in this case, the peak in the around of 100°C is characteristic of the removal of moisture and very light volatile components. As can be seen from the TG curves, the mass of the sample begins to decrease from about 100 ºC for each heating rate analysed. The second peak is excluded because it is located at around 200°C, which is too low for a pyrolysis process.

On the basis of the thermogravimetric analysis carried out at a heating rate of 10°C/min and following the considerations made for the carob samples, the operating temperatures for the experimental test of slow pyrolysis of the digestate under investigation were chosen.

The pyrolysis was carried out at a heating rate of 10 °C/min from room temperature to *i.e.* 400°C, close to the last peak of thermal degradation. The mass yield of the products, calculated from the mass balance of the system as in following equation, is shown in Figure 11.

$$m_{biochar} = m_{feed} - m_{liquid} - m_{gas}$$

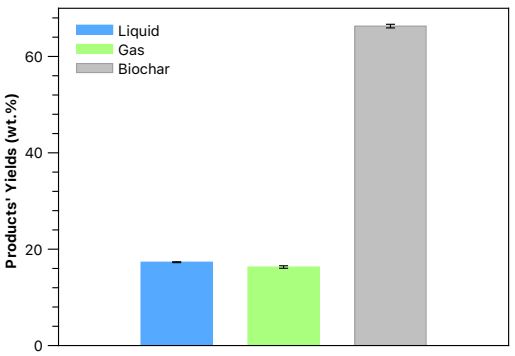

Figure 11 *Products' Yields of digestate pyrolysis*

As expected, the yield of biochar is high and is equal to 66 wt.%. Indeed, the proximate analysis of the digestate, characterised by high fixed carbon content and residual ash, predicted this result. However, the yields of the liquid and gaseous fractions are comparable, both around 17% by weight. These results correspond to those reported in the literature for similar compounds [13], [14].

2.1.2.4. Digestate-derived Biochar (dBC) Properies

The biochar obtained from pyrolysis of digestate (*d*BC) has been fully characterized. Firstly, the HHV of the solid fractions, which is the amount of heat released by the unit mass once it has been burned and the products have returned to a temperature of 25 °C (including the latent heat of vaporisation of water), was determined using a Parr 6200 calorimeter. The HHVs of the solid fractions is equal to 9.7 MJ/kg.

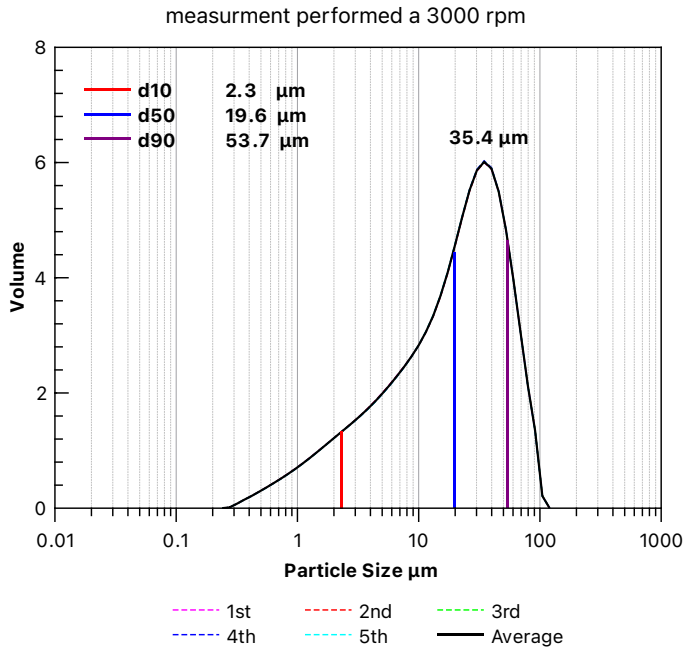

Figure 12 *Curve of diameter distribution and d10, d50 and d90 factors for dBC produced at different temperatures from the pyrolysis of digestate.*

To improve quality of *d*BC particles, after pyrolysis, the resulting biochar was ground in a mechanic mortar and sieved to below 45 µm. In Figure 12 the particle-size distribution curve after milling and sieving process is reported. The final size of *d*BC particles has been measured using a granulometer with ultrasound treatment with a stirrer velocity of 3000 rpm. The factor, d10, d50 and d90 that represent the maximum diameter values of 10%, 50% and 90% of the particles, respectively, were calculated. According to the SEM morphology (see Figure 13 (b,c)), almost all the particles have a diameter smaller than 100 µm: thanks to the d10 factor, it is possible to state that at least 10% of the particles have a diameter smaller than 2.3 µm. In fact, sonication during the Mastersizer measurement breaks up the agglomerates and brings them into solution. The sieving process was efficient: the maximum of the particle size distribution curves is equal to 35.4 µm and it is certain that 90 v.% of the particles have a diameter lower than 53.7 µm.

In order to chemically characterise the biochar, ATR-FTIR analysis of the *d*BC was carried out and compared with the digestate prior to pyrolysis, and EDX measurements of the char were carried out. It is possible to compare the digestate spectra with a biomass spectrum, knowing that the digestate was mainly composed of the organic fraction. Indeed, the ATR-FTIR spectra show a reduction of several characteristic lignocellulosic bands, for example: The broad band between 3300-3600 cm^{-1} with a maximum at 3288 cm^{-1} (ν_{OH}, OH stretching vibrations of hydrogen-bonded hydroxyl groups), the two peaks at 2920 and 2948 cm^{-1} (asymmetric and symmetric CH stretching vibrations of aliphatic groups), the peak at 1628 cm^{-1} (related to aromatic C=C stretching and C=O stretching modes). Instead, there are bands whose intensity increases after the pyrolysis process: the peak at 1420 cm^{-1}, related to aromatic structural vibrations, the peak at 1026 cm^{-1}, normally related to C-O stretching, the two peaks at 876 and 778 cm^{-1}, related to aromatic C-H deformation modes [15]–[17].

Thermal cracking is responsible for breaking chemical bonds to rearrange them into new functional groups. The reduction of hydrogen-bonded hydroxyl groups, aliphatic groups, and C=C and C=O aromatic groups (which appears to be partial rather than complete) can be attributed to incomplete thermal degradation of the feedstock. As stated before, at 400°C, hemicellulose, cellulose and some lignin degradation occurred. The rearrangement of these chemical structures as a result of the pyrolysis process can be seen by the increase in certain bands, such as: the peak at 1420 cm^{-1}, related to aromatic structural vibrations, the peak at 1026 cm^{-1}, normally related to C-O stretching, the two peaks at 876 and 778 cm^{-1}, related to aromatic C-H deformation modes [15]–[17].

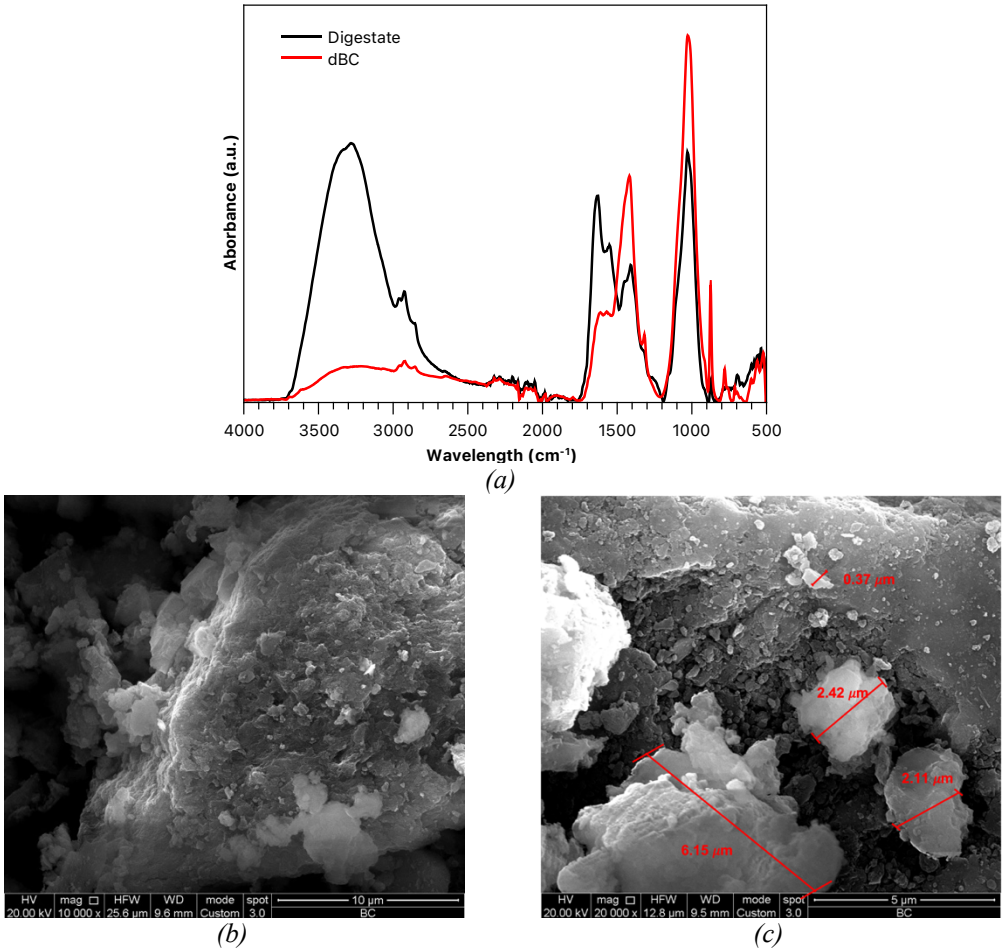

Figure 13 *(a) ATR-FTIR spectra before and after pyrolysis and SEM micrographs at (b) 10000x and (c) 20000x*

Furthermore, EDX analysis has been carried out for the characterisation of the elemental composition of the *d*BC surface at two different magnifications: 50x and 1000x, to evaluate the elemental concentration of the *d*BC in qualitative and quantitative terms. Although some elemental concentrations differ by a few percentage points, the sample results are homogeneous. However, there is an intrinsic error in weight determination for all atoms with an atomic weight less than sodium. Nevertheless, several elements have been detected by EDX spectroscopy, from carbon to iron and titanium, as shown in Figure 4 and Table 2. It can be stated that *d*BC is mainly carbon and oxygen. Other components present in significant

amounts include: aluminium, silica, phosphorus, potassium and calcium. It is important to highlight the presence of iron in low concentration [18]–[20], for the following characterisation of the composite. The inhomogeneity of OFMSW and its inorganic components, such as bones and table salt, present in the initial food waste, are responsible for the high diversity and quantity of inorganic contents.

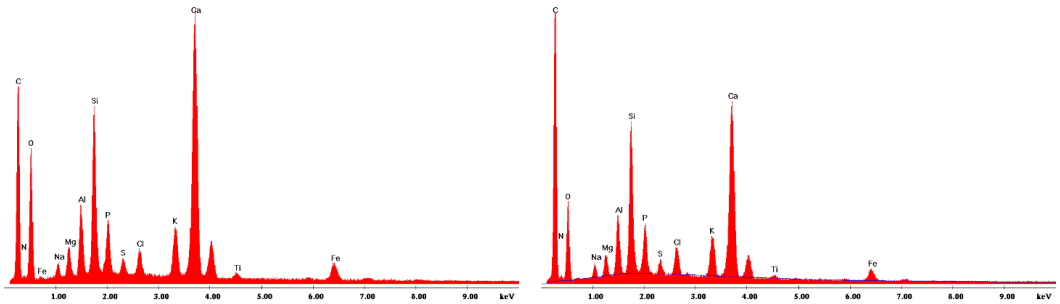

(a) *(b)*

Figure 14 *EDX spectra of biochar obtained by slow pyrolysis of digestate at 400 °C and 1 atm at (a) 50x and (b) 1000x of magnitude.*

Table 7 EDAX analysis and Elemental concentration

Element	**50x [wt.%]**	**1000x [wt.%]**	**Element**	**50x [wt.%]**	**1000x [wt.%]**
C	49.44	62.74	*P*	1.40	1.29
N	3.68	4.09	*S*	0.37	0.34
O	24.99	16.23	*Cl*	0.61	0.69
Na	0.85	0.72	*K*	1.38	1.12
Mg	1.11	0.78	*Ca*	8.30	5.49
Al	2.06	1.66	*Ti*	0.24	0.15
Si	4.37	3.84	*Fe*	1.20	0.83

The radical scavenging activities of the *d*BC particles were investigated in order to assess their chemical activity. In particular, the kinetics of scavenger activities of *d*BC was determined from the decrease in absorbance at 517 nm of each sample caused by the interaction of DPPH and *d*BC upon dispersion in methanol solution as a function of time keeping constant the *d*BC amount, see Figure 15. The graph shows that after 15 min the scavenging efficiency is already equal to 25 %, and it achieve 50 % after less than 4 hours. At 24h, at the end of measurement, results equal to 90%.

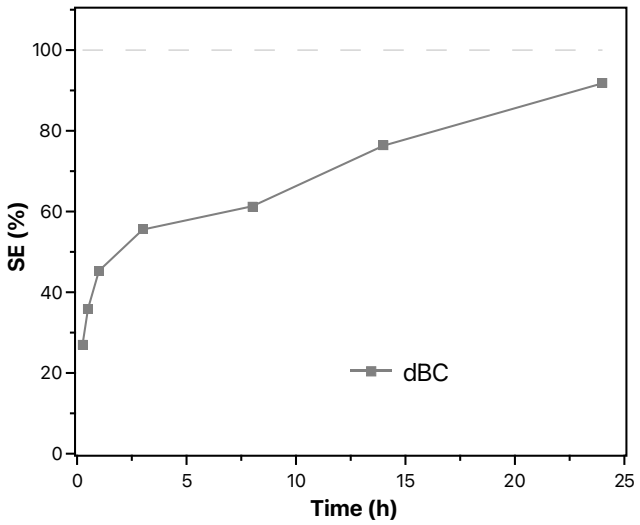

Figure 15 *Scavenging Efficiency of 1 mg/ml of solid as function of time*

2.1.3. Endings

In this chapter, two different bio-wastes were first characterised in order to select the operating conditions for the slow pyrolysis process. Later, the slow pyrolysis has been counted, also characterising the product yields of the pyrolysis. Finally, the particles were characterised with the intention of using the solid residue as a filler for reinforced photo-resistant composite materials. Chemical characterisation by elemental composition and/or EDX analysis and spectroscopic analysis was carried out. Morphology, particle size distribution and evaluation of radical scavenging activity and efficiency were also studied.

Regarding the carob waste, it has a high level of fixed carbon that makes it suitable for converting into value-added biochar to reinforce biocomposite applications. After pyrolysis, the carbon content of *cw*BC increases as the temperature of the pyrolysis process increases. However, at lower pyrolysis temperatures, *cw*BC particles showed higher scavenging efficiency. In fact, BC280 showed the faster free radical scavenging kinetics in DPPH solution, which will be confirmed in the composite photo-oxidation study in a later chapter. However, the study of the scavenging efficiency as a function of *cw*BC concentration in DPPH solution showed that above a concentration of 5 mg/ml, BC340 and BC400 offered comparable scavenging efficiencies to BC280. Moreover, the three different size distribution curves are a direct result of the differences in chemical structure and composition related to the pyrolysis temperature condition and the consequent fragility, since the grinding conditions were the same for the three particles. In particular, the particle size decreases as the pyrolysis temperature increases. This result will obviously have an impact on the dispersion and mechanical stability of the composites produced, which will be discussed in the later chapter (see 2.4.).

On the other hand, digestate, the result of the digestion of the organic fraction of municipal solid waste (OFMSW), is suitable for biogas production due to its high concentration of volatile compounds. Moreover, a high amount of ash was also

found, and the high variety and quantity of inorganic contents are attributed to the inhomogeneity of OFMSW and its inorganic components, such as bones and common salt, present in the original food waste. Furthermore, a better particle size distribution curve than that obtained with locust bean was obtained by pressing and sieving the biochar after the pyrolysis process. Good radical scavenging kinetics were obtained and a higher concentration of functional groups on the surface was detected.

References

[1] R. Teresi *et al.*, 'Improvement of oxidation resistance of polymer-based nanocomposites through sonication of carbonaceous nanoparticles', *Ultrasonics Sonochemistry*, vol. 61, Mar. 2020, doi: 10.1016/j.ultsonch.2019.104807.

[2] Y. T. Shieh and W. W. Wang, 'Radical scavenging efficiencies of modified and microwave-treated multiwalled carbon nanotubes', *Carbon*, vol. 79, no. 1, pp. 354–362, 2014, doi: 10.1016/j.carbon.2014.07.077.

[3] X. Zhang *et al.*, 'Interaction of tannic acid with carbon nanotubes: Enhancement of dispersibility and biocompatibility', *Toxicology Research*, vol. 4, no. 1, pp. 160–168, Jan. 2015, doi: 10.1039/c4tx00066h.

[4] L. J. R. Nunes, J. C. De Oliveira Matias, and J. P. Da Silva Catalão, 'Introduction', in *Torrefaction of Biomass for Energy Applications*, Elsevier, 2018, pp. 1–43. doi: 10.1016/B978-0-12-809462-4.00001-8.

[5] M. Volpe, D. Panno, R. Volpe, and A. Messineo, 'Upgrade of citrus waste as a biofuel via slow pyrolysis', *Journal of Analytical and Applied Pyrolysis*, vol. 115, pp. 66–76, Sep. 2015, doi: 10.1016/j.jaap.2015.06.015.

[6] X. Shi and J. Wang, 'A comparative investigation into the formation behaviors of char, liquids and gases during pyrolysis of pinewood and lignocellulosic components', *Bioresource Technology*, vol. 170, pp. 262–269, Oct. 2014, doi: 10.1016/j.biortech.2014.07.110.

[7] R. W. Nachenius, F. Ronsse, R. H. Venderbosch, and W. Prins, 'Biomass Pyrolysis', in *Advances in Chemical Engineering*, vol. 42, Elsevier, 2013, pp. 75–139. doi: 10.1016/B978-0-12-386505-2.00002-X.

[8] B. Sizirici, Y. H. Fseha, I. Yildiz, T. Delclos, and A. Khaleel, 'The effect of pyrolysis temperature and feedstock on date palm waste derived biochar to remove single and multi-metals in aqueous solutions', *Sustainable Environment Research*, vol. 31, no. 1, Dec. 2021, doi: 10.1186/s42834-021-00083-x.

[9] M. Rasapoor, B. Young, R. Brar, A. Sarmah, W.-Q. Zhuang, and S. Baroutian, 'Recognizing the challenges of anaerobic digestion: Critical steps toward improving biogas generation', *Fuel*, vol. 261, p. 116497, Feb. 2020, doi: 10.1016/j.fuel.2019.116497.

[10] N. Kanaujia and J. Singh, '13 - Composition, characteristics and challenges of OFMSW for biogas production: Influence of mechanism and operating parameters to improve digestion process', in *Advanced Organic Waste Management*, C. Hussain and S. Hait, Eds., Elsevier, 2022, pp. 207–223. doi: 10.1016/B978-0-323-85792-5.00025-3.

[11] H. Shin, 'Hydrogen production from food waste in anaerobic mesophilic and thermophilic acidogenesis', *International Journal of Hydrogen Energy*, vol. 29, no. 13, pp. 1355–1363, Oct. 2004, doi: 10.1016/j.ijhydene.2003.09.011.

[12] I. Ogwang, H. Kasedde, B. Nabuuma, J. B. Kirabira, and J. D. Lwanyaga, 'Characterization of Biogas Digestate for Solid Biofuel Production in Uganda', *Scientific African*, vol. 12, p. e00735, Jul. 2021, doi: 10.1016/j.sciaf.2021.e00735.

[13] Y. Wen, Z. Shi, S. Wang, W. Mu, P. G. Jönsson, and W. Yang, 'Pyrolysis of raw and anaerobically digested organic fractions of municipal solid waste: Kinetics, thermodynamics, and product characterization', *Chemical Engineering Journal*, vol. 415, p. 129064, Jul. 2021, doi: 10.1016/j.cej.2021.129064.

[14] S. Ghysels *et al.*, 'Integrating anaerobic digestion and slow pyrolysis improves the product portfolio of a cocoa waste biorefinery', *Sustainable Energy Fuels*, vol. 4, no. 7, pp. 3712–3725, 2020, doi: 10.1039/D0SE00689K.

[15] Y. Lee *et al.*, 'Comparison of biochar properties from biomass residues produced by slow pyrolysis at 500°C', *Bioresource Technology*, vol. 148, pp. 196–201, Nov. 2013, doi: 10.1016/j.biortech.2013.08.135.

[16] Y. Liu, Z. He, and M. Uchimiya, 'Comparison of Biochar Formation from Various Agricultural By-Products Using FTIR Spectroscopy', *MAS*, vol. 9, no. 4, p. p246, Mar. 2015, doi: 10.5539/mas.v9n4p246.

[17] G. Socrates, *Infrared and Raman Characteristic Group Frequencies Tables and Charts*, Third Edition. Wiley, 2001.

[18] N. T. Dintcheva, S. Al-Malaika, E. Morici, and R. Arrigo, 'Thermo-oxidative stabilization of poly(lactic acid)-based nanocomposites through the incorporation of clay with in-built antioxidant activity', *Journal of Applied Polymer Science*, vol. 134, no. 24, Jun. 2017, doi: 10.1002/app.44974.

[19] F. P. La Mantia, N. T. Dintcheva, V. Malatesta, and F. Pagani, 'Improvement of photo-stability of LLDPE-based nanocomposites', *Polymer Degradation and Stability*, vol. 91, no. 12, pp. 3208–3213, Dec. 2006, doi: 10.1016/j.polymdegradstab.2006.07.014.

[20] L. Botta, R. Scaffaro, F. P. La Mantia, and N. T. Dintcheva, 'Effect of different matrices and nanofillers on the rheological behavior of polymer-clay nanocomposites: Rheological Behavior of Polymer-Clay Nanocomposites', *J. Polym. Sci. B Polym. Phys.*, vol. 48, no. 3, pp. 344–355, Feb. 2010, doi: 10.1002/polb.21896.

2.2. Preliminary Experimental Feasibility Study. Could Biochar replace conventional carbon particles?

Thanks to the study in the previous chapter, it is clear to us how the use of biomass for the production of carbonaceous particles can lead to advantages in the production of reinforcing and antioxidant fillers. It is known from the literature that carbon particles such as carbon black, graphene and carbon nanotubes have largely played this role over the last few decades.

Therefore, in this chapter, a comparison was made between the radical scavenging efficiency of carbon black (CB) and a commercial biochar (*c*BC*)* in order to compare the antioxidant activity of these two particles and the suitability of *c*BC to replace CB. Polypropylene (PP), a material for which we have a good understanding of carbon black behaviour, was chosen to compare the contribution to rheological and mechanical behaviour.

Considering that among carbonaceous particles, biochar (*c*BC) is more similar to carbon black (CB) in terms of shape ratio and chemical structure, the following section compares composites filled with biochar and carbon black at a concentration of 4 wt%. Furthermore, hybrid composites filled with both *c*BC and CB (*c*BC: CB weight ratios of 1:3, 2:2 and 3:1 wt%) have been studied, also considering partial substitution of CB with *c*BC. This comparison was also carried out in the case of composites in which the filler concentration of CB and *c*BC was in a hybrid form with the concentration of graphene.

2.2.1. Materials and Methods

2.2.1.1. Materials

Polypropylene Moplen ® X30G produced by LyondellBasell (LyondellBasell, Ferrara, Italy) with a melt flow index (M.F.I.) of 8 g/10 min (230 °C/2.16 Kg) and density 0.90 g/cm^3 was used for nanocomposite preparation.
Carbon Black, CB, (Super P®) is a fine black powder and it has been supplied by MTI Corporation, Richmond, CA 94804–3809, USA. Its main properties are: density: 0.16 g/cm^3; volatiles ≤ 0.15%; particles size = 40 nm; specific surface area = 62 m^2/g; ash ≤0.10%;
Graphene nanoplatelets (GnPs), under the trade name xGnP®, grade C, with average diameter between 1 and 2 μm, an average thickness lower than 2 nm, and a specific surface area of about 750 m2/g were supplied by XG Sciences Inc (Lansing, MI, USA).
Commercial Biochar powder (*c*BC), used in the food industry (Spigadoro, Perugia, Italy) was selected as filler. In particular, as indicated in the supplier's technical data sheet, this biochar was obtained from the pyrolysis of birch and beech wood.

2.2.1.2. Composites formulation

Polypropylene was used as the polymer matrix and was melt-mixed with carbonaceous filler using a coronating twin-screw extruder OMC (OMC, Saronno, Italy) with a screw diameter of 19 mm and length to diameter ratio of 35 mm. The temperature profile for polypropylene and nanocomposites was 130–140–150–160–170–180–190 °C (die), with screw speed set at 220 rpm and the gravimetric feeder set at 12 rpm.

Carbonaceous fillers in the PP matrix were either pure additives or in hybrid concentrations to achieve a total carbon content of 4 wt%. The carbonaceous particles used are described below. Sample codes with relative polymer and filler concentrations are given in Table 8.

Table 8 Sample code name with relative weight concentration

Sample	**PP** [wt.%]	***c*BC** [wt.%]	**CB** [wt.%]	**GNP** [wt.%]
PP	100			
PP/4*c*BC	96	4		
PP/4CB	96	4		
PP/4GNP	96	4		
PP/2*c*BC2CB	96	2	2	
PP/1*c*BC3CB	96	1	3	
PP/3*c*BC1CB	96	3	1	
PP/2*c*BC2GNP	96	2		2
PP/2CB2GNP	96		2	2

2.2.1.3. Particles Characterizations

The 1,1.diphenyl-2-pycryl (DPPH, supplied by Sigma Aldrich) free radical scavenging assay was carried out [1]–[3]. First, a methanol solution of DPPH (10^{-4} M) was prepared, then 1 mg of solid was placed in 2 ml of this solution for 24h at 25 °C. The solutions were kept at 25 °C during the time required by the measurement. Then the supernatant liquid was removed, and the UV-vis spectrum recorded at different step times achieving 24h in a Beckmann DU-800 spectrometer. Spectra were recorded on a spectrophotometer equipped with a Peltier temperature controller. Scavenging efficiency values were calculated by the following equation:

$$Radical\ Scavenging\ Efficiency\ (\%) = \frac{A - B}{A - 0.1} \times 100$$

where A is the absorbance at 517 nm of the DPPH solution and B the one of the DPPH solution after contact with the solid.

2.2.1.4. Composites characterization

Rheological tests were performed using a strain-controlled rheometer (mod. ARES G2 by TA Instrument, New Castle, DE, USA) in parallel plate geometry (plate diameter 25 mm). The complex viscosity (η^*) and storage (G') and loss (G'') moduli were measured by performing frequency scans from $\omega = 10^{-2}$ to 10^{2} rad/s at the same processing temperatures. The strain amplitude was $\gamma = 5\%$, which preliminary strain sweep experiments proved to be low enough to be in the linear viscoelastic regime.

Tensile tests were performed on rectangular specimens using a universal testing machine (Instron model 3365, Rochdale, UK) according to ASTM D882. The tests were performed at a tensile speed of 1 mm/min for 1 min to evaluate the Young's modulus, calculated as the slope of the initial linear portion of the engineering stress-strain curves, and then the speed was increased to 10 mm/min until the specimen broke. The average values for elongation at break, EB, modulus of elasticity, E, and tensile strength, TS, were calculated.

2.2.2. Results and Discussion

The radical scavenging activities of CB and *c*BC particles were investigated in order to assess their chemical activity. In particular, the kinetics of scavenger activities was determined from the decrease in absorbance at 517 nm of each sample caused by the interaction of DPPH and carbonaceous particle upon dispersion in methanol solution as a function of time keeping constant the particle amount, see Figure 16. The graph shows that carbon black and biochar have similar kinetics of radical scavenging, with an increase in the first 6 hours and then remaining constant. Furthermore, the scavenging efficiency of biochar is always higher than that of carbon black, regardless of time.

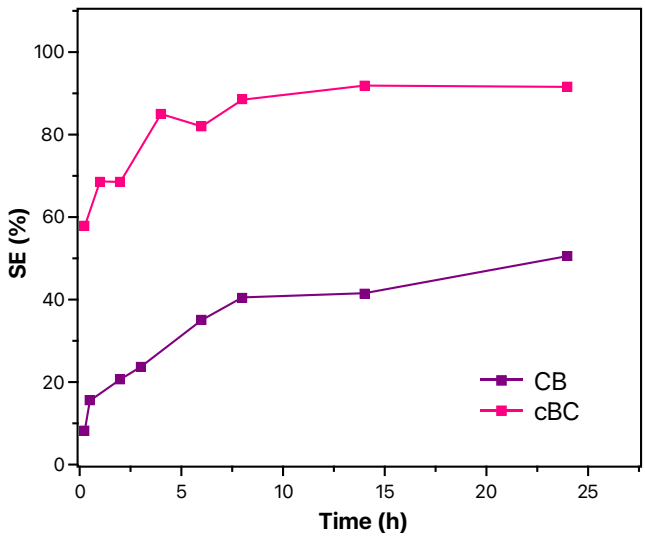

Figure 16 *Scavenging efficiency as a function of time*

The rheological behaviour of *c*BC-containing composites compared to that of unfilled PP was evaluated by oscillatory measurements. Figure 17(*a-e)* shows the complex viscosity, dynamic storage and loss modulus, distinguishing between the PP matrix filled with only one type of carbonaceous particle and the PP-based

composites filled with a hybrid concentration of carbonaceous particles, with the aim of achieving 4 wt% of the total amount of filler. For PP/4*c*BC, a global decrease in complex viscosity is highlighted by the curve, with an increase in complex viscosity at low angular frequency, due to the irregular shape of *c*BC and the consequent high interaction between the polymer chain and the biochar particles, which reduces chain mobility. In contrast, the addition of 4 wt% CB and GNP reduces the Newtonian behaviour of the pure PP matrix, showing an increase in the complex viscosity value, especially for the CB composite. In composite materials containing hybrid fillers, conventional carbonaceous fillers (CB and GNP) have been partially replaced by biochar particles. For PP/3*c*BC1CB, again a plasticising effect is highlighted by the curve, more similar to the composite with only 4 wt. % of *c*BC. By the decreasing of *c*BC particles from 3 to the 2 wt. % the complex viscosity values increase to be comparable to the ones of PP matrix, and moreover for the PP/1*c*BC3CB sample. Since biochar shown conductive properties [4], a further comparison was made for the replacement of carbon black with biochar particles in hybrid composites containing CB and GNP, which are well known for thermal and electrical conduction applications[5]. For processability point of view, complex viscosity of the two-hybrid composite (PP/2CB2GNP and PP/2*c*BCGNP) showed the same rheologic behaviour, improving the sustainability with the reducing of oil derived carbon fillers, such as CB and GNP.

Figure 17(*c-e)* shows the dynamic storage and loss modulus as a function of frequency, distinguishing all the samples studied into three groups: *(c)* PP-based with only one carbonaceous particle added, *(d)* hybrid composition of *c*BC and CB composites, varying the ratio between the two carbonaceous particles, and *(e)* hybrid composition in the presence of GNP particles; all the composite systems are compared with a pure PP matrix. In all frequency range, all investigated sample showed a liquid-like behaviour, with G''>G'. With the addition of carbon particles, the low frequency terminal slopes of G' and G" vary depending on the carbonaceous particles added to the PP matrix as shown in Table 1. When 4 wt% of oil derived

carbonaceous particles are added, a significant increase in the terminal slope of both G' and G" is highlighted. The situation is different for PP/4*c*BC where there is an imperceptible increase in the G' slope and a significant reduction in the G" slope. Consistent with these results, for composites containing biochar and carbon black at different weight ratios, as the carbon black content increases, both the G' and G" slopes increase. On the other hand, for hybrid composites based on GNP, corresponding to a complex viscosity curve, nothing changes with the addition of biochar or carbon black as a complementary filler, but the G' and G" slopes are higher with respect to the pure PP matrix.

The mechanical properties of the PP-based composites were evaluated by tensile analysis and the mechanical properties obtained, Young's modulus, tensile strength and elongation at break are summarised in Figure 18. Looking at PP-based composites with only one carbonaceous particle added, carbon black and biochar showed a great influence on the mechanical properties, increasing the Young's modulus by about 25% without reducing the elongation at break too much. 4 wt% GNP made no difference to the mechanical properties. For hybrid composite of *c*BC and CB, as the increase of *c*BC with respect to CB concentration, Young modulus increase, while maintaining constant tensile strength, and with no different contribution in varying elongation at break. For hybrid composites, unlike CB, the ability of *c*BC to disperse creates a network capable of increasing stiffness while maintaining a constant elongation at break of the final composites.

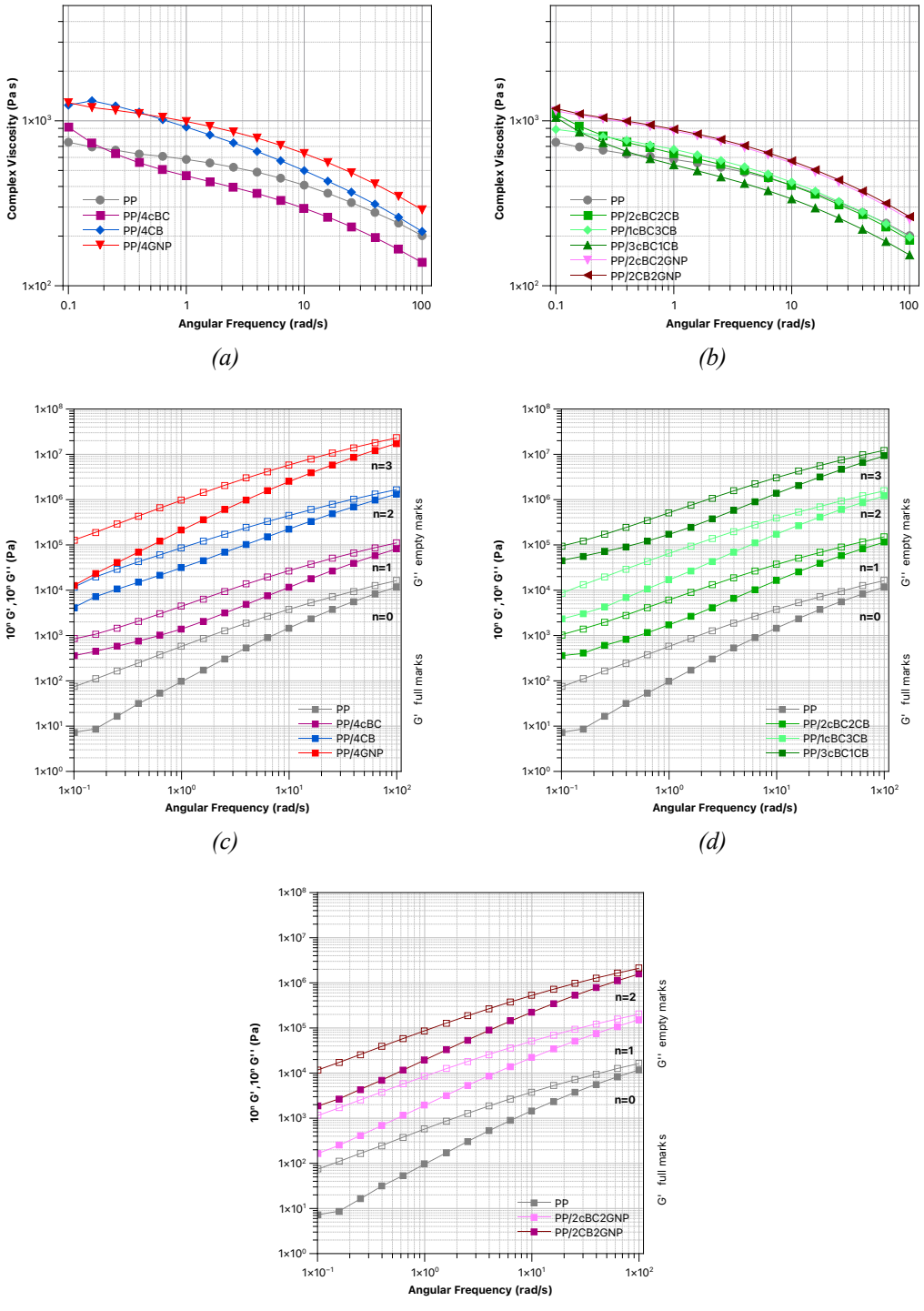

Figure 17 *Rheological behaviour of PP-based composite: (a-b) Complex Viscosity; (c-d-e) Storage G' and Loss G'' Modulus for neat PP and carbon-containing composites*

Table 9 G' and G" terminal slope at low frequency

	PP	**PP/4*c*BC**	**PP/CB**	**PP/4GNP**
G' [Pa/rad s^{-1}]	100.47	110.66	294.37	219.36
G''[Pa/rad s^{-1}]	557.63	378.51	813.32	934.12

	PP/1*c*BC3CB	**PP/2*c*BC2CB**	**PP/3*c*BC1CB**	**PP/2*c*BC2GNP**	**PP/2CB2GNP**
G' [Pa/rad s^{-1}]	164.35	152.28	137.17	197.17	815.81
G''[Pa/rad s^{-1}]	624.15	565.61	465.6	197.19	834.46

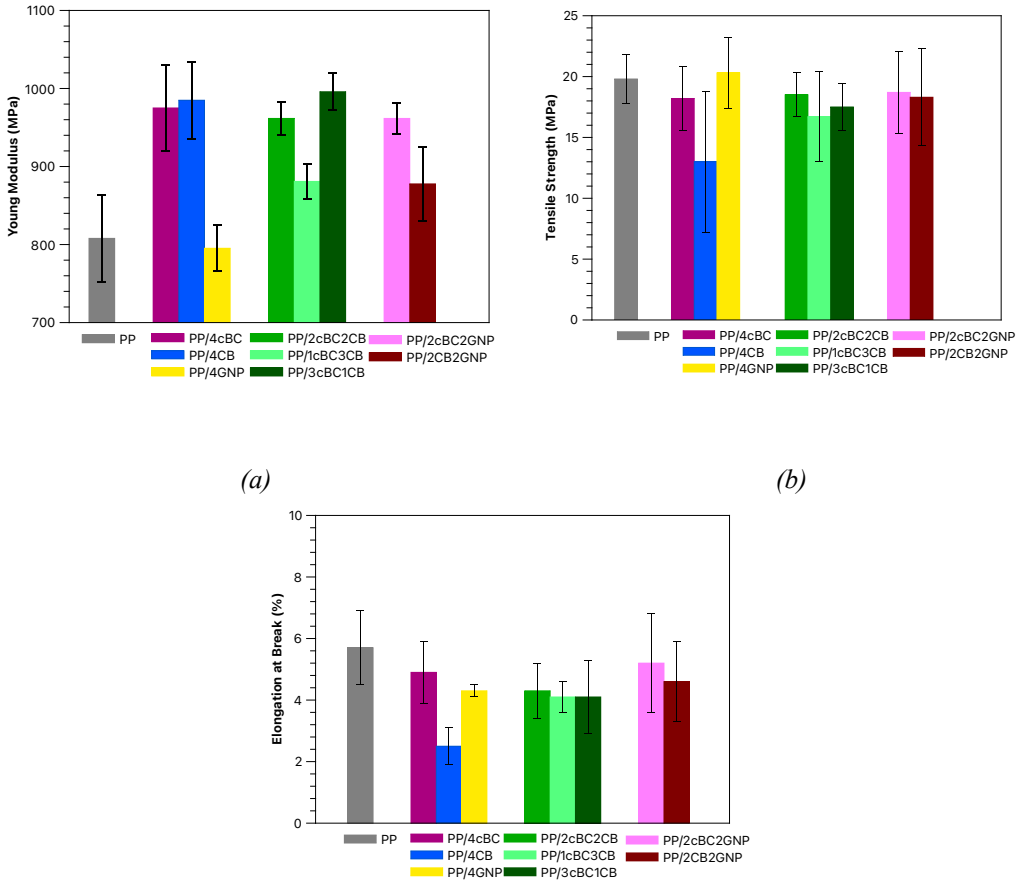

Figure 18 *(a) Young Modulus (b) Tensile Strength and (c) Elongation at Break of pp-based composites*

2.2.3. Endings

In this short chapter, an attempt was made to understand whether biochar particles could partially or fully replace carbon black as a reinforcing and antioxidant filler. Firstly, the scavenging efficiency in DPPH solution was investigated and it was shown that the scavenging efficiency of commercial biochar, *c*BC particles is much higher than that of carbon black, CB.

In terms of the rheological behaviour of the composites, the presence of *c*BC in polypropylene appears to have a plasticising effect, which can be advantageous depending on the processing chosen for the composite formulation. This plasticising effect is shown both for the pure *c*BC filled composite and, proportionally to the concentration of *c*BC with respect to CB, for the hybrid *c*BC:CB composites. When *c*BC replaces CB in the hybrid compound with GNP, the rheological behaviour remains unchanged.

In terms of mechanical properties, the presence of *c*BC particles acts as a reinforcing agent that is absolutely comparable to that offered by carbon black. This behaviour is confirmed both in pure addition and in comparison with pure CB in the PP matrix, as well as in the presence of hybrid fillers, both as co-fillers with carbon black or with graphene.

Reference

[1] R. Teresi *et al.*, 'Improvement of oxidation resistance of polymer-based nanocomposites through sonication of carbonaceous nanoparticles', *Ultrasonics Sonochemistry*, vol. 61, Mar. 2020, doi: 10.1016/j.ultsonch.2019.104807.

[2] Y. T. Shieh and W. W. Wang, 'Radical scavenging efficiencies of modified and microwave-treated multiwalled carbon nanotubes', *Carbon*, vol. 79, no. 1, pp. 354–362, 2014, doi: 10.1016/j.carbon.2014.07.077.

[3] X. Zhang *et al.*, 'Interaction of tannic acid with carbon nanotubes: Enhancement of dispersibility and biocompatibility', *Toxicology Research*, vol. 4, no. 1, pp. 160–168, Jan. 2015, doi: 10.1039/c4tx00066h.

[4] M. Giorcelli and M. Bartoli, 'Development of Coffee Biochar Filler for the Production of Electrical Conductive Reinforced Plastic', *Polymers*, vol. 11, no. 12, p. 1916, Nov. 2019, doi: 10.3390/polym11121916.

[5] L. Valentini *et al.*, 'Synergistic effect of graphene nanoplatelets and carbon black in multifunctional EPDM nanocomposites', *Composites Science and Technology*, vol. 128, pp. 123–130, May 2016, doi: 10.1016/j.compscitech.2016.03.024.

2.3. Preliminary Experimental Feasibility Study. Commercial Biochar as a filler for PBAT-based composites

This chapter discusses the preparation of a biocomposite based on poly(butylene adipate-co-terephthalate) (PBAT) as a biopolymer matrix and commercial biochar (*c*BC) as a filler. The *c*BC used in this chapter is commercially available in order to define the useful concentration of *c*BC particles in the PBAT matrix and to evaluate the PBAT/*c*BC interaction. The addition of *c*BC resulted in an improvement of the modulus of elasticity while maintaining high values of deformation. The commercial biochar was characterised by DPPH assay to evaluate the radical scavenging efficiency. The biochar was then added to PBAT at different concentrations. The formulated composite was characterised by morphological, mechanical and thermal analysis. In addition, accelerated degradation tests monitored by spectroscopic analysis and tensile tests showed that the filler induced a photo-oxidative resistance on PBAT by delaying the degradation phenomena.

2.3.1. Materials and Methods

2.3.1.1. Materials

PBAT (ecoflex® F Blend C1200, BASF, SE, Ludwigshafen, Germany) is a film grade with a melt flow rate (MFR) of 2.7-4.9 g/10 min (190 ◦C, 2.16 kg), density in the range 1.25-1.27 g/cm3 and melting temperature in the range 110-120 ◦C. Commercial biochar powder (hereafter referred to as *c*BC) used in the food industry (Spigadoro, Perugia, Italy) was selected as filler. As indicated in the supplier's technical data sheet, this biochar was obtained from the pyrolysis of birch and beech wood.

2.3.1.2. Composites Formulation

PBAT/*c*BC composites were melt-mixed using a Brabender batch mixer (Brabender, model PLE330, Duisburg, Germany). PBAT was also processed under the same conditions for comparison. To avoid hydrolytic chain scission during processing, PBAT and biochar were dried overnight under vacuum at 70 °C and 105 °C, respectively. In addition, prior to melt processing, PBAT and 5 wt.%, 10 wt.% or 20 wt.% of *c*BC particles were pre-mixed in the solid state and then fed into the batch mixer at 170 °C with a rotor speed of 60 rpm for 5 min. Specimens were then obtained by compression moulding using a laboratory press (Carver, Wabash, IN, USA) at 170 ◦C for 2 min at a pressure of 100 bar.

2.3.1.3. Particle Characterization

The 1,1.diphenyl-2-pycryl (DPPH, supplied by Sigma Aldrich) free radical scavenging assay was carried out [1]–[3]. First, a methanol solution of DPPH (10^{-4} M) was prepared, then 1 mg of solid was placed in 2 ml of this solution for 24h at 25 °C. The solutions were kept at 25 °C during the time required by the measurement. Then the supernatant liquid was removed, and the UV-vis spectrum recorded at different step times achieving 24h in a Beckmann DU-800 spectrometer. Spectra were recorded on a spectrophotometer equipped with a Peltier temperature controller. Scavenging efficiency values were calculated by the following equation:

$$Radical\ Scavenging\ Efficiency\ (\%) = \frac{A - B}{A - 0.1} \times 100$$

where A is the absorbance at 517 nm of the DPPH solution and B the one of the DPPH solution after contact with the solid.

2.3.1.4. Composites Characterization

The morphology of biochar particles and biocomposites has been under investigation. A Quanta 200 ESEM, FEI (Hillsboro, OR, USA) Scanning Electron Microscope (SEM) was used to observe the morphology of all materials. For PBAT-based biocomposites, each sample was fractured in liquid nitrogen and the fracture surface analysed; biochar particles were observed unaltered.

Tensile tests were performed on rectangular specimens using a universal testing machine (Instron model 3365, Rochdale, UK) according to ASTM D882. The tests were performed at a tensile speed of 1 mm/min for 1 min to evaluate the Young's modulus, calculated as the slope of the initial linear portion of the engineering stress-strain curves, and then the speed was increased to 10 mm/min until the specimen broke. The average values for elongation at break, EB, modulus of elasticity, E, and tensile strength, TS, were calculated.

For the thermal characterisation of the materials, differential scanning calorimetry (Setaram, model DSC131, Lyon, France) was performed. Analyses were carried out under a protective atmosphere (nitrogen). Samples of similar weight (~5 mg) were subjected to heat/cool/heat ramps at a scanning speed of 10 °C/min in the temperature range of 30-190 °C. The PBAT crystallinity (χ) was calculated using the following equation [4]:

$$\chi = \frac{\Delta H_m}{\Delta H_{100} \times W_p}$$

where ΔH_m is the enthalpy of fusion, ΔH_{100} is the enthalpy of fusion of 100% crystalline polymer and W_p is the weight fraction of polymer. For PBAT ΔH_{100} = 114 J g^{-1} [5].

2.3.1.5. Degradation Study

A Q-UV/se accelerated weathering tester (Q-Labs Corp., Westlake, OH, USA) with eight UVB-313 lamps was used to subject all samples to photo-oxidation. Samples were exposed at 70 ◦C to an irradiance of 0.89 W/m^2 (at a wavelength of $\lambda = 313$ nm) and monitored every 24 h.

To understand the chemical composition and follow the functional group changes during accelerated weathering, FTIR-ATR analysis was performed on both the pure PBAT matrix and the PBAT/*c*BC composites (Perkin-Elmer FT-IR/NIR Spectrum 400, Waltham, MA, USA). Tensile tests were also carried out on photo-oxidised samples to monitor the evolution of main mechanical properties.

2.3.2. Results and Discussion

The radical scavenging activities of *c*BC particles were investigated in order to assess their chemical activity (see also chapter 2.2.2). In particular, the kinetics of scavenger activities was determined from the decrease in absorbance at 517 nm of each sample caused by the interaction of DPPH and carbonaceous particle upon dispersion in methanol solution as a function of time keeping constant the particle amount, see Figure 19. The graph shows that the kinetics of biochar radical scavenging efficiency consists of an increase in the first 6 hours and then remaining constant. Furthermore, the scavenging efficiency of biochar is high regardless of time.

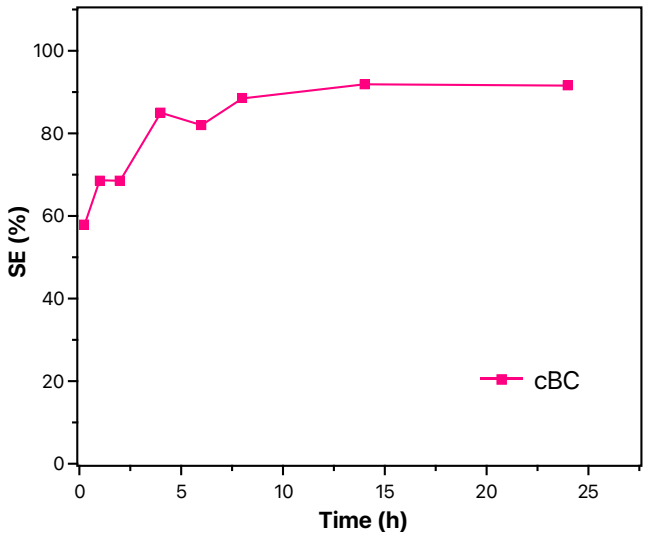

Figure 19 *Scavenging efficiency as a function of time*

SEM analysis was carried out to investigate the morphology of both *c*BC microparticles and PBAT/*c*BC composites. In Figure 20, micrographs of *c*BC particles are shown at two different magnitudes in order to observe the *c*BC surface and 3D structure and the general dimension of all particles. *c*BC showed porous and almost parallelepipedal structure, with different granulometry: from 65 μm to lower dimension. The porous structure is imparted by the fact that birch and beech wood is pyrolysed for the production of *c*BC, and the lignocellulose structure is preserved by

the process. The elongated and coarse pores are due to the retention of the original wood skeleton, which is also preserved by the rapid release of gaseous products during pyrolysis [6].

Figure 21 shows micrographs of the nitrogen cracked surface of PBAT and PBAT/*c*BC composites. The PBAT cross section, see Figure 21 (a), appears smooth and homogeneous. No variation in dispersion is observed as the *c*BC concentration is varied, all composites show uniform dispersion of the embedded filler. In addition, as already noted in Figure 20(b), a wide granulometry distribution is also evident in the case of the biocomposites. The morphology suggests a good matrix/filler interfacial adhesion, it is not always easy to distinguish where the particle ends, and the matrix begins. Furthermore, in Figure 21(c), it appears that some PBAT matrix has penetrated into the porous structure of the biochar particles. This result is probably due to the affinity between the PBAT polymer and the biochar particles, which seems to be independent of the filler concentration.

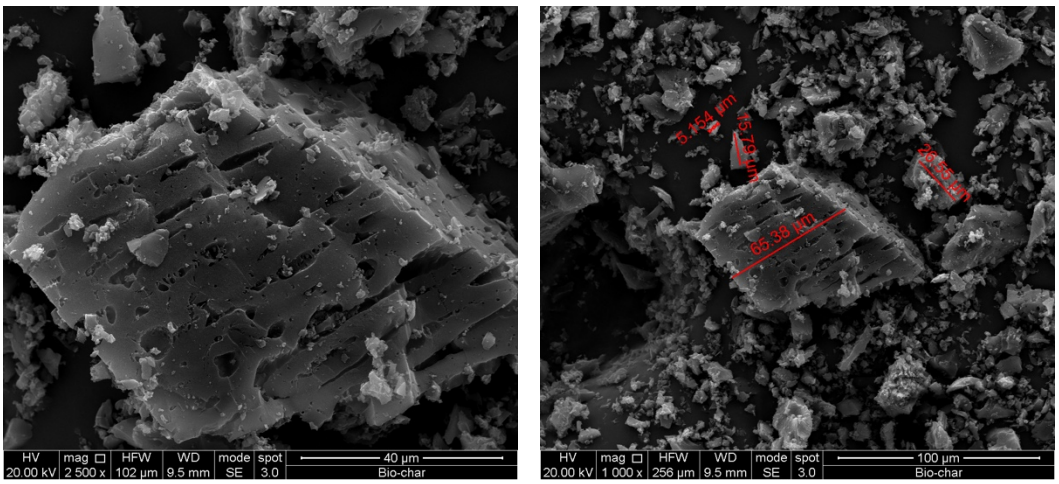

(a) *(b)*

Figure 20 *SEM micrographs of cBC at (a) 2 500 x and (b) 1 000 x*

The thermograms recorded by DSC during the second heating scan of the compression moulded samples are shown in Figure 22. PBAT shows the typical thermogram of an almost amorphous polymer, characterised by a small endothermic peak at 129.5°C, due to the melting phenomenon of the small fraction of crystalline

phase (7%). Whatever the *c*BC concentration, adding *c*BC filler caused minimal decrease in crystallinity compared to pure PBAT. In fact, PBAT remains almost amorphous in spite of the addition of filler, and this was to be expected since PBAT is a random copolymer characterised by low crystallinity due to the intrinsic irregularity of its structure, which inhibits the crystallisation process [7]. Nevertheless, as can be seen in Table 10, a slight increase in the T_m from 129.5 °C to 133.0 °C can be observed when 20 wt.% of *c*BC is added to PBAT. This latter result confirms some compatibility between *c*BC and PBAT as reported in previous studies [8].

Tensile testing was used to mechanically characterise the specimens obtained after compression moulding. The resulting trends in Young's modulus, tensile strength and elongation at break are shown in Figure 23. The addition of 5 wt. % filler had no effect on the Young's modulus but had a significant effect on the tensile strength with a reduction of 50% and the elongation at break with a reduction of 37%. The elastic modulus of PBAT/*c*BC 10% and PBAT/*c*BC 20% increased by approximately 33% and 93% respectively compared to PBAT. The increase in Young's modulus can be attributed to: the reinforcing effect of *c*BC on the matrix due to the good adhesion observed in the SEM analysis, and the relative effective concentration of *c*BC and the lack of increase in crystallinity observed in the DSC thermograms. Nevertheless, a significative reduction of tensile strength and elongation at break has been highlighted also for PBAT/*c*BC 10% and PBAT/*c*BC 20%. Both properties reduce in value as the increase of *c*BC concentration in PBAT matrix.

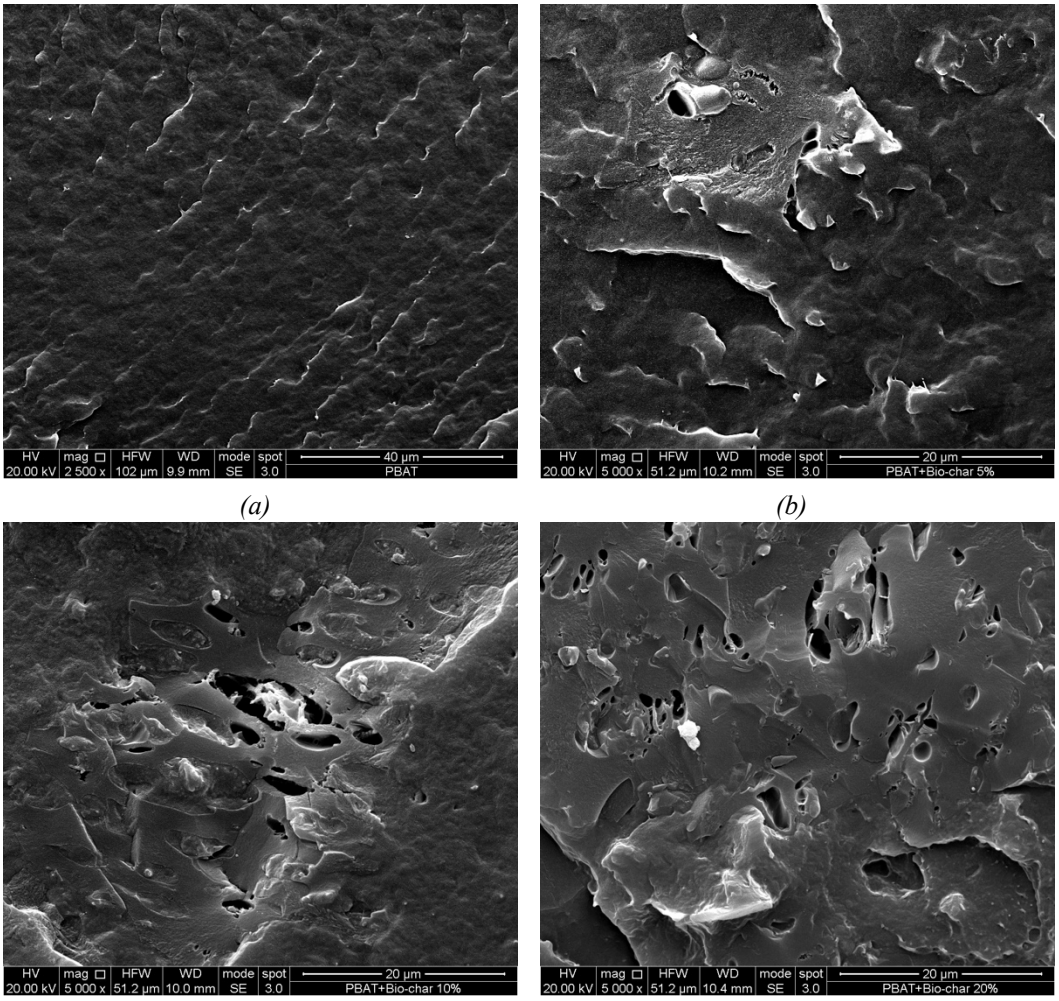

Figure 21 *SEM micrographs of (a) pristine PBAT, (b) PBAT/cBC 5%, (c) PBAT/cBC 10% and (d) PBAT/cBC 20%*

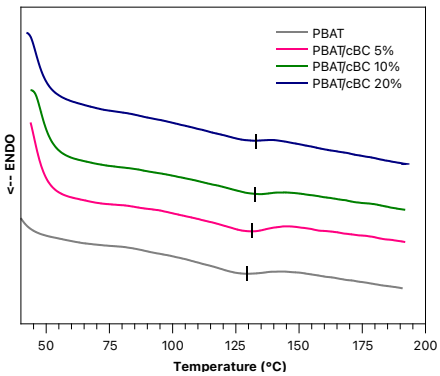

Figure 22 *DSC thermograms recorded during the Second heating scan.*

Table 10 DSC data from the second heating scan of a PBAT-based composite with the addition of commercial cBC.

Sample Name	ΔH_m [J/g]	χ [-]	T_m [°C]
PBAT	8.04	7.0	129.5
PBAT/*c*BC 5%	5.97	5.2	131.2
PBAT/*c*BC 10%	5.90	5.1	132.7
PBAT/*c*BC 20%	7.11	6.2	133.0

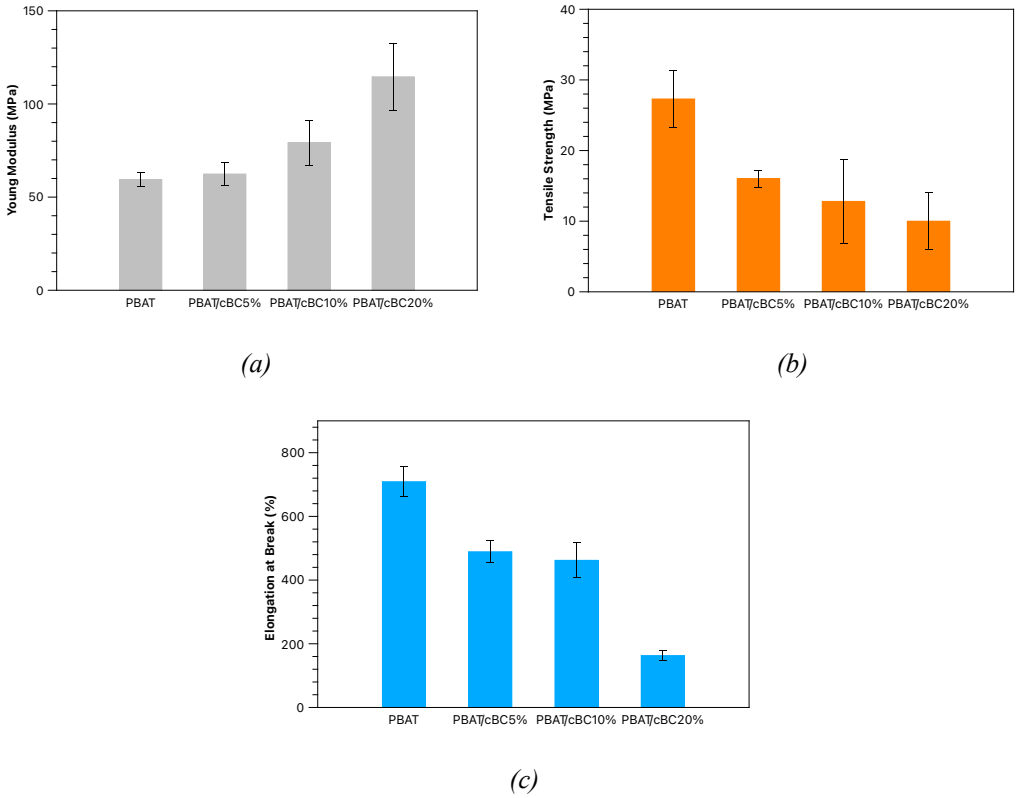

Figure 23 *(a) Young Modulus (b) Tensile Strength and (c) Elongation at Break of PBAT/cBC composites at different cBC content*

Despite the good matrix-filler adhesion and the good compatibility observed between PBAT and *c*BC, the decrease in tensile strength of the biocomposites can be attributed to the premature failure of the sample, which is expected when rigid particles are added to a ductile polymer matrix, and in some way the filler/matrix and filler/void interfaces could possibly act as stress concentrators in composites [9].

A Q-UV/SE accelerated weathering tester was used to subject all samples to a photo-oxidation process, and then samples were monitored by variation of tensile properties as a function of time. These results were correlated with FTIR spectra.

A proper photooxidative stability is a key parameter for a film application [10], therefore, considering the conclusions that came from the mechanical properties thesis, the tensile properties and the variation of the FT-IR spectra were monitored without PBAT/*c*BC 20%. Figure 24 shows the dimensionless Young's modulus and elongation at break, obtained as the ratio between the values as a function of time and the value at time zero, before exposure to photooxidation. As shown in Figure 24(a), the Young's modulus increases with increasing photooxidation time, as observed for semi-crystalline polymers. In the case of virgin PBAT, the increase can be attributed to cross-linking phenomena that occur as a result of chain reactions triggered by the presence of oxygen in radical form. In the end, materials from a ductile behaviour are involved in brittle behaviour. Interestingly, the presence of 5 wt.% and 10 wt.% *c*BC in the PBAT matrix reduces these phenomena, especially for PBAT/*c*BC 10%. Figure 24(b) shows the dimensionless elongation at break as a function of exposure time, and this property is the main parameter normally affected by the structural and morphological changes of the polymers caused by photooxidation [11]. This graph also highlights the half time of elongation at break, a parameter evaluated as the time at which the elongation at break is half of the initial elongation. This time is considered the maximum time the film can be used [11]. The half time for pure PBAT results in 17h, whereas for PBAT/*c*BC 5% and PBAT/*c*BC10% the half time was calculated and results in 32h and 36h respectively. Thus, *c*BC increases the photo-oxidation resistance of PBAT and more than doubles its stability, especially for PBAT/*c*BC 10%. This result was predictable from the DPPH analysis.

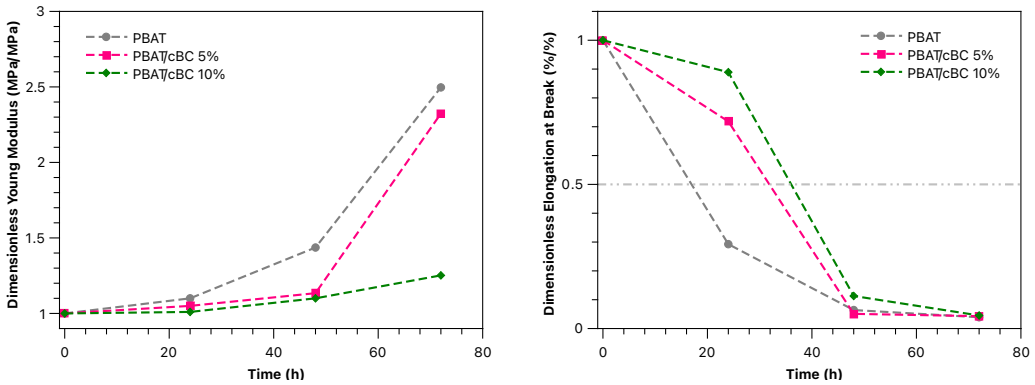

(a) *(b)*

Figure 24 *(a) Dimensionless Young Modulus and (b) Dimensionless Elongation at Break as a function of photo-oxidation time*

Another important approach to investigate the chemical transformations that normally occur during photooxidative exposure of polymer matrices is FTIR-ATR analysis. The spectra were collected every 24 hours and are shown in Figure 25.

In Figure 25 the insets correspond to a zoom on the wavelengths 3700-2700 cm^{-1} and 1850-1550 cm^{-1}, which are critical regions for highlighting the chemical modification that occurred during the photooxidative degradation. In all the spectra, the typical bands are easily recognizable. Firstly, the -OH vibration is visible in the broad band between 3700 and 3100 cm^{-1} and increases with increasing exposure time. The symmetric and antisymmetric CH_2 stretching can be assigned to the peaks at 2857 and 2874 cm^{-1}. Furthermore, at 1710 cm^{-1} the strong peak related to the C=O carbonyl group appears, with a sharp peak representing the CH_2 groups at 720 cm^{-1}. The C-O bond in the ester linkage was observed around 1275-1250 cm^{-1}[12], [13]

All these signals are significantly affected by the photodegradation phenomena, changing their intensity (*i.e.* width and height of the peaks) as a function of the exposure time. In Figure 25(a), where the photodegradation process of pristine PBAT has been shown by means of recorded spectra, a significant reduction and broadening of the peak relative to C=O is reported. In fact, the left shoulder (1790-

1750 cm^{-1}) suggests the formation of free C=O and the right shoulder (1590-1630 cm^{-1}) represents the formation of a lower molecular weight ester.

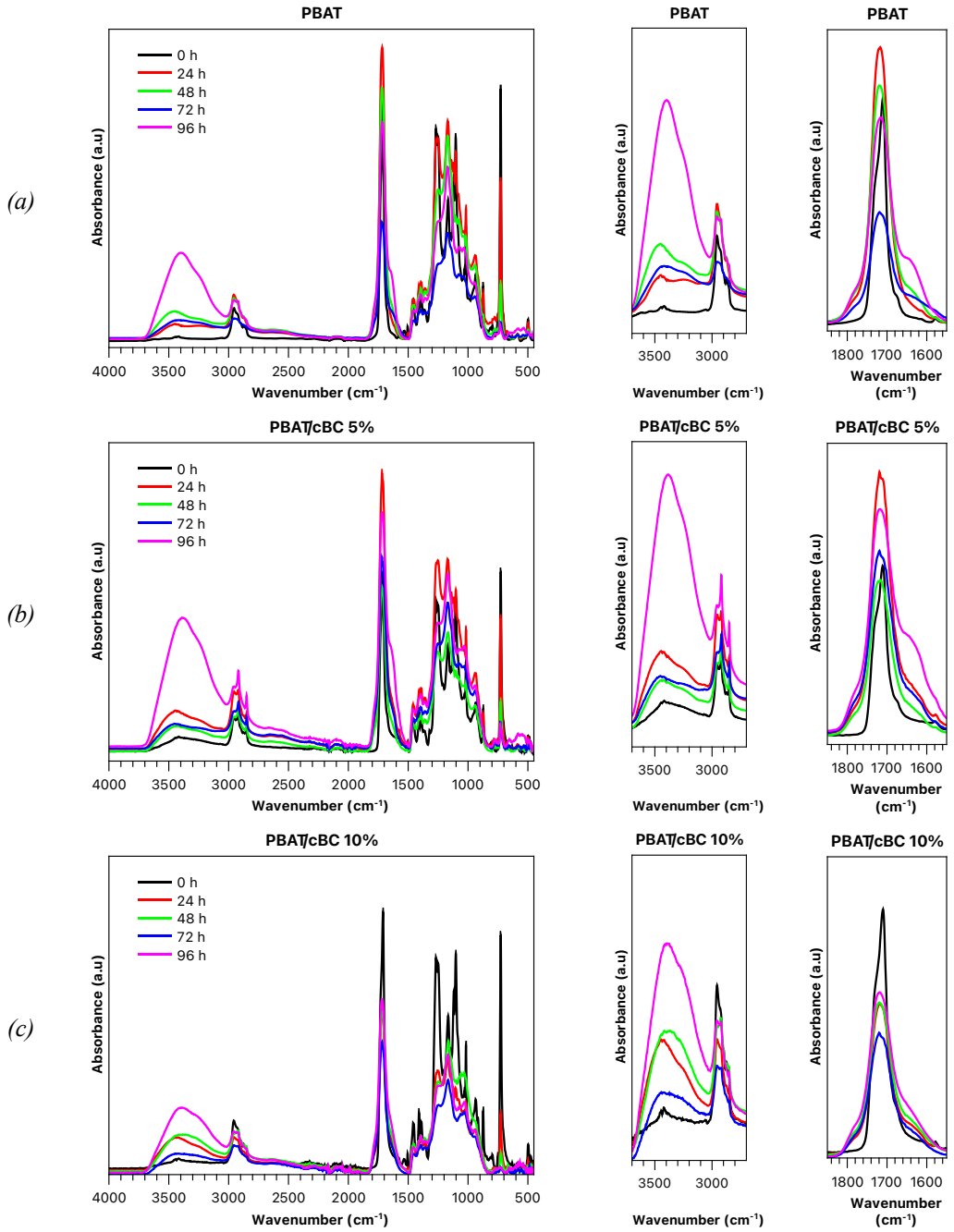

Figure 25 *FTIR spectra as a function of photo-oxidation time of (a) pristine PBAT, (b) PBAT/cBC 5% and (c) PBAT/cBC 10%*

All these phenomena suggest the occurrence of a Norrish I [14] chain scission reaction. Moreover, as already mentioned, the increase of the broad band in the

corresponding region of -OH stretching suggests: the formation of hydrogen bonded compounds (3530 *c-1*), free peroxide or peroxide in the molecular chain (3440 cm^{-1}), indicating a photo-oxidative reaction. All these results suggest an autocatalytic reaction of the carbonyl end groups, *i.e.* Norrish II reactions [14].

Interestingly, this chemical modification, which is consistent with dimensionless elongation at break and Young's modulus graphs, was found to be less intense for PBAT/*c*BC 5% and PBAT/*c*BC 10%, particularly after 24 hours. These results, which are also consistent with the DPPH particle analysis, suggest that *c*BC particles are exploited to protect against degradation.

2.3.3. Endings

The properties of PBAT-based composites filled with commercial biochar particles were evaluated in this chapter. All PBAT/*c*BC composites showed uniform filler dispersion and good adhesion within the selected biopolymer matrix. This resulted in an increase in the modulus of elasticity. However, a dramatic reduction in elongation at break was observed in the PBAT/*c*BC 20 wt.% samples.

In addition, by delaying the degradation phenomena of the polymer matrix, the presence of the filler induced a photo-oxidative resistance on PBAT. This result was even more pronounced for PBAT/*c*BC 10 wt.% than for PBAT/*c*BC 5 wt.%. It opens up the possibility of using PBAT-based films in outdoor applications.

Reference

[1] R. Teresi *et al.*, 'Improvement of oxidation resistance of polymer-based nanocomposites through sonication of carbonaceous nanoparticles', *Ultrasonics Sonochemistry*, vol. 61, Mar. 2020, doi: 10.1016/j.ultsonch.2019.104807.

[2] Y. T. Shieh and W. W. Wang, 'Radical scavenging efficiencies of modified and microwave-treated multiwalled carbon nanotubes', *Carbon*, vol. 79, no. 1, pp. 354–362, 2014, doi: 10.1016/j.carbon.2014.07.077.

[3] X. Zhang *et al.*, 'Interaction of tannic acid with carbon nanotubes: Enhancement of dispersibility and biocompatibility', *Toxicology Research*, vol. 4, no. 1, pp. 160–168, Jan. 2015, doi: 10.1039/c4tx00066h.

[4] G. Infurna *et al.*, 'Biochar Particles Obtained from Agricultural Carob Waste as a Suitable Filler for Sustainable Biocomposite Formulations', *Polymers*, vol. 14, no. 15, p. 3075, Jul. 2022, doi: 10.3390/polym14153075.

[5] V. Titone, F. P. La Mantia, and M. C. Mistretta, 'The Effect of Calcium Carbonate on the Photo-Oxidative Behavior of Poly(butylene adipate-co-terephthalate)', *Macromolecular Materials and Engineering*, vol. 305, no. 10, Oct. 2020, doi: 10.1002/mame.202000358.

[6] Q. Zhang, M. U. Khan, X. Lin, H. Cai, and H. Lei, 'Temperature varied biochar as a reinforcing filler for high-density polyethylene composites', *Composites Part B: Engineering*, vol. 175, p. 107151, Oct. 2019, doi: 10.1016/j.compositesb.2019.107151.

[7] T. T. Santos *et al.*, 'Effect of filler type on properties of PBAT/organoclay nanocomposites', *Polym. Bull.*, vol. 77, no. 2, pp. 901–917, Feb. 2020, doi: 10.1007/s00289-019-02778-z.

[8] S.-J. Xiong *et al.*, 'Economically Competitive Biodegradable PBAT/Lignin Composites: Effect of Lignin Methylation and Compatibilizer', *ACS Sustainable Chem. Eng.*, vol. 8, no. 13, pp. 5338–5346, Apr. 2020, doi: 10.1021/acssuschemeng.0c00789.

[9] V. Fiore, L. Botta, R. Scaffaro, A. Valenza, and A. Pirrotta, 'PLA based biocomposites reinforced with Arundo donax fillers', *Composites Science and*

Technology, vol. 105, pp. 110–117, Dec. 2014, doi: 10.1016/j.compscitech.2014.10.005.

[10] F. La Mantia, L. Ascione, M. Mistretta, M. Rapisarda, and P. Rizzarelli, 'Comparative Investigation on the Soil Burial Degradation Behaviour of Polymer Films for Agriculture before and after Photo-Oxidation', *Polymers*, vol. 12, no. 4, p. 753, Mar. 2020, doi: 10.3390/polym12040753.

[11] L. Botta, N. Tz. Dintcheva, and F. P. La Mantia, 'The role of organoclay and matrix type in photo-oxidation of polyolefin/clay nanocomposite films', *Polymer Degradation and Stability*, vol. 94, no. 4, pp. 712–718, Apr. 2009, doi: 10.1016/j.polymdegradstab.2008.12.017.

[12] S. Mohanty and S. K. Nayak, 'Biodegradable nanocomposites of poly (butylene adipate-co-terephthalate) (PBAT) with organically modified nanoclays', *Int J Plast Technol*, vol. 14, no. 2, pp. 192–212, Dec. 2010, doi: 10.1007/s12588-010-0018-y.

[13] Y. Cai, J. Lv, and J. Feng, 'Spectral Characterization of Four Kinds of Biodegradable Plastics: Poly (Lactic Acid), Poly (Butylenes Adipate-Co-Terephthalate), Poly (Hydroxybutyrate-Co-Hydroxyvalerate) and Poly (Butylenes Succinate) with FTIR and Raman Spectroscopy', *J Polym Environ*, vol. 21, no. 1, pp. 108–114, Mar. 2013, doi: 10.1007/s10924-012-0534-2.

[14] T. Kijchavengkul, R. Auras, M. Rubino, E. Alvarado, J. R. Camacho Montero, and J. M. Rosales, 'Atmospheric and soil degradation of aliphatic-aromatic polyester films', *Polymer Degradation and Stability*, vol. 95, no. 2, pp. 99–107, Feb. 2010, doi: 10.1016/j.polymdegradstab.2009.11.048.

2.4. Biochar Particles from Carob Waste as a filler for PBAT-based composites.

The aim of this chapter is to give new life to agricultural carob waste by pyrolysing it to make it suitable as an interesting filler for biocomposite formulation. The preparation and characterisation of the particles has already been discussed in chapter 2.1.2.1. In this chapter, the formulation of biocomposites prepared by adding carob waste derived biochar particles (*cw*BC) to poly(butylene adipate co-terephthalate) (PBAT) at two different concentrations, *i.e.* 10 and 20 wt.%, will be discussed. As previously discussed, the *cw*BC were prepared using three pyrolysis processing temperatures (*i.e.* 280, 340 and 400 °C). The resulting particles from the pyrolysis process (BC280, BC340 and BC400) were considered as suitable fillers for PBAT. Morphological, thermal, mechanical and rheological characterisations were carried out to characterise all the biocomposites. In addition, accelerated weathering, monitored by both tensile test and spectroscopic analysis, was carried out and the results obtained show that even the laboratory biochar particles produced in our laboratories by pyrolysis of a different feedstock can have a beneficial effect on the photo-oxidation delay of the PBAT matrix.

2.4.1. Materials and Methods

2.4.1.1. Materials

Poly(butylene adipate-co-terephthalate), (PBAT; commercial Ecoflex® F Blend C1200, BASF, SE, Ludwigshafen, Germany) is a film grade with a melt flow rate (MFR) of 2.7-4.9 g/10 min (190◦C, 2.16 kg), a density in the range of 1.25-1.27 g/cm3 and a melting temperature in the range of 110-120°C.

Biochar particles (*cw*BC) were produced from carob waste after syrup extraction for carob candy production and from slow pyrolysis for fuel production. The procedure for slow pyrolysis process is reported in detail in chapter 2.1.1.4 Experimental apparatus and Procedure. The biochar particles are named BC280, BC340 and BC400 as a result of pyrolysis at three different temperatures, *i.e.,* 280, 340 and 400°C. Residual biochar from these three different pyrolysis conditions was milled at the same process conditions.

2.4.1.2. Biocomposites Formulation

Compounding of the biocomposites was carried out using a Brabender mixer at 170°C with a mixing speed of 50 rpm for 5 min. Prior to compounding, PBAT and *cw*BC were dried at 60°C under vacuum to avoid hydrolysis during compounding. The three different samples BC280, BC340 and BC400 were added at 10 wt% and 20 wt%. These concentrations were chosen as a result of previous work on commercial biochar (chapter 2.3). The mixture was then pelletised. In addition, the neat PBAT was subjected to the same processing conditions in order to be comparable with the composites. After drying for 24 hours in a vacuum oven at 60°C to avoid hydrolysis, thin films (about 200 μm thick) of neat PBAT and of all the composites were obtained by compression moulding using a Carver Laboratory Press at a pressure of 1500 psi for 5 minutes at 170°C.

2.4.1.3. Feedstock and Biochar characterization

Biochar particles has been produced in the contest of this research. Feedstock characterization test for decision of operative condition and the characterization test of resulting biochar particles it has been already described in 2.1.1.2 and in chapter 2.1.1.5, respectively.

2.4.1.4. Biocomposites Characterization

Rheological tests were performed using a strain-controlled rheometer (ARES G2, TA Instrument, New Castle, DE, USA) in parallel plate geometry (plate diameter 25 mm). Frequency scans from 10^{-2} to 10^{2} rad/s were performed to measure complex viscosity (η*) and storage (G′) and loss (G″) moduli at the same processing temperatures. The strain amplitude was set at 5%, which was found to be low enough to be in the linear viscoelastic regime in preliminary experiments with strain sweeps. A scanning electron microscope (SEM, Quanta 200 ESEM, FEI, Hillsboro, OR, USA) was used to examine the microstructure of the biocomposites. Prior to the SEM analysis, the samples were fractured in liquid nitrogen. To avoid electrostatic charging under the electron beam, the fractured surface of each sample was sputtered (Scancoat Six Edwards, Crawley, UK) with a thin layer of gold for 90 s in an argon atmosphere.

The melting enthalpies of all samples were measured by DSC using a Shimadzu (Japan) DSC-60 instrument at a heating rate of 10 °C/min from T ambient to 170 °C, as an average of five measurements. All samples of similar weight (~7 mg) were subjected to heating/cooling/heating and the thermal parameters were evaluated on the second heating scan, erasing the previous thermal history. The PBAT crystallinity, χc, was calculated using the equation:

$$\chi_c = \frac{\Delta H_m}{\Delta H_{100} - W_p} \times 100$$

Where ΔH_m is the enthalpy of fusion, ΔH_{100} is the enthalpy of fusion of 100% crystalline polymer and W_p is the weight fraction of polymer. For PBAT ΔH_{100}=114 J g^{-1} [1].

Tensile tests were performed on rectangular specimens using a universal testing machine (Instron model 3365, UK) according to ASTM D882. The tests were performed at a tensile speed of 1 mm/min for 1 min to evaluate the Young's modulus, and then the speed was increased to 10 mm/min until the specimen broke. Average

values were calculated for elongation at break, EB, modulus of elasticity, E, and tensile strength, TS.

A dynamic mechanical analyser model DMA +50 (Metravib, Limonest, France) was used to perform dynamic mechanical thermal tests (DMTA) in tensile configuration. The test was performed on three specimens (w×h =10 mm×30 mm) of each composite from room temperature to 120 °C. The heating rate was 2 °C/min. For some composites, measuring was stopped before reaching 120 °C. The frequency was set at 1 Hz, and a prior static displacement of 2x10-5 m and a prior dynamic displacement of 10^{-5} m were set.

2.4.1.5. Degradation Study

All samples were subjected to photo-oxidation using a Q-UV/se accelerated weathering tester (Q-Lab Corporation) with eight UVB-313 lamps. The samples were exposed at 70°C to an irradiance of 0.89 W/m^2 (at a wavelength λ=313 nm) and monitored every 24 hours.

FTIR-ATR analysis was carried out on both the pure PBAT matrix and the PBAT/*cw*BC composites (Perkin-Elmer FT-IR/NIR Spectrum 400, Waltham, MA, USA) to understand the chemical composition and follow the change in functional groups during accelerated weathering. Tensile tests were also performed on the photo-oxidised samples. These tests were used to monitor the variation of the main mechanical properties.

2.4.2. Results and Discussion

Oscillatory measurements were used to evaluate the rheological behaviour of virgin PBAT and all PBAT biocomposites. The complex viscosity trends as a function of frequency for each system are shown in Figure 26(a-c). As the amount of filler incorporated increases, a progressive increase in the complex viscosity of the biocomposites can be observed. It is noteworthy that a low frequency yield behaviour is observed for all composites, and this phenomenon is more pronounced for composites with the highest *cw*BC content. As shown in Figure 26(d-e), the increase in complex viscosity with *cw*BC content is also reflected in an increase in storage modulus G'. Again, the effect of incorporating *cw*BC was higher as the filler content in the polymer matrix increased and more pronounced at low frequencies. In fact, when 20 wt.% filler is added to the PBAT matrix, an increase in the storage modulus of one order of magnitude is observed at low frequencies. This behaviour is generally due to high polymer-filler and filler-filler interactions, which limit the relaxation of the macromolecules. Therefore, as the *cw*BC content increases, a reduction in the chain mobility of PBAT is likely to occur. For all pyrolysis temperatures, the Newtonian behaviour exhibited by pure PBAT tends to progressively disappear as the amount of *cw*BC in the composites increases.

Figure 27 shows the micrographs of the nitrogen fractured surface of PBAT/*cw*BC composites. The composites formulated with particles obtained at the three different pyrolysis temperatures are compared. Furthermore, for the sake of brevity, the morphology variation as a function of *cw*BC concentration is reported only for PBAT/BC280 samples. The morphology of the fractured surface of all PBAT/*cw*BC composites suggests a good matrix/filler interfacial adhesion in all systems and this can probably be attributed to the affinity between the PBAT matrix and the filler, already found in the previous chapter 2.3. It is noteworthy that the affinity doesn't depend on the *cw*BC content and on the pyrolysis temperature at which the composites were obtained. Also here, as already observed and discussed for *cw*BC

particles (see chapter 2.1.2.1), the filler at lower pyrolysis temperature showed a marked lignocellulosic structure, different from the one obtained at 400°C, which appears predominantly carbonaceous.

Figure 28 shows the DSC thermograms recorded at a heating rate of 10°/min for all the samples studied. Table 11 lists the main properties resulting from the thermal cycle. The presence of *cw*BC particles results in a slight increase in T_m compared with pure PBAT, and in a slight increase in T_m with an increase in the pyrolytic temperature for the 10 wt.% load. In addition, the T_m is almost constant for the composites with 20 wt.% *cw*BC. However, the total crystalline phase content in the bio-composites is significantly reduced by the addition of *cw*BC and it decreases with the increase of particle loading and with the increase of pyrolysis temperature at which the biochar particles are produced. Thus, the presence of dispersed fillers doesn't act as nucleating agent for PBAT matrix and in this case hinders crystallisation process. PBAT remains almost amorphous despite the addition of fillers and this was expected as PBAT is a random copolymer characterised by low crystallinity due to the intrinsic irregularity of its structure, which inhibits the crystallisation process [2].

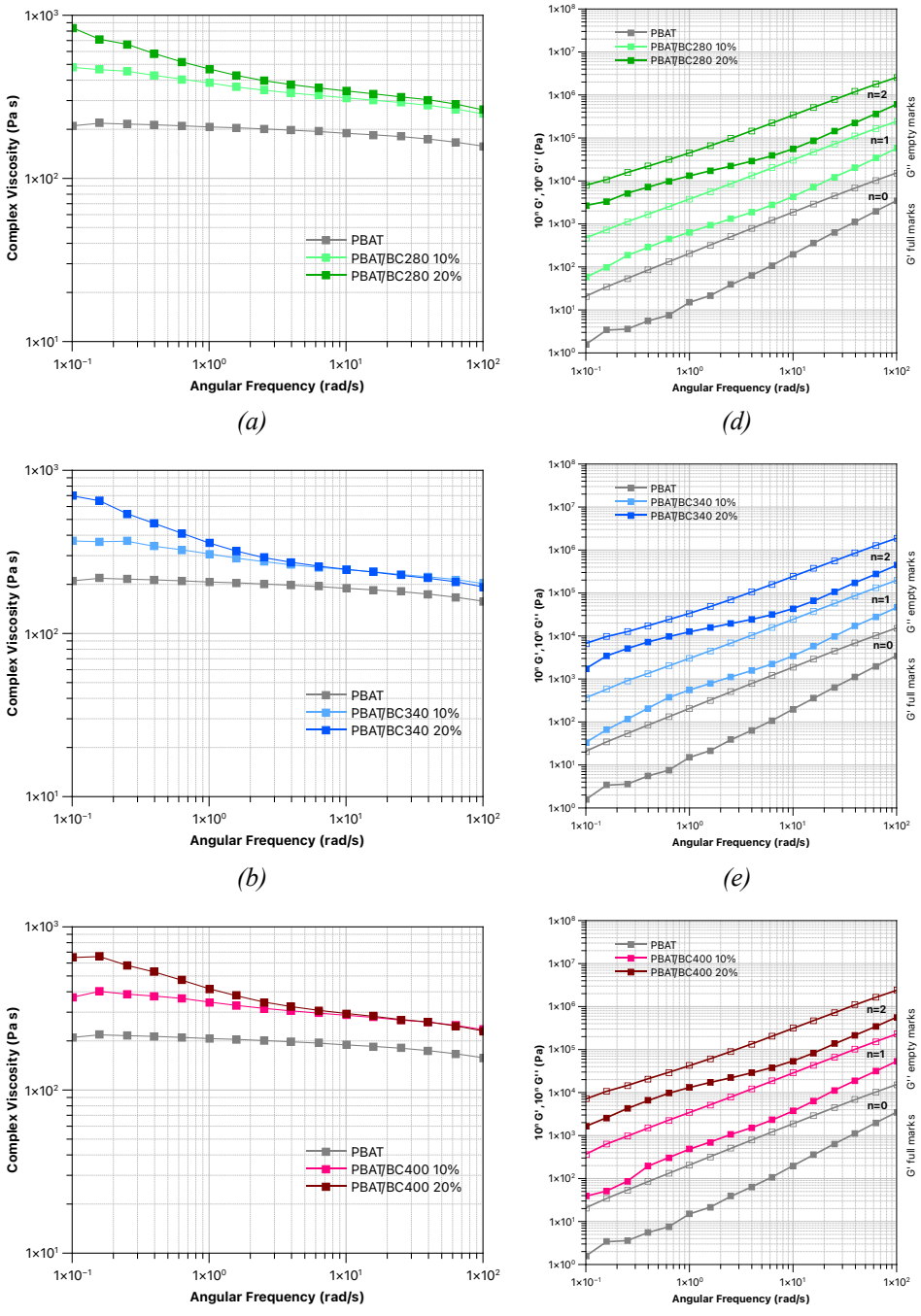

Figure 26 *Rheological behaviour of PBAT-based composite: (a-b-c) Complex Viscosity; (d-e-f) Storage G' and Loss G'' Modulus*

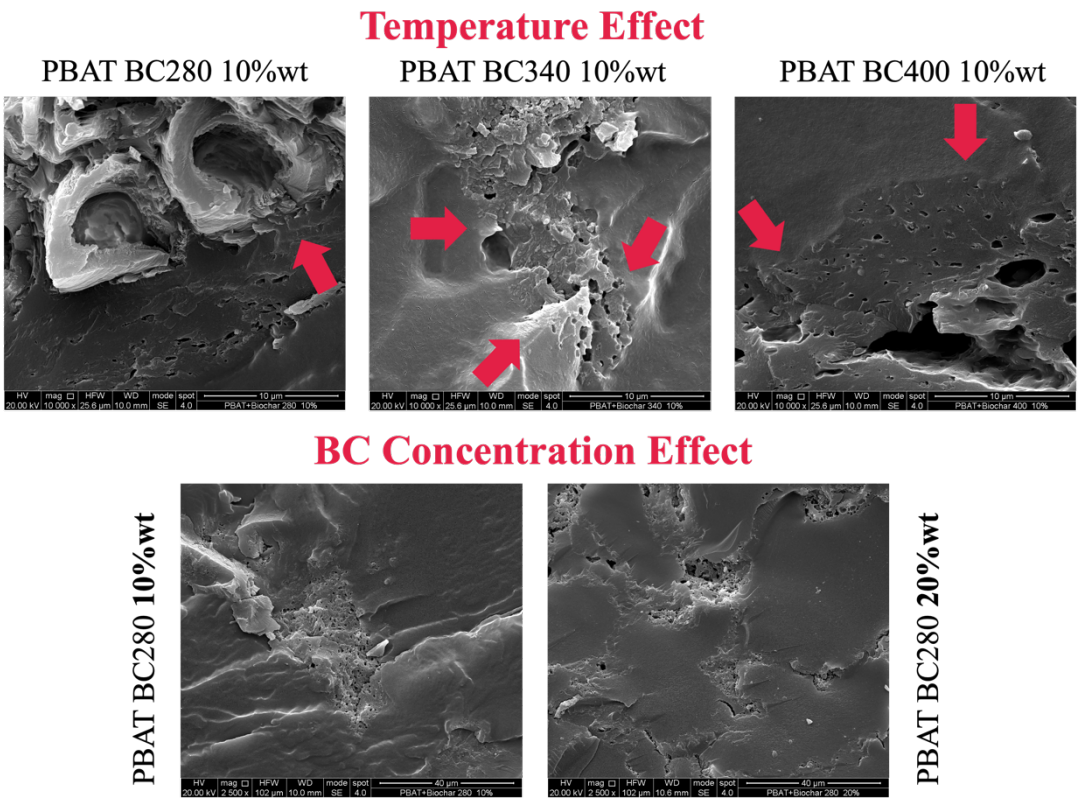

Figure 27 *SEM micrographs of biocomposites as a function of pyrolysis temperature (top) and as a function of varying biochar concentration (bottom).*

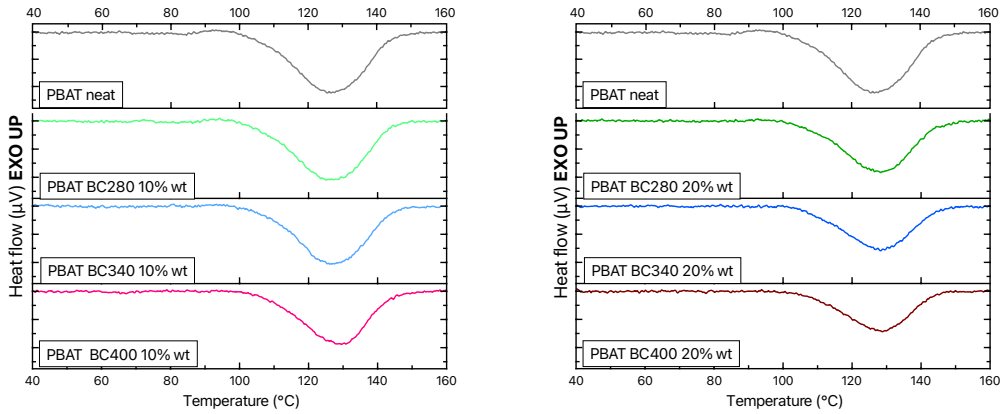

(a) *(b)*

Figure 28 *DSC curves of second heating scan of PBAT/cwBC biocomposites containing cwBC at (a) 10 %wt. and (b) 20 %wt.*

Table 11 DSC data from the second heating scan of a PBAT-based composite with the addition of cwBC, obtained by pyrolysing carob waste at different temperatures.

	T_m [°C]	T_{onset} [°C]	T_{offset} [°C]	ΔH [J/g]	χ [%]
PBAT neat	126.7±1.48	110.4±1.10	141.1±1.20	35.5±0.26	31.4±0.28
PBAT BC280 10%wt	125.5±1.26	112.4±2.02	144.1±2.39	32.8±0.49	32.0±0.58
PBAT BC340 10%wt	126.1±2.27	114.1±1.14	138.2±1.28	29.8±0.29	29.1±0.26
PBAT BC400 10%wt	129.5±1.30	116.5±1.46	141.2±1.57	28.2±0.30	27.5±0.19
PBAT BC280 20%wt	128.3±1.60	116.0±1.16	142.9±1.33	26.1±0.23	28.6±0.51
PBAT BC340 20%wt	128.3±1.28	106.1±1.06	139.0±1.09	24.1±0.43	26.4±0.21
PBAT BC400 20%wt	128.7±1.30	115.1±1.44	142.6±1.35	20.1±0.24	22.9±0.29

The mechanical properties of the PBAT-based composites were evaluated by tensile test and dynamic mechanical analysis; the obtained mechanical properties, modulus of elasticity, tensile strength, and strain at break are shown in Figure 29(a-c). The trends of E' *vs.* T for all the composites are shown in Figure 29(d). With increasing *cw*BC load and pyrolysis temperature, the tensile values, *i.e.* E and TS, increase. As expected, the ductile behaviour of PBAT changes to a rigid behaviour with the addition of carbonaceous particles. However, a consistent increase of +140% of the modulus is obtained when BC400 is added at 20 wt.%, probably due to the lower global dimension of these particles, as already shown in the previous paragraph. The smaller size of the particles allows a more uniform dispersion, which is confirmed by the SEM analysis, and increases the surface area of the interface between the matrix and *cw*BC.

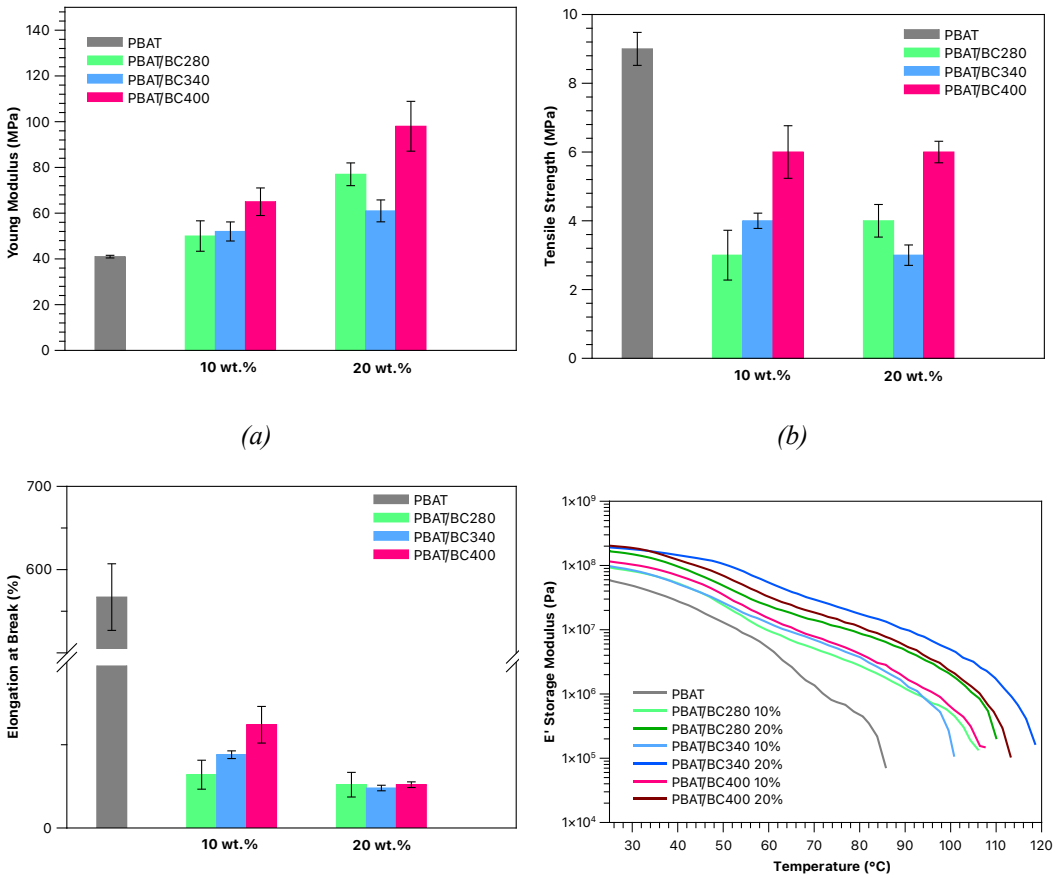

Figure 29 *Main mechanical properties, i.e., (a) Young's Modulus, E, (b) Tensile Strength, TS, and (c) Elongation at Break, EB, and (d) Storge Modulus, E', vs Temperature of PBAT/cwBC biocomposites*

The storage modulus curves, E', of all the composites studied are shown as a function of temperature in Figure 29(d). The storage modulus at low temperature increases with increasing *cw*BC loading and its pyrolysis temperature, following the same trend as the modulus of elasticity. Furthermore, E' decreases with increasing temperature for all samples. However, the presence of particles influences the softening temperature of the samples. At 10 wt.% load, the variation of the pyrolysis temperature at which the *cw*BC particles were obtained doesn't significantly affect the E'(*T*) curves, see Figure 29(d).

In order to study the oxidation resistance of polymeric biocomposites, the photo-oxidation behaviour is a key parameter. Therefore, the variation of mechanical

properties as a function of irradiation time has been under observation. Figure 30 shows the dimensionless variations of the main mechanical properties. As a ratio between the values at a given irradiation time and the value before exposure to photooxidation, both the dimensionless deformation at break and the dimensionless Young's modulus were obtained. In addition, it is possible to identify the half time of the strain at break from the dimensionless strain at break trends, as the time at which the values are half of the initial value (it is evaluated as the time at which the strain at break decreases by 50% with respect to the initial value). This is the maximum time that polymer films can be used. After this time, the ductility of the film is lost [3].

Dimensionless elongation at break of pure PBAT shows a significant reduction in ductility behaviour after 24 h of photoirradiation, with a half-time of 14 h. Biocomposites, on the other hand, almost don't reach the half time of elongation at break after a complete cycle of photooxidation (72h). Thus, the addition of *cw*BC particles delays the ageing phenomena, probably both by UV absorption (being carbonaceous particles) and by scavenging action, as demonstrated by the DPPH assay discussed above and according to the literature [4]. The delay in photodegradation phenomena is more pronounced for *cw*BC obtained at lower pyrolysis temperature, and this could be explained considering that the lower the pyrolysis temperature at which the particles are obtained, the higher their radical scavenging efficiency, also according to the DPPH assay (see Figure 8 in chapter 2.1.2.1).

Consistent with the DPPH assay, where increasing the total amount of biochar in solution has achieved SE=100% regardless of the pyrolysis temperature, also in the composite, as increasing the total amount of *cw*BC in the PBAT matrix, the dimensionless elongation at break result is not affected by the pyrolysis temperature. In relation to the elongation at break, the Young's modulus increases as a function of irradiation time, and this behaviour is more pronounced as the filler load decreases and as the pyrolysis temperature at which the *cw*BC was obtained increases.

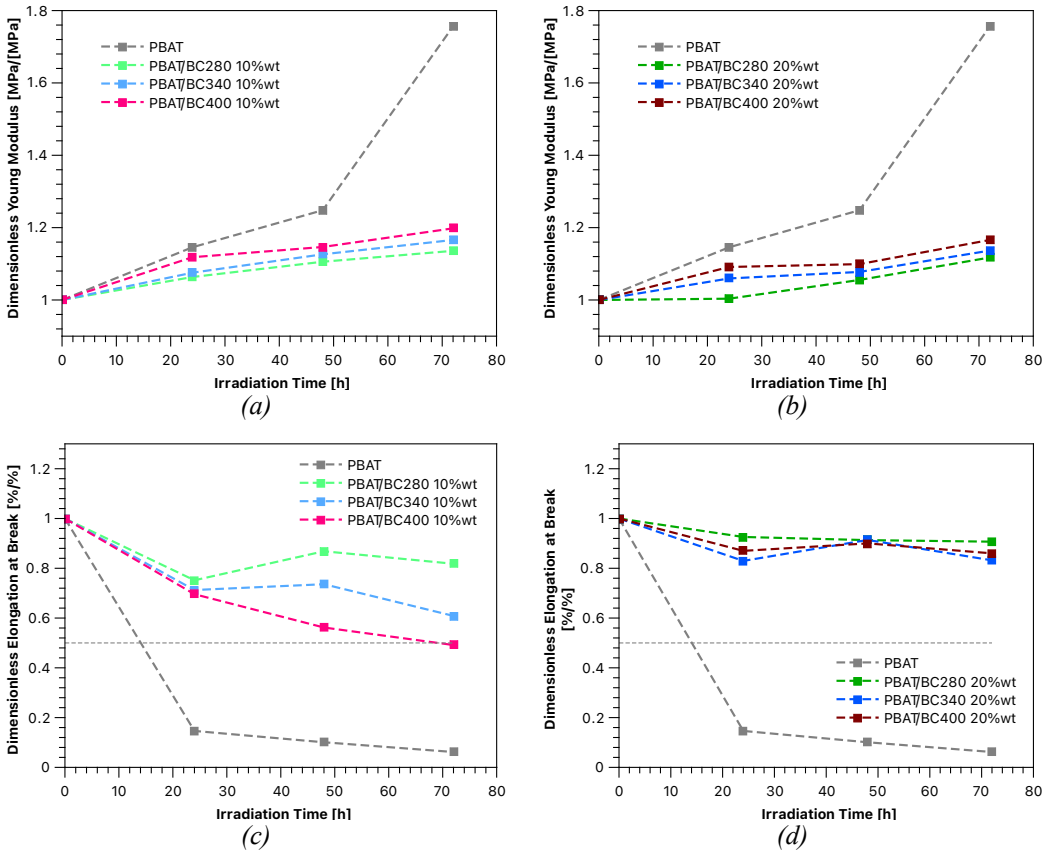

Figure 30 *Trends of (a-b) dimensionless elongation at break and (c-d) dimensionless modulus of elasticity of PBAT/cwBC biocomposites as a function of photooxidation time.*

Complementary ATR-FTIR analysis is also carried out to monitor the ageing behaviour of neat PBAT and PBAT based composites during weathering testing. Selected spectra of neat PBAT, PBAT/BC280 10 wt.% and PBAT/BC400 10 wt.% are shown in 31, with two insets for each spectrum, highlighting the main chemical changes that occur during photooxidation. The typical bands of PBAT are seen in 31(a): a broad band of -OH between 2700 and 3000 cm^{-1}, the two peaks related to the CH_2 stretching vibration at 2956 and 2865 cm^{-1}, the strong peak of C=O at 1710 cm^{-1}, a clear peak representing the CH_2 groups at 720 cm^{-1} and two peaks related to the C-O bond in the ester bond are present at 1275 and 1250 cm^{-1}. All these signals have a tendency to change their intensity as a function of UV irradiation time, highlighting that photodegradation of the PBAT matrix takes place.

It's clearly visible a reduction of C=O functional groups since the decrease and shift of the neat peak at 1710 cm^{-1}, with the creation of a left shoulder, indicates the formation of free C=O due to the occurrence of chain scission by means of Norrish I scission reaction, according to the literature [4], [5]. Furthermore, the appearance of peaks/shoulders at 3410 and 3440 cm^{-1} due to autocatalytic photo-oxidation reactions can be related to the occurrence of Norrish II reaction, which leads to the formation of free OOH and/or peroxide. In the 31(b-c), the two composites containing 10% by weight of *cw*BC obtained at lower and higher pyrolysis temperatures are compared to the neat matrix. In order to correlate the two different effects on the variation of the mechanical properties, these two compositions were chosen for the sake of brevity. Indeed, the variation of the functional group peaks exposed for the neat PBAT matrix appears less intense, which also helps to explain the better mechanical stability.

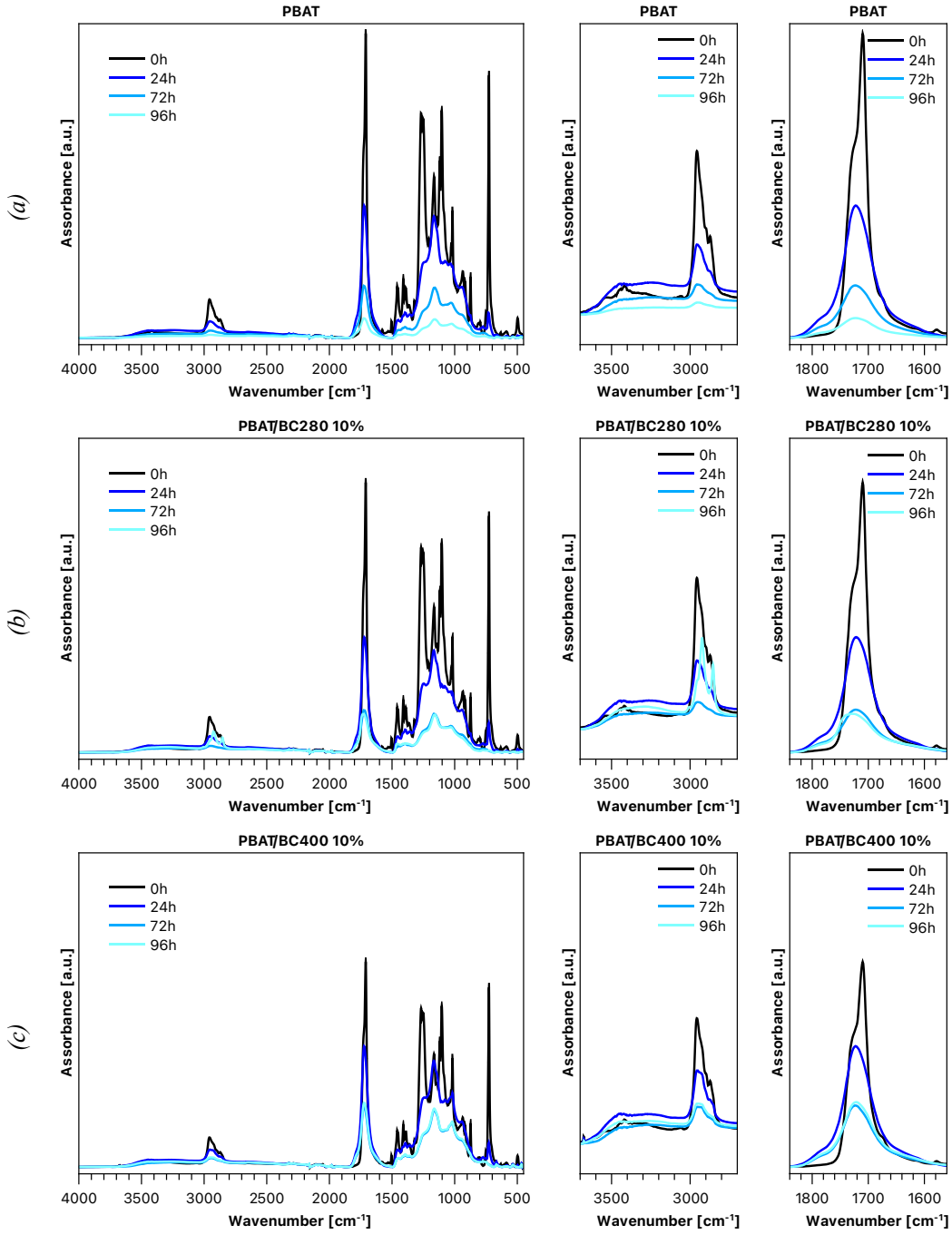

Figure 31 *FTIR-ATR spectra as a function of photo-oxidation time of (a) neat PBAT, (b) PBAT/BC280 10% and (c) PBAT/BC400 10%*

2.4.3. Endings

This chapter investigated the use of biochar particles obtained in our laboratories pyrolysing carob waste after glucose extraction, a waste of a local carob-candy factory, as a suitable filler for PBAT-based biocomposites. The biochar particles, as a result of three different pyrolysis process temperatures, were added to PBAT matrix and the properties of the produced biocomposites were investigated.

The different pyrolysis temperatures result in different particle dimensions, as seen in section 2.1.2.1. In particular, BC400 results in a smaller dimension. This results in better dispersion of the BC400 particles in the polymer matrix and better tensile and rheological properties and thermal stability of the resulting composite compared to composites filled with particles obtained at lower temperatures.

Moreover, in chapter 2.1.2.1, it was seen how increasing the pyrolysis temperature decreases the absorption kinetics of free radicals in DPPH solution, resulting in particles obtained at a lower pyrolysis temperature having a higher radical scavenging efficiency. The study of particle scavenging activity also showed that it was sufficient to slightly increase the concentration of biochar obtained at higher temperatures to obtain comparable scavenging activity. This trend was also confirmed for the mechanical behaviour of the composite as a function of photooxidation time. In fact, by adding 10 wt.% of particles within the PBAT matrix, the graphs of the dimensionless elongation at break as a function of the photo-oxidation time showed that *(i)* in the case of BC400, the half time (the time at which the value is half of the initial one) is reached at the end of the photo-oxidation cycle, *(ii)* in the case of BC280, the dimensionless elongation at break remains almost constant and close to one. Instead, by adding 20 wt.%, the mechanical behaviour of the resulting composites with BC280, BC340 or BC400 is comparable and approximately equal to 1 throughout the photo degradation cycle.

References

[1] V. Titone, F. P. La Mantia, and M. C. Mistretta, 'The Effect of Calcium Carbonate on the Photo-Oxidative Behavior of Poly(butylene adipate-co-terephthalate)', *Macromolecular Materials and Engineering*, vol. 305, no. 10, Oct. 2020, doi: 10.1002/mame.202000358.

[2] T. T. Santos *et al.*, 'Effect of filler type on properties of PBAT/organoclay nanocomposites', *Polym. Bull.*, vol. 77, no. 2, pp. 901–917, Feb. 2020, doi: 10.1007/s00289-019-02778-z.

[3] L. Botta, N. Tz. Dintcheva, and F. P. La Mantia, 'The role of organoclay and matrix type in photo-oxidation of polyolefin/clay nanocomposite films', *Polymer Degradation and Stability*, vol. 94, no. 4, pp. 712–718, Apr. 2009, doi: 10.1016/j.polymdegradstab.2008.12.017.

[4] L. Botta, R. Teresi, V. Titone, G. Salvaggio, F. P. La Mantia, and F. Lopresti, 'Use of biochar as filler for biocomposite blown films: Structure-processing-properties relationships', *Polymers*, vol. 13, no. 22, Nov. 2021, doi: 10.3390/polym13223953.

[5] T. Kijchavengkul, R. Auras, M. Rubino, E. Alvarado, J. R. Camacho Montero, and J. M. Rosales, 'Atmospheric and soil degradation of aliphatic-aromatic polyester films', *Polymer Degradation and Stability*, vol. 95, no. 2, pp. 99–107, Feb. 2010, doi: 10.1016/j.polymdegradstab.2009.11.048.

2.5. Biochar Particles from Digestate Pyrolysis as a filler for PBAT:PLA-based composites.

This study investigates the effect of biochar as a filler for biopolymer blends, with a focus on the effect of the biopolymer weight ratio on the final biochar-added blends. The blends studied in this work were obtained by varying the weight ratio of polybutylene adipate-co-terephthalate (PBAT) and polylactic acid (PLA) due to their great importance in packaging and agricultural fields. PBAT:PLA based biocomposites have been formulated by adding biochar particles, keeping the filler loading constant at 10 wt.%, a concentration chosen based on the results of previous results. Biochar has been produced in our laboratories by the slow pyrolysis of the digestate obtained from the anaerobic digestion of the organic fraction of municipal solid waste (OFMSW). Digestate feedstock and digestate-derived biochar (*d*BC) formulation and characterization, has been already discussed in chapter 2.1.2.3. The inhomogeneity of the feedstock is responsible for content and high diversity of inorganics in biochar surface that led to a particular interaction polymer/filler. The effect of *d*BC on PBAT and PLA biopolymer matrices is different, and for the blend compositions the relative weight ratio between PBAT and PLA plays an important role. Furthermore, the biocomposite blend has been fully characterised: rheological, morphological, mechanical, and dynamic-mechanical characterisations have been carried out, highlighting how the properties results strongly influenced by the presence of *d*BC in the blend. In addition, a study of the viscous molar mass of the two polymer matrices when processed in the presence or absence of *d*BC particles highlight that a strong chemical interaction occurs between PLA and *d*BC particles, unlike PBAT and *d*BC.

2.5.1. Materials and Methods

2.5.1.1. Materials

Poly(butylene adipate-co-terephtalate), PBAT, (commercial Ecoflex® F Blend C1200, BASF, SE, Ludwigshafen, Germany) is a film grade with a melt flow rate (MFR) of 2.7-4.9 g/10min (190°C, 2.16 kg), a density in the range of 1.25-1.27 g/cm3 and a melting temperature in the range of 110-120°C. Poly(Lactic Acid), PLA, (commercial Ingeo ® 4032D, NatureWorks, USA), having a MFI equal to 7 g/10 min (at 210°C and 2.16 kg), a density of 1.24 g/cm^3 and a melting point between 155 and 170°C. Biochar used in this work has been produced in our lab, it follows the entire procedure.

Biochar particles were produced pyrolysing digestate (*d*BC), the by-product of anaerobic digestion of organic Fraction of Municipal Solid Waste for biogas production. The slow pyrolysis process is described in detail in the 2.1.1.4 Experimental apparatus and Procedure section. Having been pyrolysed at 400 °C, the biochar was ground and sieved.

2.5.1.2. Bio-blend formulation

Prior to processing, biopolymer pellets and *d*BC particles were dried at 60°C under vacuum to avoid hydrolysis phenomena. The biocomposite formulation was then carried out by means of a batch mixer (Brabender model PLE330, Duisburg, Germany) at 170°C, at a mixing speed of 50 rpm for 5 min, with simultaneous addition of *d*BC and polymer matrix. Sample codes with relative polymer and filler concentrations are given in Table 12.

Table 12 Sample code name with relative weight concentration

Sample	PBAT [wt.%]	PLA [wt.%]	*Sample*	PBAT [wt.%]	PLA [wt.%]	*d*BC [wt.%]
PBAT:PLA 100:0	100	0	PBAT:PLA/*d*BC 100:0/10	90	0	10
PBAT:PLA 75:25	75	25	PBAT:PLA/*d*BC 75:25/10	67.5	22.5	10
PBAT:PLA 50:50	50	50	PBAT:PLA/*d*BC 50:50/10	45	45	10
PBAT:PLA 25:75	25	75	PBAT:PLA/*d*BC 25:75/10	22.5	67.5	10
PBAT:PLA 0:100	0	100	PBAT:PLA/*d*BC 0:100/10	0	90	10

2.5.1.3. Feedstock and Biochar characterization

Biochar particles has been produced in the contest of this research. Feedstock characterization test for decision of operative condition and the characterization test of resulting biochar particles it has been already described in 2.1.1.2 and in chapter 2.1.1.5, respectively.

2.5.1.4. Biocomposites Characterization

The rheological tests were carried out using a strain-controlled rheometer (mod. ARES G2 from TA Instrument, New Castle, DE, USA) in a parallel plate geometry (plate diameter 25 mm). Frequency scans from $\omega = 10^{-2}$ to 10^{2} rad/s were used to measure complex viscosity (η^*) and storage (G') and loss (G'') moduli at the same processing temperatures. The strain amplitude was $\gamma = 5\%$. Preliminary strain sweep experiments indicated that this was low enough to be in the linear viscoelastic regime.

A scanning electron microscope (SEM, Quanta 200 ESEM, FEI, Hillsboro, OR, USA) was used to examine the microstructure of the biocomposites. Prior to the SEM analysis, the samples were fractured in liquid nitrogen. To avoid electrostatic charging under the electron beam, the fractured surface of each sample was sputtered (Scancoat Six Edwards, Crawley, UK) with a thin layer of gold for 90 s in an argon atmosphere.

Tensile tests were performed on rectangular specimens using a universal testing machine (Instron model 3365, Rochdale, UK) in accordance with ASTM D882. The tests were performed at a tensile speed of 1 mm/min for 1 minute to evaluate Young's modulus, and then the speed was increased to 10 mm/min until the specimen broke. The average values for elongation at break, EB, modulus of elasticity, E, and tensile strength, TS, were calculated.

A dynamic mechanical analyser model DMA +50 (Metravib, Limonest, France) was used to perform dynamic mechanical thermal tests (DMTA) in tensile configuration. The test was carried out from room temperature to 140°C at a heating rate of 5 °C/min for three specimens (10 mm × 30 mm) of each composite. The frequency was set to 1 Hz and the dynamic displacement was set to 5×10^{-5} m.

The intrinsic viscosity [η] was measured using an iVisc LMV 830 capillary viscometer (Lauda Proline PV 15, Lauda-Königshofen, Germany) equipped with a Ubbelohde (K = 0.005) capillary viscometer in an oil bath thermostated at 27 °C. Each material was dissolved in THF with stirring at 50 °C for 1 hour to prepare the solution at a concentration of 0.2 wt%. To evaluate the intrinsic viscosity of the composites, each composite was dissolved in THF, the solid fraction was then removed using filter paper, the resulting solution was cast and a 0.2% w/w solution was then prepared. Flow times were measured in triplicate for each sample until the standard deviation was below 0.5 s. Solomon-Ciuta [1] intrinsic viscosity values were calculated using equation:

$$[\eta] = \frac{\sqrt{2}}{c}\sqrt{\eta_{sp} - \ln \eta_{rel}}$$

where c is the concentration of the polymer solution, η, η_{sp} and η_{rel} are, respectively, intrinsic, specific and relative viscosity. The solution viscosity of each sample was obtained by averaging 5 flow measurements. The viscosimetric molecular weight (M_v) was calculated using Mark-Houwink's equation:

$$[\eta] = KM_v^a$$

The parameter values of the Mark-Houwink constants, a and K, depend upon the specific polymer-solvent system. For PLA-THF, $K = 1.74 \cdot 10^{-4}$ and $a = 0.736$. For PBAT-THF, $K = 1.5 \cdot 10^{-4}$ and $a = 0.766$ [3].

2.5.2. Results and Discussion

Figure 32 shows the complex viscosity of bioblend and biocomposite as a function of angular frequency. In Figure 32(a), the curves show that the pristine samples (PBAT:PLA 0:100 and PBAT:PLA 100:0) have the same complex viscosity at low frequency, with a Newtonian behaviour of pure PLA, unlike PBAT, which shows a more pronounced decrease in complex viscosity with increasing angular frequency. In fact, unlike PLA, PBAT shows a narrower Newtonian range, exhibiting a shear-thinning behaviour already from 1 rad/s to higher angular frequency tested. Accordingly, in blend formulation, the addition of PBAT limits the Newtonian range, with the shear thinning tendency becoming more pronounced with increasing PBAT content. For blends dominated by one of the two matrices (PBAT:PLA 75:25 and PBAT:PLA 25:75), the complex viscosity at low frequency becomes higher than that of the pure matrix, with the appearance of a stress-strain behaviour at low frequency, suggesting a change in morphology. However, a more balanced behaviour between the two matrices is observed for PBAT:PLA 50:50. This phenomenon depends on the higher shear that occurs between the two phases and is a classic result for immiscible polymer blends. Indeed, for immiscible polymers, the formation of droplets of the minor phase within the major phase is responsible for an increase of the complex viscosity. For the blend in which PBAT and PLA are equivalent, as visible later in the morphology section, no droplet formation is visible and the morphology results in an elongated co-continuous phase that result responsible of an easier sliding of the polymer chain under shear [4], [5]. Thus, the blends have a higher complex viscosity at low frequency and a pronounced shear thinning behaviour in the frequency range, indicating a high interaction between the two matrices [6], [7], with a decrease of the complex viscosity at higher frequency due to the disentanglement of the molecular chain [8], [9].

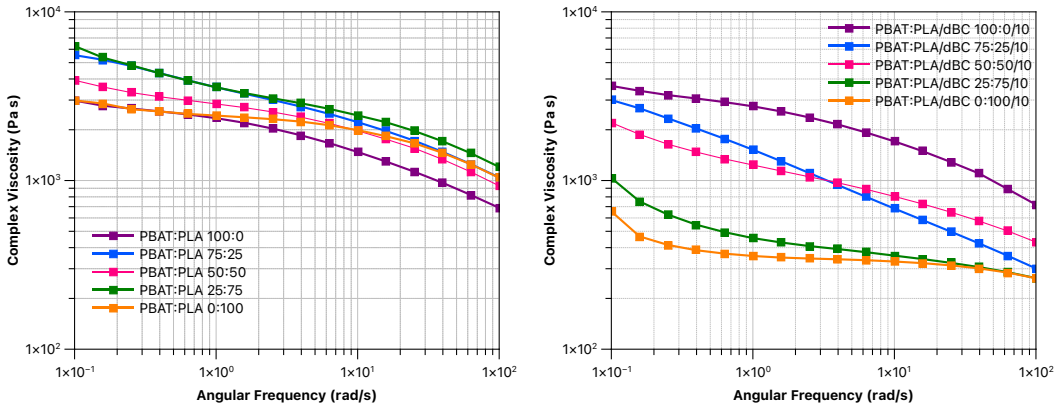

(a) *(b)*

Figure 32 *Complex Viscosity as a function of angular frequency of PBAT:PLA blends (a) without and (b) with 10 wt.% of dBC particles*

As shown in Figure 33, two different rheological behaviours are determined by the addition of 10 wt.% *d*BC to pristine PBAT or pristine PLA. Indeed, as seen in previous chapters (see 2.3 and 2.1.2.3) the addition of 10 wt.% of *d*BC to the PBAT matrix determines a global increase of the composite viscosity, as shown by Figure 33(a). On the contrary, as shown in Figure 33(b), for pure PLA the addition of 10 wt.% of *d*BC completely modifies the rheological behaviour with a significant decrease of the complex viscosity and a stress-strain behaviour at low frequency. This behaviour is usually observed when a plasticiser is added to a polymer matrix or when degradation phenomena occur.

Turning to the study of composite blends, the rheological behaviour depends on the weight ratio between PBAT:PLA to mean the balance between their two antithetic behaviours. Figure 32(b) shows the rheological behaviour of composite blends. As is the case with PLA composites, at low frequency the complex viscosity decreases with increasing PLA content in the blend. The presence of *d*BC particles and their interaction with the polymer blend is more visible in the stress-strain behaviour at low frequency when the amount of PLA exceeds the amount of PBAT in the biopolymer blend. Instead, the PBAT:PLA/*d*BC 75:25/10 complex viscosity has a more pronounced angular frequency dependence. The PBAT:PLA/*d*BC 50:50/10

showed both stress-yield behaviour and a pronounced decrease in complex viscosity with increasing angular frequency.

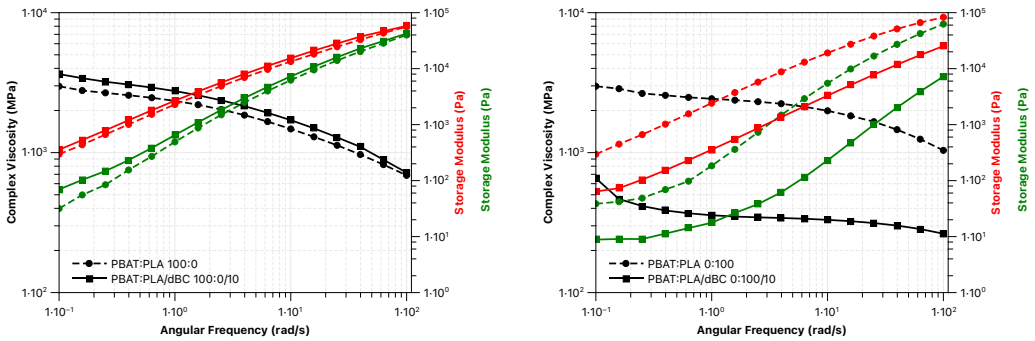

(a) *(b)*

Figure 33 *Rheological behaviour of (a) PBAT:PLA 100:0 with and without 10 wt.% of dBC particles and (b) PBAT:PLA 0:100 0 with and without 10 wt.% of dBC particles*

Figure 34 shows the SEM images of the nitrogen-fractured surface for the PBAT:PLA blends with different composition ratios, showing a typical two-phase structure According to the rheological behaviour, the morphology changes with increasing PLA content in the PBAT:PLA blend. As shown in the first column of Figure 7, the morphology changes from spherical droplets (PBAT:PLA 75:25) to a co-continuous elongated structure (PBAT:PLA 50:50) and back to spherical droplets [10], [11]. In composite SEM images, the average size of *d*BC particles in biopolymer blends appears to be smaller than the dimension shown by the particles (see Figure 12 and Figure 13 in chapter 2.1.2.3). This phenomenon is probably due to the shear stress experienced by *d*BC during melt mixing, which also favours a deagglomeration of smaller particles seen in Figure 3b, which appear homogeneous and well dispersed in the biopolymer blend.

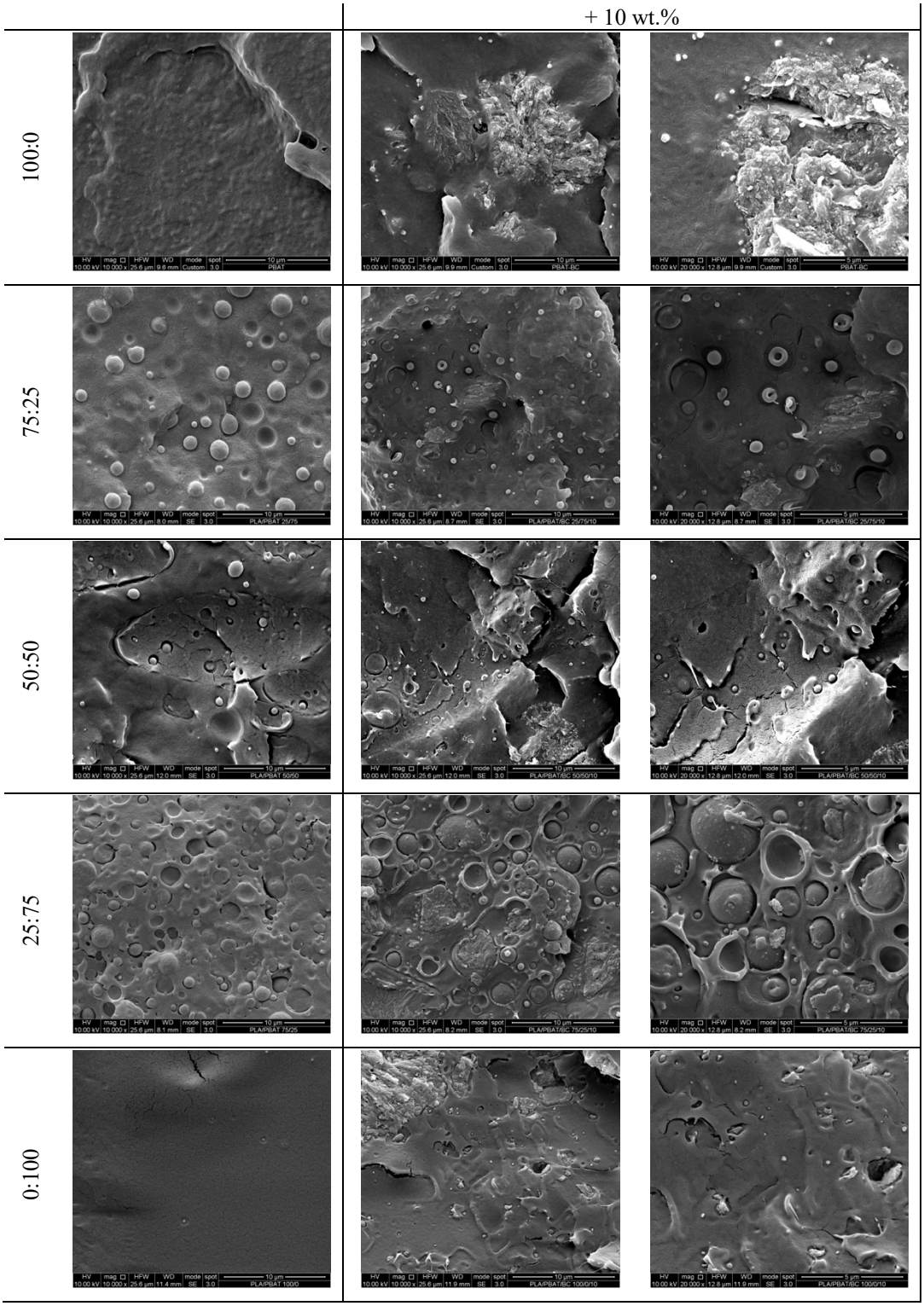

Figure 34 *SEM images of blend varying PBAT:PLA weight ratio, with and without 10 wt.% of dBC*

The reduction in particle size that occurs during melt mixing could lead to an increase in the polymer/filler interface area. As a result, the interaction between *d*BC and the biopolymer blend was enhanced. Also in this case, and in accordance with the rheological behaviour, this interaction led to a change in morphology depending on the PBAT:PLA weight ratio. Concerning the addition of *d*BC to pristine PBAT matrix, a good adhesion and dispersion between biopolymer matrix and *d*BC particles was shown, as already reported in a previous chapters (see 2.3 and 2.4). When added to pristine PLA matrix, a good dispersion is achieved. However, a dissection between polymer matrix and *d*BC occurs, with clear gaps surrounding *d*BC particles. Moreover, in the presence of *d*BC, when PLA is the minor phase (PBAT:PLA/*d*BC 75:25/10), its droplets homogeneously distributed in the PBAT matrix change from spherical shape to "donut" shape, with a global reduction of the mean particle diameter. Conversely, when PBAT is the minor phase (PBAT:PLA/*d*BC 25:75/10), the homogeneously distributed PBAT droplet retains the spherical shape. In this case, the major phase of PLA changes its morphology and shows a "volcano" shape around the PBAT droplet. For PBAT:PLA/*d*BC 50:50/10, a co-continuous elongated structure appears to be preserved, although the PLA appears slightly damaged.

Tensile testing and dynamic mechanical analysis were used to study the mechanical properties. Figure 35 shows blend mechanical properties, namely Young's modulus, tensile strength and elongation. As expected, for the blend without *d*BC (black line), as the PBAT content in the biopolymer blend increases, a transition from a rigid material to a ductile material is observed. This goes from a higher young modulus and lower elongation at break values for pure PLA to a lower young modulus and higher elongation at break values for pure PBAT. In line with the rheological behaviour and morphology, the presence of *d*BC has *(i)* a reinforcing role for PBAT that, as it is aspect, moves the mechanical behaviour of PBAT from ductile to rigid, and *(ii)* a reduction in mechanical properties for PLA. Consequently, for the blend composition, when PBAT is the main phase, *d*BC shows a small reinforcing role,

while when PLA is the main phase, biocomposites show a reduction in mechanical properties. Nevertheless, for PBAT:PLA/*d*BC 50:50/10, an increase in Young's modulus, tensile strength occurs without much variation in elongation at break, probably due to the preservation of the co-continuous elongated morphology and a good dispersion of *d*BC in the blend.

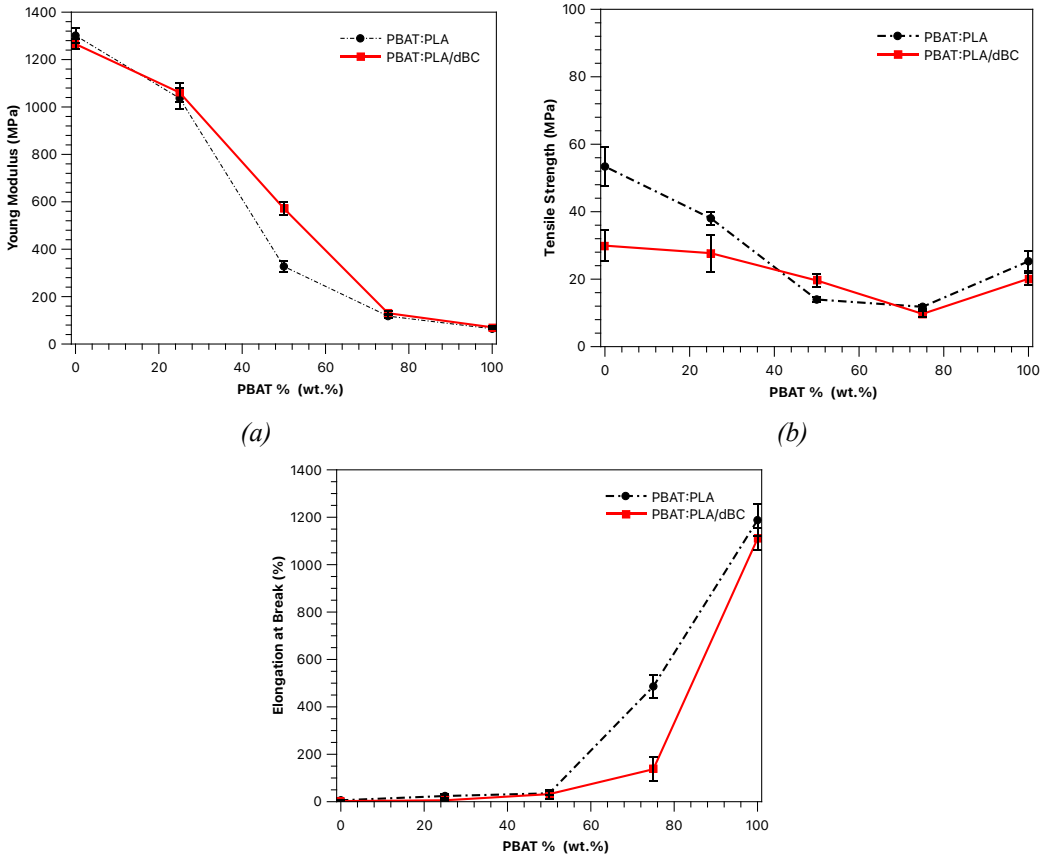

Figure 35 *(a) Young Modulus, (b) Tensile Strength and (c) Elongation at Break of PBAT:PLA blends without and with 10% of dBC particles as a function of PBAT content in biopolymer blend.*

The results of the DMA analysis are shown in Figure 36 as the variation of the logarithm of the storage moduli and the damping factor with temperature. The storage modulus, E', and the damping factor, tanδ, for the blend and the blend filled with 10 wt.% *d*BC as a function of temperature are shown in Figure 36, from room

temperature to 140°C, where possible. As expected, the first observation is related to the differences in the storage modulus at room temperature and in the shape of the storage modulus curve between the pure PBAT and the blend with PBAT in the main concentration with respect to the pure PLA and the blend with PLA in the main concentration. Instead, for the PBAT:PLA 50:50 blend, the mechanical behaviour of PLA prevails, with a storage modulus at room temperature comparable to that of pure PLA and a pronounced increase in a E' (with a maximum at ≈130 °C) due to the cold crystallisation phenomena of PLA. A second observation is related to the shape of the damping factor curve: the main peak at tanδ is related to the T_g of PLA, since that of PBAT is normally observed around -30÷-20 °C. Figure 36(b) shows how the T_g of PLA in the blend remains constant at 70.3±0.6°C, and the increase in magnitude is consistent with the increase in PLA content in the blend: namely, PBAT, the rubbery phase, acts as a stress concentrator. When the blends are filled with 10 wt.% *d*BC, the first observation is the shift towards a lower value of E' of the PBAT:PLA/*d*BC 75:25/10 and PBAT:PLA/*d*BC 50:50/10 blends (Figure 36(c)), coherent with the tensile properties already shown. The storage moduli below the glass transition temperature of PLA are lower for all PBAT:PLA weight ratios, except for pure PBAT. This behaviour is consistent with the tensile properties and rheological behaviour. Moreover, a different shape with a double shoulder in the E' curves, caused by PLA cold crystallisation phenomena. As for the damping factor, a significant reduction in the size of the main peaks related to T_g is observed, indicating a lower damping capacity in the presence of *d*BC. Furthermore, a shift towards a lower value of T_g is observed with the increase of PLA in the blend, from 71.4 °C for PBAT:PLA/*d*BC 75:25/10 to a T_g of 66.4 °C for PBAT:PLA/*d*BC 25:75/10. The slight decrease in glass transition temperature with increasing PLA in the biocomposite blend and the decrease in peak size is consistent with the behaviour observed with rheological analysis. We hypothesize that the decrease in storage moduli below the glass transition temperature and the decrease in T_g are due to a

possible degradation of the PLA polymer chain, caused by the presence of *d*BC in the blend.

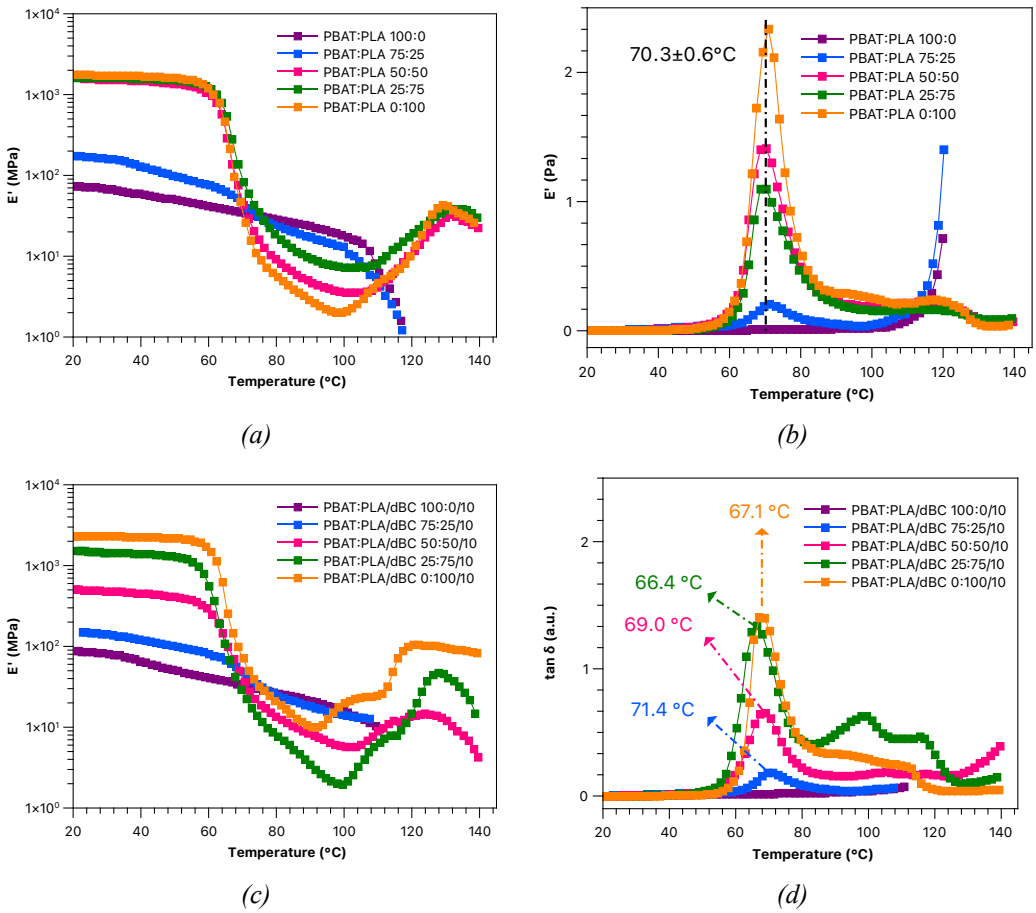

Figure 36 *Storage modulus and damping factor graphs for biopolymer blend (a,b) without and (c,d) with 10 wt.% of dBC.*

In order to evaluate the degradation phenomena likely to be suggested by the previous characterisation, a measurement of the molecular weight was carried out by means of intrinsic viscosity measurements and correlated to the molecular weight M_v by means of Mark-Houwink constants. Table 13 shows the results of the capillary viscosimetry carried out on PBAT and PLA, with and without 10 wt.% of *d*BC. Each material was dissolved in THF with stirring at 50 °C for 1 hour to prepare the solution at the concentration of 0.2 wt.%. To evaluate the intrinsic viscosity of the composites,

each composite was dissolved in THF, then the solid fraction was removed using filter paper, the resulting solution was poured and then a 0.2 wt.% solution was prepared. The viscous molar mass of the biocomposites has been compared with that of the pure matrix, which was subjected to the same process condition.

Table 13 Viscous molar mass, intrinsic viscosity, and dimensionless values of molar mass of PBAT and PLA with and without 10 wt.% of dBC.

	M_v^0	η		M_v	η	$\frac{M_v}{M_{v0}}$
	[g/mol]	[dL/g]		[g/mol]	[dL/g]	[-]
PBAT:PLA 100:0	5.32×10^4	0.63	*PBAT:PLA/dBC 100:0/10*	5.79×10^4	0.67	1.08
PBAT:PLA 0:100	1.58×10^5	1.17	*PBAT:PLA/dBC 0:100/10*	7.91×10^4	0.7	0.50

The table highlights that the M_v of PBAT, processed in the presence of in the absence of *d*BC, maintains its viscous molar mass constant, with a dimensionless value of the molar mass almost equal to one. For PLA, the dimensionless molar mass is actually 0.5, whereas a significant reduction of the viscous molar mass has been highlighted. For PBAT, the loading of *d*BC as a reinforcing filler leads to an increase in mechanical and rheological properties. Instead, the reduction in viscosity and molar mass of PLA suggests a scission of the molecular chains induced by the presence of *d*BC in the composite. This result is probably due to the fact that *d*BC causes or accelerates the degradation of PLA, thereby reducing the molar mass [12], [13].

2.5.3. Endings

In this chapter, a fully biodegradable biopolymer blend based on PBAT and PLA matrices was prepared by varying the weight ratio between the two biopolymer matrices. The biochar added to the different biopolymer blends was obtained in our laboratories using digestate as a feedstock. Initially, the digestate and the digestate-derived biochar were fully characterised (see chapter 2.1.2.3). For biocomposites blend rheological behaviour, the addition of *d*BC modifies complex viscosity depending particularly on PLA interaction with *d*BC particles, and consequently on the increase of PLA matrix in polymer blend. From the mechanical characterisation of the filled blend, it is evident that degradation phenomena occur caused by the interaction between PLA and *d*BC particles. From the morphological characterisation, it is clear how different is the interaction between *d*BC particles and the two different polymer matrices, showing an overall good *d*BC dispersion in the polymer matrix, even if a better interfacial adhesion was highlighted in the presence of PBAT matrix, and some degradative evidence was found on PLA matrix. Thus, the rheological, morphological and mechanical behaviour of *d*BC filled blends highlight the challenges of using *d*BC particles as filler for PLA or PLA based blends. Indeed, degradation phenomena when *d*BC interacts with the PLA matrix have been confirmed by means of a capillary viscosimeter, evaluating the viscous molar mass of the two polymers matrix processed in the absence and in the presence of *d*BC particles. In fact, a significant reduction in the molecular weight of PLA is probably due to a strong interaction between PLA and the residual inorganic elements present on the *d*BC surface after pyrolysis. In short, the excellent properties of *d*BC particles obtained from digestate pyrolysis could certainly be used as a filler for biopolymer blends, although the composition of the blend is a determining factor.

Reference

[1] A.-A. A. Abdel-Azim, A. M. Atta, M. S. Farahat, and W. Y. Boutros, 'Determination of intrinsic viscosity of polymeric compounds through a single specific viscosity measurement', *Polymer*, vol. 39, no. 26, pp. 6827–6833, Dec. 1998, doi: 10.1016/S0032-3861(98)00184-0.

[2] Q. Meng, M.-C. Heuzey, and P. J. Carreau, 'Control of thermal degradation of polylactide/clay nanocomposites during melt processing by chain extension reaction', *Polymer Degradation and Stability*, vol. 97, no. 10, pp. 2010–2020, Oct. 2012, doi: 10.1016/j.polymdegradstab.2012.01.030.

[3] M. F. Andrade *et al.*, 'Influence of Gamma Radiation on the Properties of Biodegradable PBAT – Poly (butylene Adipate co-terephthalate) Active Films with Orange Essential Oil', *Macromol. Symp.*, vol. 394, no. 1, p. 2000057, Dec. 2020, doi: 10.1002/masy.202000057.

[4] A. Codou, A. Anstey, M. Misra, and A. K. Mohanty, 'Novel compatibilized nylon-based ternary blends with polypropylene and poly(lactic acid): morphology evolution and rheological behaviour', *RSC Adv.*, vol. 8, no. 28, pp. 15709–15724, 2018, doi: 10.1039/C8RA01707G.

[5] C. Lacroix, M. Grmela, and P. J. Carreau, 'Relationships between rheology and morphology for immiscible molten blends of polypropylene and ethylene copolymers under shear flow', *Journal of Rheology*, vol. 42, no. 1, pp. 41–62, Jan. 1998, doi: 10.1122/1.550943.

[6] H. Moustafa, N. El Kissi, A. I. Abou-Kandil, M. S. Abdel-Aziz, and A. Dufresne, 'PLA/PBAT Bionanocomposites with Antimicrobial Natural Rosin for Green Packaging', *ACS Appl. Mater. Interfaces*, vol. 9, no. 23, pp. 20132–20141, Jun. 2017, doi: 10.1021/acsami.7b05557.

[7] A. Pietrosanto, P. Scarfato, L. Di Maio, M. R. Nobile, and L. Incarnato, 'Evaluation of the Suitability of Poly(Lactide)/Poly(Butylene-Adipate-co-Terephthalate) Blown Films for Chilled and Frozen Food Packaging Applications', *Polymers*, vol. 12, no. 4, p. 804, Apr. 2020, doi: 10.3390/polym12040804.

[8] X. Li *et al.*, 'The morphological, mechanical, rheological, and thermal properties of PLA/PBAT blown films with chain extender', *Polym Adv Technol*, vol. 29, no. 6, pp. 1706–1717, Jun. 2018, doi: 10.1002/pat.4274.

[9] Y. Deng, C. Yu, P. Wongwiwattana, and N. L. Thomas, 'Optimising Ductility of Poly(Lactic Acid)/Poly(Butylene Adipate-co-Terephthalate) Blends Through Co-continuous Phase Morphology', *J Polym Environ*, vol. 26, no. 9, pp. 3802–3816, Sep. 2018, doi: 10.1007/s10924-018-1256-x.

[10] S. Su, M. Duhme, and R. Kopitzky, 'Uncompatibilized PBAT/PLA Blends: Manufacturability, Miscibility and Properties', *Materials*, vol. 13, no. 21, p. 4897, Oct. 2020, doi: 10.3390/ma13214897.

[11] K. Li, J. Peng, L.-S. Turng, and H.-X. Huang, 'Dynamic rheological behavior and morphology of polylactide/poly(butylenes adipate-co-terephthalate) blends with various composition ratios', *Adv. Polym. Technol.*, vol. 30, no. 2, pp. 150–157, Jun. 2011, doi: 10.1002/adv.20212.

[12] R. Arrigo, M. Bartoli, and G. Malucelli, 'Poly(lactic Acid)-biochar biocomposites: Effect of processing and filler content on rheological, thermal, and mechanical properties', *Polymers*, vol. 12, no. 4, Apr. 2020, doi: 10.3390/POLYM12040892.

[13] R. Scaffaro, F. Sutera, M. C. Mistretta, L. Botta, and F. P. La Mantia, 'Structure-properties relationships in melt reprocessed PLA/hydrotalcites nanocomposites', *Express Polym. Lett.*, vol. 11, no. 7, pp. 555–564, 2017, doi: 10.3144/expresspolymlett.2017.53.

Conclusion

The aim of this work was the formulation and characterization of biocomposites reinforced with biochar particles, the by-product of pyrolysis. Biochar represents a second-level waste product that holds great promise for materials science in the last ten years. The focus of this research was the employment of this particles to obtain biodegradable materials, with particular attention to energy optimisation, through the slow pyrolysis of two types of organic waste. The dissertation sought to answer some questions regarding the formulation of biodegradable and biobased composites reinforced with biochar particles, and whether and how such composites could play a role in applications such as agriculture.

Firstly, it has been produced biochar from two different sources. The pyrolysis sources were selected from production waste with the aim of valorising the waste itself. In addition, the slow pyrolysis process used to produce biochar was primarily aimed at producing good quality fuel and gas, and the resulting biochar, which is still waste, was evaluated as a reinforcing filler. In addition to the valorisation of the waste itself, the choice of a processing waste can be useful as a feedstock targeting process has necessarily already been carried out.

The first source used for the production of biochar is in fact the processing waste of carob fruit after removal of sugars and nutrients for the production of sweets by a local factory. The carobs were then characterised as a post-production input and three different pyrolysis temperatures were selected, taking into account the degradation peaks shown in the feedstock analysis. The three pyrolysis temperatures resulted in different liquid, gas and solid yields and, as far as this research was concerned, different physicochemical properties of the resulting char. In view of the studies

carried out through literature review, it was decided to use all three types of char products as fillers for the production of biocomposites.

The second source used as a feedstock for pyrolysis was digestate. In the waste management sector, digestate is the solid and residual product resulting from the anaerobic digestion of waste for the production of fuel and gas. In the case of our research, the digestate was provided by a regional waste management company that supplied digestate from the treatment of the organic fraction of municipal solid waste. Due to the inhomogeneity of the source (*e.g.* different types of food, residual bones) for digestate production, the characteristics of the resulting biochar after the pyrolysis process are very different from those obtained with carob.

After the biochar was produced and before it was added to polymer matrices for biocomposites formulations, preliminary studies were carried out.

The first question was whether it could have properties comparable to conventional carbon particles such as carbon black. Firstly, the scavenging efficiency with DPPH assay was investigated comparing carbon black (CB) with commercial biochar (*c*BC) and it was shown that the scavenging efficiency of commercial biochar particles is much higher than that of carbon black. Samples were prepared using polypropylene (PP) as the matrix, as it is a well-known matrix. PP-based composites loaded with CB and *c*BC were then compared. In addition, a study of hybrid polypropylene-based composites with varying weight ratios between biochar and carbon black was carried out. Finally, the possibility of replacing carbon black with biochar in carbon black/graphene (GNP) hybrid composites was investigated by comparing the properties of PP/CB:GNP with those of PP/*c*BC:GNP.
In terms of the rheological behaviour of the composites, the presence of *c*BC in polypropylene appears to have a plasticising effect, which can be advantageous depending on the processing chosen for the composite formulation. This plasticising

effect is shown both for the pure *c*BC filled composite and, proportionally to the concentration of *c*BC with respect to CB, for the hybrid PP/*c*BC:CB composites. When *c*BC replaces CB in the hybrid compound with GNP, the rheological behaviour remains unchanged. In terms of mechanical properties, the presence of *c*BC particles acts as a reinforcing agent that is absolutely comparable to that offered by carbon black. This behaviour is confirmed both in pure addition and in comparison, with pure CB in the PP matrix, as well as in the presence of hybrid fillers, both as co-fillers with carbon black or with graphene.

Having established that biochar could be suitable as a filler due to its higher scavenging capacity, a commercial biochar used in the food industry, derived from the pyrolysis of birch and beech wood, was evaluated for the production of a biocomposite based on poly(butylene adipate-co-terephthalate) (PBAT) as a biopolymer matrix and commercial biochar as a filler. The first experimental section was carried out using commercial *c*BC to determine the processing conditions for biocomposite formulation. All PBAT/*c*BC composites showed uniform filler dispersion and good adhesion within the selected biopolymer matrix. The addition of *c*BC resulted in an improvement of the modulus of elasticity while maintaining high values of deformation. The biochar was then added to PBAT at different concentrations. In addition, by delaying the degradation phenomena of the polymer matrix, the presence of the filler induced a photo-oxidative resistance on PBAT. This result was even more pronounced for PBAT/*c*BC 10 wt.% than for PBAT/*c*BC 5 wt.%. It opens up the possibility of using PBAT-based films in outdoor applications.

In this context, a study was carried out on PBAT-based composites with biochars produced in our laboratory at three different pyrolysis temperatures from carob waste (*cw*BC*)*. The biochar particles, as a result of three different pyrolysis process temperatures, were added to PBAT matrix. The focus was on the variation of the final properties of the composite as a function of the pyrolysis temperature used.

The different pyrolysis temperatures result in different particle dimensions, and, in particular, BC400 results in a smaller dimension. This results in better dispersion of the BC400 particles in the polymer matrix and better tensile and rheological properties and thermal stability of the resulting composite compared to composites filled with particles obtained at lower temperatures. It was seen how increasing the pyrolysis temperature decreases the absorption kinetics of free radicals in DPPH assay, resulting in particles obtained at a lower pyrolysis temperature having a higher radical scavenging efficiency. The study of particle scavenging activity also showed that it was sufficient to slightly increase the concentration of biochar obtained at higher temperatures to obtain comparable scavenging activity. This trend was also confirmed for the mechanical behaviour of the composite as a function of photooxidation time. In fact, by adding 10 wt.% of particles within the PBAT matrix, the dimensionless elongation at break as a function of the photo-oxidation time showed that *(i)* in the case of BC400, the half time (the time at which the value is half of the initial one) is reached at the end of the photo-oxidation cycle, *(ii)* in the case of BC280, the dimensionless elongation at break remains almost constant and close to one. Instead, by adding 20 wt.%, the mechanical behaviour of the resulting composites with BC280, BC340 or BC400 is comparable and approximately equal to 1 throughout the photo degradation cycle.

Finally, a study was carried out on the use of biochar as a filler in biopolymer blends, using as a filler digestate-derived biochar (*d*BC). A fully biodegradable biopolymer blend based on PBAT and PLA matrices was prepared by varying the weight ratio between the two biopolymer matrices. For biocomposites blend rheological behaviour, the addition of *d*BC modifies complex viscosity depending particularly on PLA interaction with *d*BC particles, and consequently on the increase of PLA matrix in polymer blend. From the mechanical characterisation of the filled blend, it is evident that degradation phenomena occur. The degradation phenomena when *d*BC interacts with the PLA matrix have been confirmed by means of a capillary

viscosimeter and a significant reduction in the molecular weight of PLA is probably due to a strong interaction between PLA and the residual inorganic elements present on the *d*BC surface after pyrolysis. In short, the excellent properties of *d*BC particles obtained from digestate pyrolysis could certainly be used as a filler for biopolymer blends, although the composition of the blend is a determining factor.

Applying the concept of waste to material, this dissertation has demonstrated the possibility of producing biochar from different feedstocks and its successful use as a filler in the formulation of composites and biocomposites. Therefore, in synthetic matrix, biochar together with other carbonaceous particles could be considered to replace carbon black. However, for a successful formulation of durable biocomposites, it should be noted that performance and durability are strictly related to *(i)* the chemical nature of the host matrix and *(ii)* the chemical nature of the feedstock from which the biochar is produced. Regarding the synergistic effect of these two factors, biochar could exert a protective action in case of photo-oxidation phenomena or pro-degradant effect processing at high temperature.
In summary, the circular economy perspective, together with the waste-to-material approach, supports the transition to sustainability and enables the formulation of innovative sustainable materials with good properties and performance.

Figure index

Table Index

Spreading Research

National Conference

1. **G. Infurna**, Marco Maniscalco, Luigi Botta, G. Caputo, Nadka. Tz. Dintcheva *"Biopolymers blend composites containing biochar particles from anaerobic urban waste digestate pyrolysis",* CATANIA (Italy), 28th may-1st June 2023

2. Dintcheva N. Tz, Lazzara G., Cavallaro G., **Infurna G.**, La Mantia F. P., Millioto S., "*Bio- Polymers Based Films Containing Naturally Occurring Fillers And Anti-Oxidants For Cultural Heritage Conservation:Formulation, Characterization And Durability",* XII INSTM CONFERENCE-XV AIMAT CONFERENCE, July 21-24, 2019 Ischia (NA)

3. **Infurna G.**, Maniscalco M., Caputo G., Botta L., Dintcheva N. Tz., *"Biopolymer based composites containing biochar particles coming from pyrolyzed agriculture waste"*, XVI AIMAT National Conference, 15 – 18 September, 2021, Cagliari

International Conference

1. **G.Infurna,** L. Botta, N. Tz. Dintcheva *"PBAT:PLA blend composite containing biochar particles from organic fraction of municipal solid waste pyrolysis"* SOFIA (Bulgaria) 3-5 September 2023

2. **G. Infurna,** L. Botta, M. Maniscalco, G. Caputo, S. Marullo, F. D'Anna, N. Tz. Dintcheva, *"Suistanable PBAT-Biocomposites containg biocharparticlesobtained by agricultural waste"* MODEST, SALINA (Italy), September 11-13, 2022

3. Dintcheva N. Tz, Lazzara G., Cavallaro G., **Infurna G.**, La Mantia F. P., Millioto S., *"Durability Of Bio-Polymers Based Films For Cultural Heritage Conservation",* 33rd PDDG Conf. 1-5 Sep 2019, Malta

4. Dintcheva N. Tz., Lazzara G., Cavallaro G., **Infurna G.**, Francesco Paolo La Mantia, "*Naturally Occurring Materials For Cultural Heritage*

Conservation", Materials in The Next Decade, MODEST, Favignana, Settembre 2019

5. *13th European Symposium on Thermal Analysis and Calorimetry (ESTAC13)*, in Palermo, Italy from 19th to 22nd September 2022, Local Committee

Paper

1. **Infurna, G.,** Caruso, G., Dintcheva, N.T. "*Sustainable Materials Containing Biochar Particles: A Review"*(2023) Polymers, 15 (2), art. no. 343, DOI: 10.3390/polym15020343

2. Morici, E., **Infurna, G**., Dintcheva, N.T. *"Ecofriendly Biopolymer-Based Nanocomposite Films with Improved Photo-Oxidative Resistance"* (2022) Materials, 15 (16), art. no. 5778, DOI: 10.3390/ma15165778

3. **Infurna, G.,** Botta, L., Maniscalco, M., Morici, E., Caputo, G., Marullo, S., D'Anna, F., Dintcheva, N.T. *"Biochar Particles Obtained from Agricultural Carob Waste as a Suitable Filler for Sustainable Biocomposite Formulations"* (2022) Polymers, 14 (15), art. no. 3075, DOI: 10.3390/polym14153075

4. Maniscalco, M., **Infurna, G**., Caputo, G., Botta, L., Dintcheva, N.Tz. *"Slow pyrolysis as a method for biochar production from carob waste: Process investigation and products' characterization"* (2021) Energies, 14 (24), art. no. 8457, DOI: 10.3390/en14248457

5. **Infurna G.,** Botta L., Ingargiola I., Maniscalco M., Caputo G., Dintcheva N. Tz. *"Biochar from digestate pyrolysis as a filler for biopolymer blends: effect of blend composition"* (2023), Journal of Polymers and the Environment, DOI: 10.1007/s10924-023-03108-1

6. **Infurna G.** Dintcheva N.T. *"Temperature effect on biochar physiochemical properties"* Book Chapter *"Biochar as Multipurpose Platform", Under Review*

7. Dintcheva, N.T., **Infurna, G.**, Baiamonte, M., D'Anna, F. *"Natural compounds as sustainable additives for biopolymers"* (2020) Polymers, 12 (4), art. no. 732 DOI: 10.3390/polym12040732

8. Marullo, S., Gallo, G., **Infurna, G.**, Dintcheva, N.T., D'Anna, F.*"Antimicrobial and antioxidant supramolecular ionic liquid gels from biopolymer mixtures"* (2023) Green Chemistry, 25 (9), pp. 3692-3704. DOI: 10.1039/d2gc04358k

9. Marullo, S., Petta, F., **Infurna, G.**, Dintcheva, N.T., D'Anna, F. *"Polysaccharide-based supramolecular bicomponent eutectogels as sustainable antioxidant materials"*(2023) Green Chemistry, DOI: 10.1039/d3gc00573a

10. **Infurna, G.**, Cavallaro, G., Lazzara, G., Milioto, S., Dintcheva, N.T., *"Effect of different processing techniques and presence of antioxidant on the chitosan film performance"* (2022) Journal of Vinyl and Additive Technology, 28 (2), pp. 343-351, DOI: 10.1002/vnl.21905

11. Dispenza, C., Sabatino, M.A., **Infurna, G.**, Dintcheva, N.T. *"Control of end-of-life oxygen-containing groups accumulation in biopolyesters through introduction of crosslinked polysaccharide particles"* (2022) Polymer Engineering and Science, 62 (2), pp. 426-436. DOI: 10.1002/pen.25855

12. D'Anna, F., Sbacchi, M., **Infurna, G.**, Dintcheva, N.T., Marullo, S.*"Boosting the methanolysis of polycarbonate by the synergy between ultrasound irradiation and task specific ionic liquids"* (2021) Green Chemistry, 23 (24), pp. 9957-9967. DOI: 10.1039/d1gc02239c

13. **Infurna, G.,** Cavallaro, G., Lazzara, G., Milioto, S., Dintcheva, N.T. *"Understanding the effects of crosslinking and reinforcement agents on the performance and durability of biopolymer films for cultural heritage protection"* (2021) Molecules, 26 (11), art. no. 3468, DOI: 10.3390/molecules26113468

14. Di Bartolo, A., **Infurna, G.**, Dintcheva, N.T. *"A review of bioplastics and their adoption in the circular economy"* (2021) Polymers, 13 (8), art. no. 1229, DOI: 10.3390/polym13081229

15. Dintcheva, N.T., **Infurna, G.**, D'Anna, F. *"End-of-life and waste management of disposable beverage cups"*(2021) Science of the Total Environment, 763, art. no. 143044, DOI: 10.1016/j.scitotenv.2020.143044

16. **Infurna, G.**, Cavallaro, G., Lazzara, G., Milioto, S., Dintcheva, N.T. *"Bionanocomposite films containing halloysite nanotubes and natural antioxidants with enhanced performance and durability as promising materials for cultural heritage protection"* (2020) Polymers, 12 (9), art. no. 1973, DOI: 10.3390/polym12091973

17. **Infurna, G.,** Teixeira, P.F., Dintcheva, N.T., Hilliou, L., La Mantia, F.P., Covas, J.A. *"Taking advantage of the functional synergism between carbon nanotubes and graphene nanoplatelets to obtain polypropylene-based nanocomposites with enhanced oxidative resistance"* (2020) European Polymer Journal, 133, art. no. 109796, DOI: 10.1016/j.eurpolymj.2020.109796

18. Marullo, S., Meli, A., Dintcheva, N.T., **Infurna, G.**, Rizzo, C., D'anna, F. *"Environmentally friendly eutectogels comprising l-amino acids and deep eutectic solvents: Efficient materials for wastewater treatment"* (2020) ChemPlusChem, 85 (2), pp. 301-311. DOI: 10.1002/cplu.202000017

International Time Abroad

Universidade Do Minho, Guimaraes (Portugal), From 16th of March to 16th of June 2022 (94 days).

Followed Didactic Activities

1. *Aten Centre Course - Misure non lineari di sforzo e deformazione nella biomeccanica dei tessuti mediante BOSE 3330*, 19th of January 2021, Prof Zingales

2. *Theory and practice of electrochemical impedance spectroscopy*, from 21st to 25th of July 2021, Prof. Monica Santamaria, Dott. Francesco Di Franco, Dott. Andrea Zaffora

3. Aten Centre Course - U*ncover the nanoworld: a complete training on Atomic Force Microscopy (AFM) and its applications,* 21st June 2022, Laboratorio di Meccanica dei materiali e dei biomateriali

4. Preparation and characterization of (bio)polymer-based micro- and nanostructured system, 20th and 21st April 2022, Prof. Scaffaro, Ing. Maio

5. 21° Scuola AIMAT "I Materiali nella Transizione Energetica", From 13rd to17th July 2022, ISCHIA, Different Teachers

6. Introduction to polymer crystallization, 20th – 23rd March 2023, Prof. Alejandro J. Müller

7. Preparation and characterization of (bio)polymer-based micro- and nanostructured systems, 17 Feb from 20th to 23rd, Prof. R. Scaffaro, Dr. E. F. Gulino

8. AUTHOR WORKSHOP – Pubblicare su UniPa Springer, 16th February 2023, Springer Event

9. Combined processing for the preparation of biopolymeric porous structures for biomedical applications, From 11st to 13rd of April 2023, Dott. Francesco Lopresti

10. Corso Formazione e Abilitazione Utilizzo SEM, 17th and 18th of July, Ing. Mario Minacapilli

11. Corso Formazione IR Spectroscopy, 6th and 7th June 2023, Prof. Rosalinda Inguanta